

# THE *UBV* COLOR EVOLUTION OF CLASSICAL NOVAE. I. NOVA-GIANT SEQUENCE IN THE COLOR-COLOR DIAGRAM

IZUMI HACHISU

Department of Earth Science and Astronomy, College of Arts and Sciences, The University of Tokyo, Komaba, Meguro-ku, Tokyo 153-8902, Japan

AND

MARIKO KATO

Department of Astronomy, Keio University, Hiyoshi, Kouhoku-ku, Yokohama 223-8521, Japan

*The Astrophysical Journal*, 785:97, 2014 April 20

## ABSTRACT

We identified a general course of classical nova outbursts in the  $B-V$  versus  $U-B$  color-color diagram. It is reported that novae show spectra similar to those of A–F supergiants near optical light maximum. However, they do not follow the supergiant sequence in the color-color diagram, neither the blackbody nor the main-sequence sequence. Instead, we found that novae evolve along a new sequence in the pre-maximum and near-maximum phases, which we call “the nova-giant sequence.” This sequence is parallel to but  $\Delta(U-B) \approx -0.2$  mag bluer than the supergiant sequence. This is because the mass of a nova envelope is much ( $\sim 10^{-4}$  times) less than that of a normal supergiant. After optical maximum, its color quickly evolves back blueward along the same nova-giant sequence and reaches the point of free-free emission ( $B-V = -0.03$ ,  $U-B = -0.97$ ), which coincides with the intersection of the blackbody sequence and the nova-giant sequence, and remains there for a while. Then the color evolves leftward (blueward in  $B-V$  but almost constant in  $U-B$ ), owing mainly to the development of strong emission lines. This is the general course of nova outbursts in the color-color diagram, which was deduced from eight well-observed novae in various speed classes. For a nova with unknown extinction, we can determine a reliable value of the color excess by matching the observed track of the target nova with this general course. This is a new and convenient method for obtaining the color excesses of classical novae. Using this method, we redetermined the color excesses of 20 well-observed novae. The obtained color excesses are in reasonable agreement with the previous results, which in turn support the idea of our general track of nova outbursts. Additionally, we estimated the absolute  $V$  magnitudes of about 30 novae using a method for time-stretching nova light curves to analyze the distance-reddening relations of the novae.

*Subject headings:* novae, cataclysmic variables — stars: individual (FH Ser, PU Vul, PW Vul, V1500 Cyg, V723 Cas)

## 1. INTRODUCTION

A classical nova is a thermonuclear runaway event on a mass-accreting white dwarf (WD) in a binary. A companion star transfers its mass to the WD via Roche-lobe overflow or a wind. When the mass of the hydrogen-rich envelope of the WD reaches a critical value, hydrogen at the bottom of the envelope ignites to trigger a hydrogen shell-flash and the binary becomes a nova. The photospheric radius of the WD envelope expands to a giant size and the spectrum of the nova resembles that of an F-supergiant at or near optical maximum. After optical maximum, the photosphere recedes into progressively deeper layers as the envelope mass decreases, mainly because of wind mass-loss (e.g. Hachisu & Kato 2006). The wind mass-loss rate gradually decreases, and optically-thick winds finally stop before the nova enters a supersoft X-ray phase. The nova outburst ends when the hydrogen shell burning extinguishes. This nova envelope evolution was calculated by Kato & Hachisu (1994) on the basis of the optically-thick nova wind theory (e.g., Kato 1983).

Despite their overall similarity, the optical light curves of novae have a wide variety of timescales and shapes (e.g., Payne-Gaposchkin 1957; Duerbeck 1981; Strobe et al. 2010, see also Figure 1). Various empirical time-scaling laws have been proposed in an attempt to recognize common pat-

terns and unify the nova light curves (see, e.g., Hachisu et al. 2008, for a summary). Recently, Hachisu & Kato (2006) found that, in terms of free-free emission, the optical and infrared (IR) light curves of several novae follow a similar decline law. Moreover, the time-normalized light curves were found to be independent of the WD mass, chemical composition of the ejecta, and wavelength. They called this the universal decline law. Subsequently, Hachisu & Kato (2007, 2009, 2010), Hachisu et al. (2008), and Kato et al. (2009) applied this universal decline law to a number of novae ( $\gtrsim 30$  novae). On the basis of this universal decline law, Hachisu & Kato (2010) theoretically explained the maximum magnitude versus rate of decline (MMRD) law of classical novae. Therefore, we confidently state that the main part of nova light curves can be interpreted in terms of free-free emission from nova ejecta outside the photosphere.

The evolution of colors is another challenging subject that attracts many researchers, who have attempted to identify common behavior among various types of novae. For example, Duerbeck & Seitter (1979) noted that the color evolutions of six novae are remarkably similar in the intrinsic  $(B-V)_0$  versus  $(U-B)_0$  color-color diagram, regardless of their different nova speed classes. These six novae, however, traced similar but different paths in the color-color diagram (see Figures 2–7 of Duerbeck & Seitter 1979). van den Bergh & Younger (1987) derived the general trends of color evolution in nova light curves, i.e.,  $(B-V)_0 = 0.23 \pm$

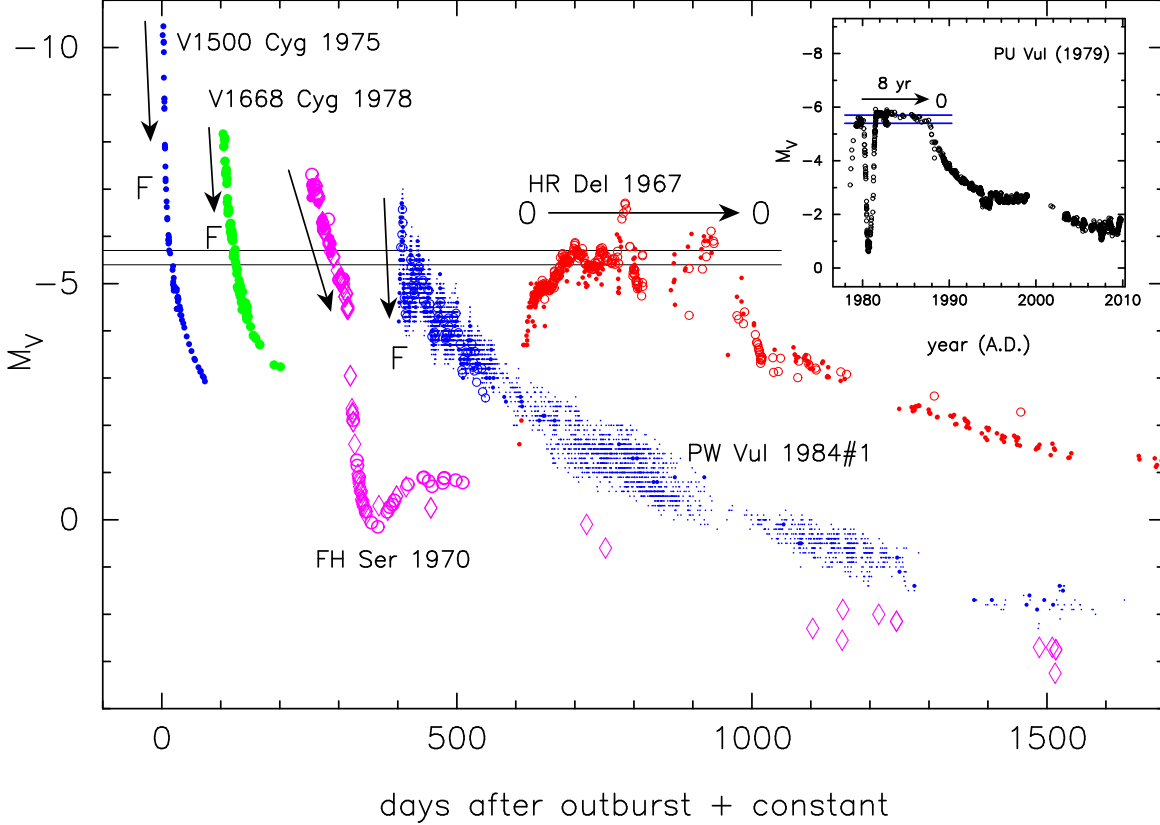


FIG. 1.— Optical light curves of six novae with different speed classes, i.e., from slow to fast, the symbiotic nova PU Vul (inset, small black open circles), very slow nova HR Del (red symbols), slow nova PW Vul (blue symbols), moderately fast nova FH Ser (magenta symbols), fast nova V1668 Cyg (green filled squares), and very fast nova V1500 Cyg (blue filled circles). Although their peak brightnesses, shapes, and decline rates are very different, we will show that their color-color evolution tracks are very similar. This indicates that these novae evolve under common physical conditions. The sources of optical data are cited in Sections 4 (PU Vul), 5.3 (HR Del), 3.1 (PW Vul), 2 (FH Ser), 3.5 (V1668 Cyg), and 3.4 (V1500 Cyg). Horizontal lines represent the absolute magnitudes of  $M_V = -5.4$  and  $M_V = -5.7$ . The distance modulus of each nova is taken from our results in Sections 2 – 5. Black arrows indicate the nova-giant sequence of each nova, followed by an optically-thick free-free emission phase (labeled F) or by an optically-thin free-free emission phase (labeled O). See text for more details.

0.06 at maximum (see also Allen 1973, for an earlier work) and  $(B-V)_0 = -0.02 \pm 0.04$  at  $t_2$ , where  $t_m$  ( $m = 2$  or  $3$ ) is the number of days during which a nova decays by the  $m$ -th magnitude from its optical maximum, and  $(B-V)_0$  is the intrinsic  $B-V$  color of the nova. These two relations, however, often show large deviations from the values obtained by other methods. Miroschnichenko (1988) found that the  $B-V$  and  $U-B$  color evolution of novae stabilizes soon after optical maximum and that this stage showed a general trend of  $(B-V)_0 = -0.11 \pm 0.02$ . He derived the extinctions,  $E(B-V)$ , of 23 novae assuming that all of them have the same  $(B-V)_0$  color at the stabilization stage, i.e.,  $E(B-V) = (B-V)_{ss} - (B-V)_0 = (B-V)_{ss} + 0.11$ , where  $(B-V)_{ss}$  is the observed  $B-V$  color at the stabilization stage. This method looks powerful but sometimes results in a large difference from the true value. (We will discuss this in more detail in Section 7.)

According to Hachisu & Kato's (2006) universal decline law, the optical fluxes in the  $UBV$  bands could be dominated by free-free emission. If this is the case, the color is simply estimated to be  $(B-V)_0 = 0.13$  and  $(U-B)_0 = -0.82$  for the optically-thin free-free emission ( $F_\nu \propto \nu^0$ ), or to be  $(B-V)_0 = -0.03$  and  $(U-B)_0 = -0.97$  for the optically-thick free-free emission ( $F_\nu \propto \nu^{2/3}$ ; see, e.g., Wright & Barlow 1975), where  $F_\nu$  is the flux at the frequency  $\nu$ . The latter value of  $(B-V)_0 = -0.03$  is close to  $(B-V)_0 = -0.02 \pm 0.04$  at  $t_2$  derived by van den Bergh & Younger (1987). However, many novae do not remain at these pivot points but evolve

further blueward.

These different trends in nova color evolution may represent different sides of the true color evolution, which we do not yet fully understand observationally or theoretically. The aim of this paper is to find a general path of nova color evolution, as Duerbeck & Seitter (1979) tried to do 30 yr ago. First, in Section 2 we analyze the moderately-fast nova FH Ser in the  $(B-V)_0 - (U-B)_0$  diagram and find a new sequence along which novae evolve when the photospheric emission dominates the optical spectrum. We call this new sequence “the nova-giant sequence” after the supergiant sequence. Then we examine the color evolution of slow and fast novae, PW Vul, V1500 Cyg, V1668 Cyg, and V1974 Cyg, in Section 3. In Section 4, we apply the tracks of color-color evolution to PU Vul and find that the tracks of color-color evolution of the slow/fast novae are common to this symbiotic nova. In Section 5, we examine two very slow novae, HR Del and V723 Cas, and show that the tracks of the color-color evolution are also common. Thus, we found that the overall trends in the color-color evolution are very similar to each other. Therefore, we propose a general course of nova outbursts in the color-color diagram for all speed classes of novae. In Section 6, we redetermine the reddening of novae by fitting the color evolution of a target nova with the general course of color evolution in the color-color diagram. In this way, we propose a new method for estimating the color excess. Discussion and conclusions follow in Sections 7 and 8, respectively. In the Appendix, we estimate the absolute mag-

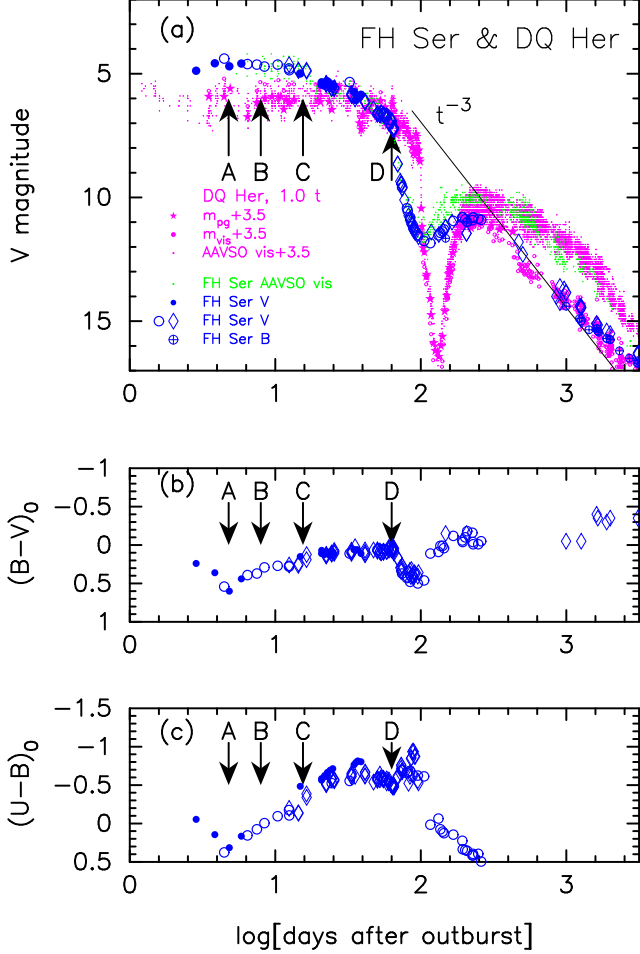


FIG. 2.— (a)  $V$  magnitude, (b)  $(B-V)_0$  color, and (c)  $(U-B)_0$  color light curves of FH Ser. The  $UBV$  data are taken from Borra & Andersen (1970, blue open circles), Osawa (1970, blue filled circles), and Burkhead et al. (1971, blue open diamonds). The  $B-V$  color of Borra & Anderson (blue open circles) is systematically bluer by 0.2 mag than the other data, so we shifted them down by 0.2 mag. Four epochs of FH Ser are specified by arrows labeled A, B, C, and D, where epoch A corresponds to the optical maximum. We add photographic ( $m_{pg}$ ) and visual ( $m_{vis}$ ) data for DQ Her, which are taken from Gaposchkin (1956). The magnitudes of DQ Her is shifted down by 3.5 mag to match them with those of FH Ser in the late  $t^{-3}$  law.

nitudes of about 30 novae, using the time-stretching method for nova light curves proposed by Hachisu & Kato (2010) to analyze the distance-reddening relation of each nova.

## 2. NOVA-GIANT SEQUENCE OF FH SER

The first example that we analyze is the moderately-fast nova FH Ser. FH Ser showed a gradual optical decay with  $t_2 = 41$  and  $t_3 = 62$  days (Warner 1995) followed by a sudden drop in brightness about 2.8 mag below the optical maximum due to dust shell formation. The  $V$  light curve is shown in Figure 1 on a linear timescale and the  $V$ ,  $(B-V)_0$ , and  $(U-B)_0$  light curves of FH Ser are shown in Figure 2 on a logarithmic timescale, where the  $UBV$  data are taken from Osawa (1970, blue filled circles), Borra & Andersen (1970, blue open circles), and Burkhead et al. (1971, blue open diamonds). The  $B-V$  color of Borra & Andersen (1970) is systematically  $\sim 0.2$  mag bluer than the others whereas their  $V$  and  $U-B$  data are reasonably consistent with those of the other groups. Therefore, we shifted Borra & Andersen's  $B-V$  data down by 0.2 mag.

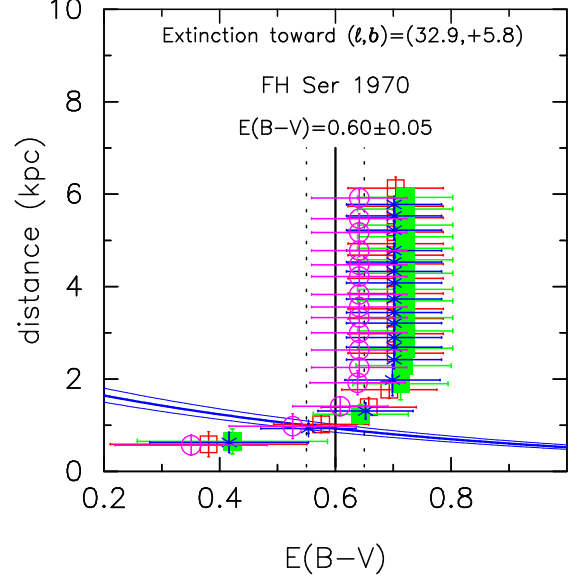


FIG. 3.— Distance-reddening relation toward FH Ser. Blue thick solid line with flanking thin solid lines denote the distance-reddening relation calculated from the distance modulus  $(m-M)_V = 11.7 \pm 0.2$ , i.e., Equation (1) together with Equation(2). Four sets of data with error bars show distance-reddening relations in four directions close to FH Ser:  $(l, b) = (32^\circ 75, 5^\circ 75)$  (red open squares),  $(33^\circ 00, 5^\circ 75)$  (green filled squares),  $(32^\circ 75, 6^\circ 00)$  (blue asterisks), and  $(33^\circ 00, 6^\circ 00)$  (magenta open circles); data are taken from Marshall et al. (2006). Vertical black solid line with flanking dotted lines represent the color excess of  $E(B-V) = 0.60 \pm 0.05$ . Two trends,  $(m-M)_V = 11.7$  (blue solid line) and Marshall et al.'s distance-reddening relations, cross consistently at  $E(B-V) \approx 0.60$  and  $d \approx 0.93$  kpc, which supports our estimate of  $E(B-V) = 0.60 \pm 0.05$ .

### 2.1. Reddening and Distance

Kodaira (1970) obtained a value of  $E(B-V) = 0.6$  for the reddening toward FH Ser using the MMRD relation and interstellar reddening relation. della Valle et al. (1997) obtained  $E(B-V) = 0.82$  from the color at optical maximum (i.e.,  $E(B-V) = (B-V)_{\max} - (B-V)_{0,\max} = 1.05 - 0.23 = 0.82$ ),  $E(B-V) = 0.61$  from the line ratio of  $H\alpha/H\beta = 5.7$ , and  $E(B-V) = 0.5$  from the equivalent width of Na I  $\lambda 5890$ . Then, della Valle et al. (1997) adopted an averaged value of  $E(B-V) = 0.64 \pm 0.16$ . Because Kodaira's  $E(B-V) = 0.60$  and della Valle et al.'s  $E(B-V) = 0.61$  coincide, we use  $E(B-V) = 0.60$  in this paper and confirm below that this value is reasonable.

The distance toward FH Ser was estimated to be  $d = 0.92 \pm 0.13$  kpc by Slavin et al. (1995), and to be  $d = 0.95 \pm 0.05$  kpc by Gilmozzi & Selvelli (2007) both from the expansion parallax method. We obtained FH Ser's distance modulus by comparing its brightness with that of DQ Her. The trigonometric parallax distance of DQ Her was obtained by Harrison et al. (2013) as  $d = 386^{+33}_{-29}$  pc. Adopting  $A_V = 3.1 \times E(B-V) = 0.31$  (Verbunt 1987), we obtain the distance modulus of DQ Her as  $(m-M)_V = A_V + 5 \log(d/10 \text{ pc}) = 0.31 + 5 \log(386^{+33}_{-29}/10) = 8.24 \pm 0.18$ . Thus, we used  $(m-M)_{V,DQ \text{ Her}} = 8.2$  for DQ Her. Figure 2(a) shows that the light curves of FH Ser and DQ Her overlap each other in the final decline phase with a brightness difference of  $\Delta V = 3.5$ . Because the timescales of these two novae are almost the same, we may consider that the brightness itself should be almost the same. Then, we obtain the distance modulus of FH Ser as

$$(m-M)_{V,FH \text{ Ser}} = (m-M)_{V,DQ \text{ Her}} + \Delta V = 8.2 \pm 0.2 + 3.5 = 11.7 \pm 0.2. \quad (1)$$

TABLE 1  
INTRINSIC TWO COLORS OF SELECTED  
NOVAE

Object	Stage	$(B-V)_0$	$(U-B)_0$
Free-Free	0 <sup>a</sup>	+0.13	-0.82
	F <sup>b</sup>	-0.03	-0.97
FH Ser	A	+0.60	+0.32
	B	+0.31	+0.10
	C	+0.15	-0.29
	D	+0.04	-0.70
PU Vul	F	-0.03	-0.97
	1	+0.15	-0.34
	B	+0.31	+0.10
	2	+0.45	+0.21
	B	+0.31	+0.10
	3(=C)	+0.15	-0.29
	4	+0.14	-0.91
	5	-0.20	-0.91
PW Vul	D	+0.04	-0.70
	C	+0.15	-0.29
	4	+0.14	-0.91
	4'	-0.08	-1.10
	5'	-0.60	-0.70
V1500 Cyg	D	+0.04	-0.70
	C	+0.15	-0.29
	4'	-0.08	-1.10
	5'	-0.60	-0.70
V1668 Cyg	D	+0.04	-0.70
	C	+0.15	-0.29
	4''	-0.05	-0.91
	5''	-0.50	-0.91
V1974 Cyg	D	+0.04	-0.70
	4''	-0.05	-0.91
	5''	-0.50	-0.91

<sup>a</sup> Optically-thin ( $F_\nu \propto \nu^0$ ).

<sup>b</sup> Optically-thick ( $F_\nu \propto \nu^{2/3}$ ).

The distance to FH Ser is estimated to be  $d = 0.93$  kpc considering  $E(B-V) = 0.60$  and the relation

$$(m-M)_V = 5 \log \left( \frac{d}{10 \text{ pc}} \right) + 3.1E(B-V). \quad (2)$$

Our distance estimate is perfectly consistent with the other values of  $d = 0.92 \pm 0.13$  (Slavin et al. 1995) and  $d = 0.95 \pm 0.05$  kpc (Gilmozzi & Selvelli 2007) mentioned above.

Marshall et al. (2006) recently published a three-dimensional dust extinction map of our galaxy in the direction of  $-100.0^\circ \leq l \leq 100.0^\circ$  and  $-10.0^\circ \leq b \leq +10.0^\circ$  with grids of  $\Delta l = 0.25^\circ$  and  $\Delta b = 0.25^\circ$ , where  $(l, b)$  are the galactic coordinates. Comparing the set of our  $E(B-V) = 0.60$  and  $d = 0.93$  kpc with the distance-reddening relation toward FH Ser given by Marshall et al. (2006), we can examine whether they are reasonable. The results are shown in Figure 3, where the galactic coordinates of FH Ser are  $(l, b) = (32.9090, +5.7860)$  and we plot four relations in directions close to FH Ser, i.e.,  $(l, b) = (32.75, 5.75)$  (red open squares),  $(33.00, 5.75)$  (green filled squares),  $(32.75, 6.00)$  (blue asterisks), and  $(33.00, 6.00)$  (magenta open circles), with error bars. The closest one is that of the green filled squares. The blue solid line of  $(m-M)_{V, \text{FH Ser}} = 11.7$  crosses the trend of these green filled squares at or near  $d = 0.93$  kpc and  $E(B-V) = 0.60$ , which is consistent with our adopted values.

## 2.2. Nova-giant Sequence in the Color-Color Diagram

The observed colors are dereddened by

$$(U-B)_0 = (U-B) - 0.64E(B-V), \quad (3)$$

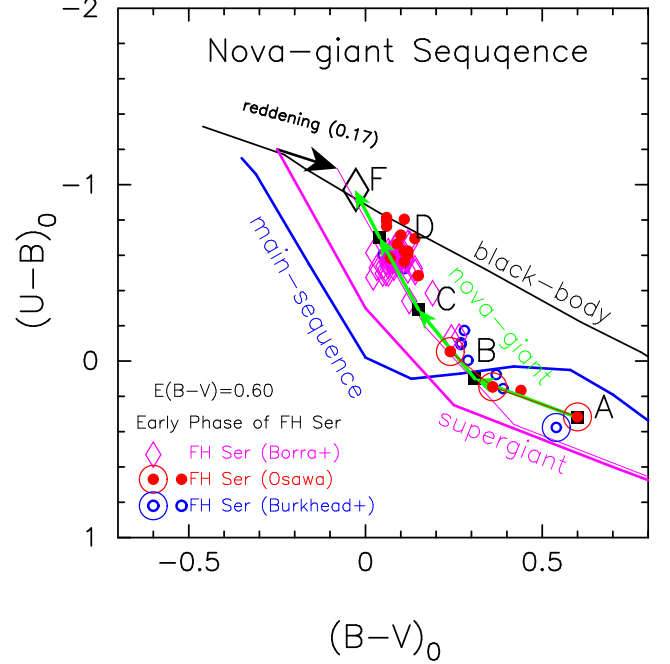


FIG. 4.— Dereddened color-color diagram of FH Ser and the nova-giant sequence. We show four evolutionary stages of FH Ser specified by A, B, C, and D in Figure 2. Each label is attached to a filled black square. Open diamond denoted by F indicates landmark for optically-thick free-free emission spectra. We define the nova-giant sequence by a line connecting points A, B, C, D, and F (green connecting arrows). Their color data are tabulated in Table 1. Three other loci are also plotted for the main-sequence (blue solid line), supergiant (magenta solid line), and blackbody (black solid line) sequences. The color data of FH Ser are taken from Osawa (1970) (red filled circles), Borra & Andersen (1970) (magenta open diamonds), and Burkhead et al. (1971) (blue open circles). Four symbols with a large open circle outside indicate data in pre-maximum phase. All other symbols represent data in post-maximum phase. Magenta thin solid line represents supergiant sequence shifted by 0.17 mag in the reddening direction, as shown at the top of the supergiant sequence by a black arrow. Most part of the nova-giant sequence overlaps the supergiant sequence shifted by  $\Delta E(B-V) = 0.17$  (thin magenta line) except the lower part (from point A to B) which is about  $\Delta(U-B) \approx -0.2$  mag bluer than the supergiant sequence.

$$(B-V)_0 = (B-V) - E(B-V), \quad (4)$$

where the factor of 0.64 is taken from Rieke & Lebofsky (1985). The dereddened colors of FH Ser are plotted in Figure 4. Here we only depict the data before the dust black-out started about 70 days after the outburst. We also plot three known sequences, the blackbody, supergiant, and main-sequence sequences, the data for which are taken from Allen (1973). We also added a point, i.e., optically-thick free-free emission spectra (open diamond denoted by F) for  $F_\nu \propto \nu^{2/3}$  (Wright & Barlow 1975).

We have frequently seen in the literature statements that the spectra of novae near maximum are similar to those of A–F type supergiants. For FH Ser, Kodaira (1970) wrote “Nova Serpentis 1970 showed a spectrum similar to F-type near its light maximum.” However, the track of FH Ser in the color-color diagram does not follow the supergiant sequence, as clearly shown in Figure 4. The shape of the FH Ser track is very similar to that of the supergiant sequence, but it is about  $\Delta(U-B) \approx -0.2$  mag bluer than the supergiant sequence. Therefore, we are forced to define a new sequence based on the data for FH Ser, which is designated by points A, B, C, D, and F from redder to bluer. In what follows, we will see that many novae evolve along this sequence when their photospheric spectra are similar to those of A–F type supergiants.



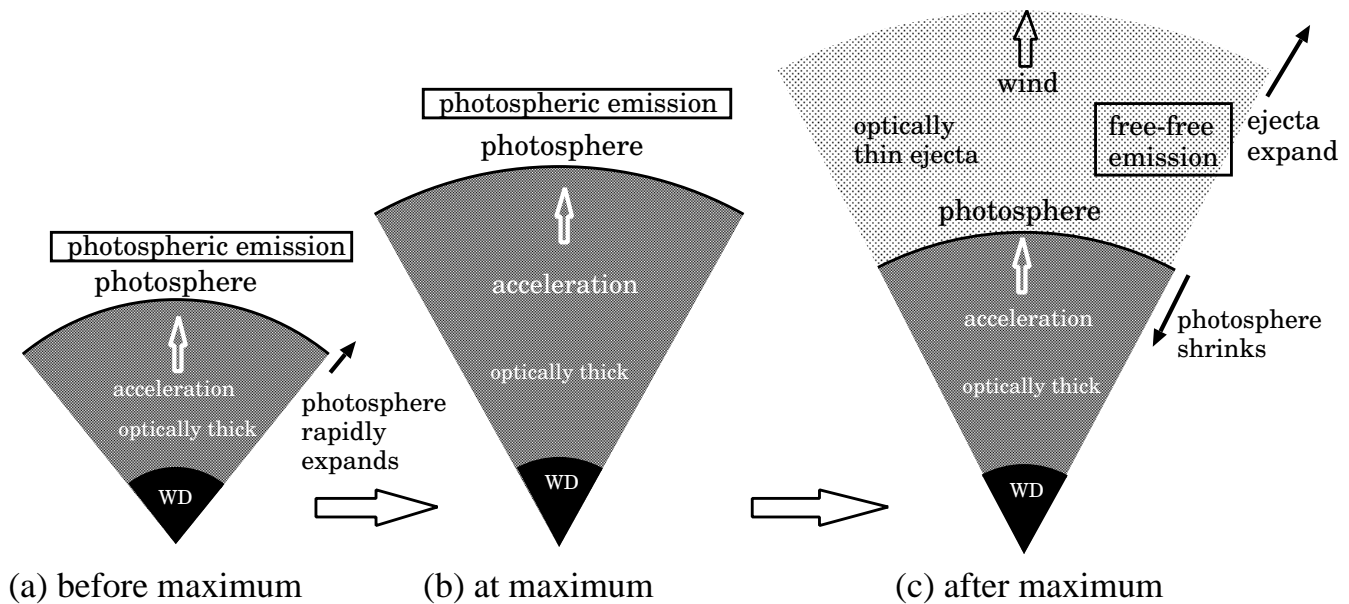


FIG. 5.— Schematic illustration of nova envelope evolution for fast and moderately fast novae. (a) Surface of expanding envelope moves almost together with optical photosphere (so-called fireball stage). (b) Photosphere reaches maximum expansion and then gradually shrinks, while ejecta are continuously expanding. At or near optical maximum, the absorption spectra resemble those of F-supergiants. (c) After optical maximum, massive, optically-thin ejecta expand, leaving pseudo-photosphere behind. More ejecta are continuously supplied by optically-thick winds. We regard this phase as an optically-thick, free-free emission phase. The spectral energy distribution (SED) is close to  $F_\nu \propto \nu^{2/3}$  in the optical (including the *UBV* bands), IR, and radio regions. Here we use the term “optically-thick wind” to describe winds that are accelerated deep inside the photosphere. On the other hand, the term “optically-thin wind” indicates winds that are accelerated outside the photosphere.

Therefore, we call this track “the nova-giant sequence” after the supergiant sequence. The color data of points A–D and F are listed in Table 1.

In the pre-maximum phase, FH Ser descends along the nova-giant sequence as shown in Figure 4 by the symbols enclosed within a larger open circle. After optical maximum, it returns along the same nova-giant sequence.

Gehrz et al. (1988) divided physical development of nova ejecta into a few distinct stages, i.e., fireball expansion, optically-thin gas expansion, and dust formation. Figure 5 illustrates the expanding nova ejecta before dust formation occurs. Figure 5(a) shows the so-called fireball stage, in which the optical photosphere moves almost together with the surface of the expanding envelope. We directly observe the photospheric emission. This photospheric emission resembles those of A–F type supergiants. In Figure 5(b), the photosphere reaches maximum expansion and detaches from the top of the ejecta. Then the photosphere recedes into progressively deeper layers while the ejecta expand continuously. Figure 5(c) corresponds to the stage after optical maximum, in which massive, optically-thin ejecta expand leaving the photosphere behind. More ejecta are continuously supplied by optically-thick winds. Here we use the term “optically-thick wind” to describe winds that are accelerated deep inside the photosphere, that is, in the optically-thick region. On the other hand, “optically-thin wind” indicates winds that are accelerated outside the photosphere, that is, in the optically-thin region.

We will show later that all novae follow the nova-giant sequence near the maximum, regardless of their speed classes and, further, that faster novae tend to have shorter excursions along the nova-giant sequence mainly because their envelopes are less massive. Slower novae tend to have longer redward journeys because of their more massive envelope masses. Among our examples, FH Ser reached the reddest part of the nova-giant sequence, up to point A in Figure 4.

Novae return along the nova-giant sequence after optical maximum and approach point F, where free-free emission dominates the spectrum, as shown schematically in Figure 5(c). In FH Ser, however, the color-color track was strongly affected by the dust blackout at point D just before it approached point F (see Figure 2).

The nova-giant sequence is about  $\Delta(U - B) \approx -0.2$  mag bluer than the supergiant sequence. This is because nova spectra resemble those of A–F supergiants near maximum regardless of the nova speed classes and we directly observe the photospheric emission of novae. However, the envelope masses of novae are much ( $\sim 10^{-4}$ ) smaller than those of normal supergiants. Thus, the Balmer jump could be shallower ( $U$  could be brighter) in novae than in normal supergiants, as shown in Section 4. This is why the position of nova-giant sequence is parallel to but  $\Delta(U - B) \approx -0.2$  mag bluer than the supergiant sequence, although nova spectra resemble those of A–F supergiants.

It may seem that the nova-giant sequence is simply the supergiant sequence and it falsely appears to differ because we happened to underestimate the extinction by an amount of  $\Delta E(B - V) \sim 0.2$ . We shifted the supergiant sequence by  $\Delta E(B - V) = 0.17$  in the direction of reddening in Figure 4 (thin magenta solid line). The bluer part of the shifted track almost coincides with the bluer part of the nova-giant sequence, but the very reddest part of the nova-giant sequence deviates from that of the shifted supergiant sequence. Therefore, these two sequences are intrinsically different. This  $\Delta(U - B) \sim -0.2$  mag difference in the redder part was already discussed by Belyakina et al. (1989) for PU Vul, as will be introduced in Section 4.1.

### 3. FREE-FREE EMISSION PHASE OF SLOW AND FAST NOVAE

In this section, we carefully study the color-color evolution of four well-observed classical novae, PW Vul, V1500 Cyg, V1668 Cyg, and V1974 Cyg, all of which show the optically-

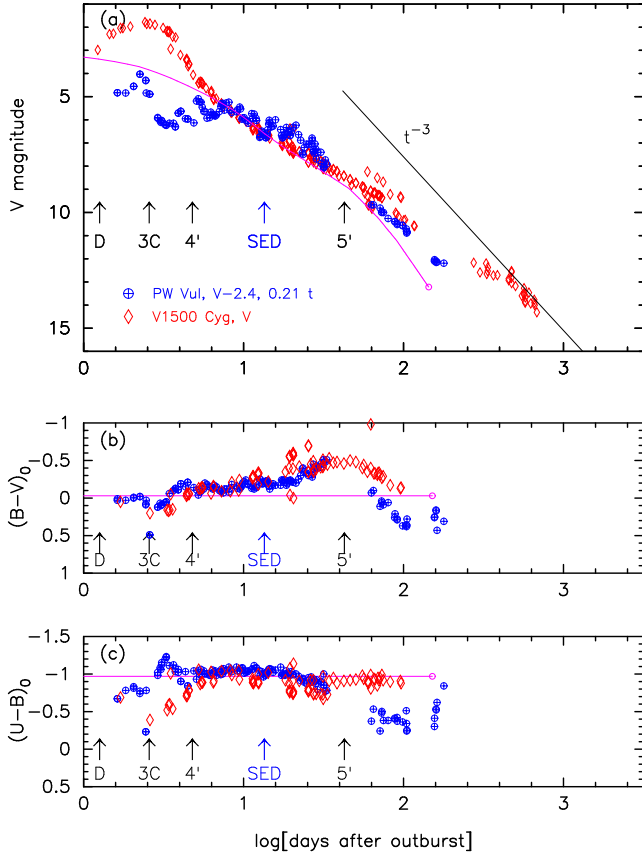


FIG. 6.— Same as Figure 2, but for PW Vul (blue open circles with plus sign inside) and V1500 Cyg (red open diamonds). We squeezed the light curves of PW Vul by 0.21 in the time direction (horizontal shift of  $\Delta \log t = -0.68$ ) and shifted its magnitudes by  $-2.4$  against those of V1500 Cyg, as indicated in the figure. We adjusted the time at  $V$  maximum of PW Vul according to that of V1500 Cyg. Magenta solid lines denote optical and color light curves of free-free emission. Several epochs are specified by labels D, C ( $=3$ ), 4', and 5' which are defined in Figures 4 and 8. Their positions in the color-color diagram are tabulated in Table 1. We also indicate the epoch of PW Vul 64 days after the outburst by “SED”, at which the spectrum of Figure 9 was secured.

thick, free-free emission dominated phase. Their  $V$ ,  $(B-V)_0$ , and  $(U-B)_0$  light curves are plotted in Figures 6 and 7 on a logarithmic timescale.

### 3.1. PW Vul

PW Vul 1984#1 was discovered by Wakuda on UT 1984 July 27.7 (Kosai 1984), about a week before the optical maximum of  $m_{V,\max} = 6.3$  on UT August 4.1. It shows a wavy structure on a smoothly-decaying light curve with  $t_2 = 83$  and  $t_3 = 147$  days (Warner 1995). Because no estimate of the outburst day was found, we assume it to be JD 2445908.0 (UT 1984 July 26.5). The light curve of PW Vul is plotted in Figure 1 on a linear timescale and in Figure 6 on a logarithmic timescale. PW Vul was observed well with *International Ultraviolet Explorer* (IUE) during the UV bright phase (e.g., Andrae et al. 1991) and also covered well by IR observation (e.g., Evans et al. 1990; Gehrz et al. 1988).

The reddening toward PW Vul was estimated to be  $E(B-V) = 0.58 \pm 0.06$  from the He II  $\lambda 1640/\lambda 4686$  ratio, and  $E(B-V) = 0.55 \pm 0.1$  from the interstellar absorption feature at  $2200\text{\AA}$  both by Andrae et al. (1991),  $E(B-V) = 0.60 \pm 0.06$  according to Saizar et al. (1991) from the He II  $\lambda 1640/\lambda 4686$  ratio,  $E(B-V) = 0.45 \pm 0.1$  according to Duerbeck et al. (1984) from the galactic extinction in the direction of the

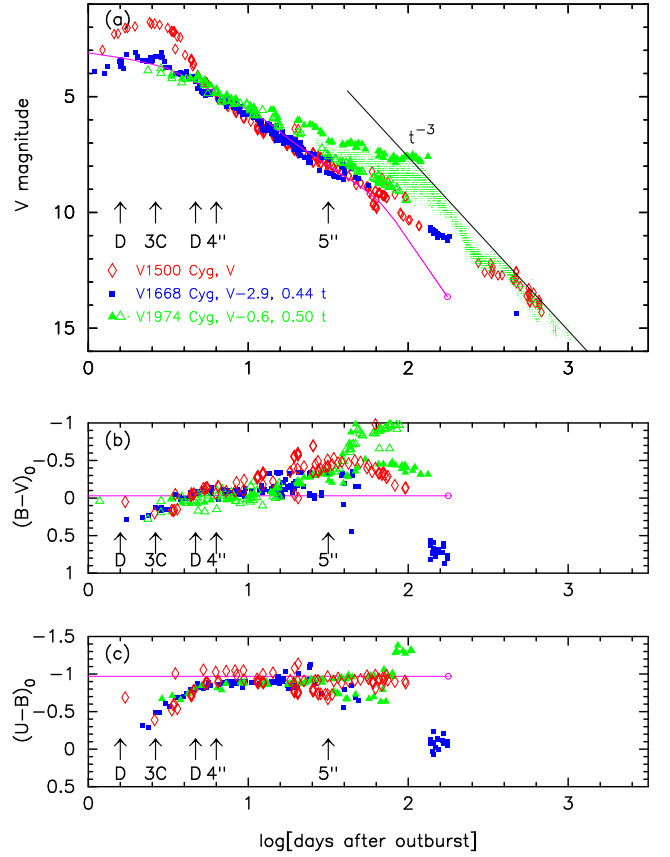


FIG. 7.— Same as Figure 6, but for V1668 Cyg (blue filled squares), V1974 Cyg (green triangles and dots), and V1500 Cyg (red open diamonds). We squeezed the light curves of V1668 Cyg and V1974 Cyg by 0.54 and 0.63 and shifted their magnitudes by  $-2.6$  and  $-0.4$ , respectively, against those of V1500 Cyg, as indicated in the figure. We adjusted the time at  $V$  maximum of V1668 Cyg and V1974 Cyg according to that of V1500 Cyg. Several epochs are specified by labels D, C ( $=3$ ), D, 4'', and 5'', which are defined in Figures 4 and 8. Their positions in the color-color diagram are tabulated in Table 1.

nova. For the last galactic absorption, we examined the galactic dust absorption map in the NASA/IPAC Infrared Science Archive<sup>1</sup>, which is calculated on the basis of recent data from Schlafly & Finkbeiner (2011) and gives  $E(B-V) = 0.43 \pm 0.02$  in the direction of PW Vul. Thus, we adopted the arithmetic mean of these four values, i.e.,  $E(B-V) = 0.55 \pm 0.1$ , in this paper.

The distance toward PW Vul was estimated to be  $d = 1.8 \pm 0.05$  kpc by Downes & Duerbeck (2000) on the basis of the expansion parallax method. Then the distance modulus in  $V$  becomes  $(m-M)_V = 5 \log(1800/10) + 3.1 \times 0.55 = 13.0$ . The maximum magnitude is calculated to be  $M_{V,\max} = m_{V,\max} - (m-M)_V = 6.3 - 13.0 = -6.7$ .

Figure 8(a) shows the intrinsic color-color diagram of PW Vul, where the  $UBV$  data of Robb & Scarfe (1995) are dereddened with  $E(B-V) = 0.55$  together with Equations (3) and (4). The nova started its color-color evolution at point D (near point F) on the nova-giant sequence and descended to near point C (or point 3), then jumped up to point 4. The nova further went up slightly and then moved downward and to the left. Then, PW Vul stayed at point 4' for a while, as shown in Figure 6 and moved gradually to point 5'. Here points 1, 2, 3, 4, and 5 will be introduced in Section 4 as a template of the symbiotic nova PU Vul (“PU Vul template”), the data for

<sup>1</sup> <http://irsa.ipac.caltech.edu/applications/DUST/>

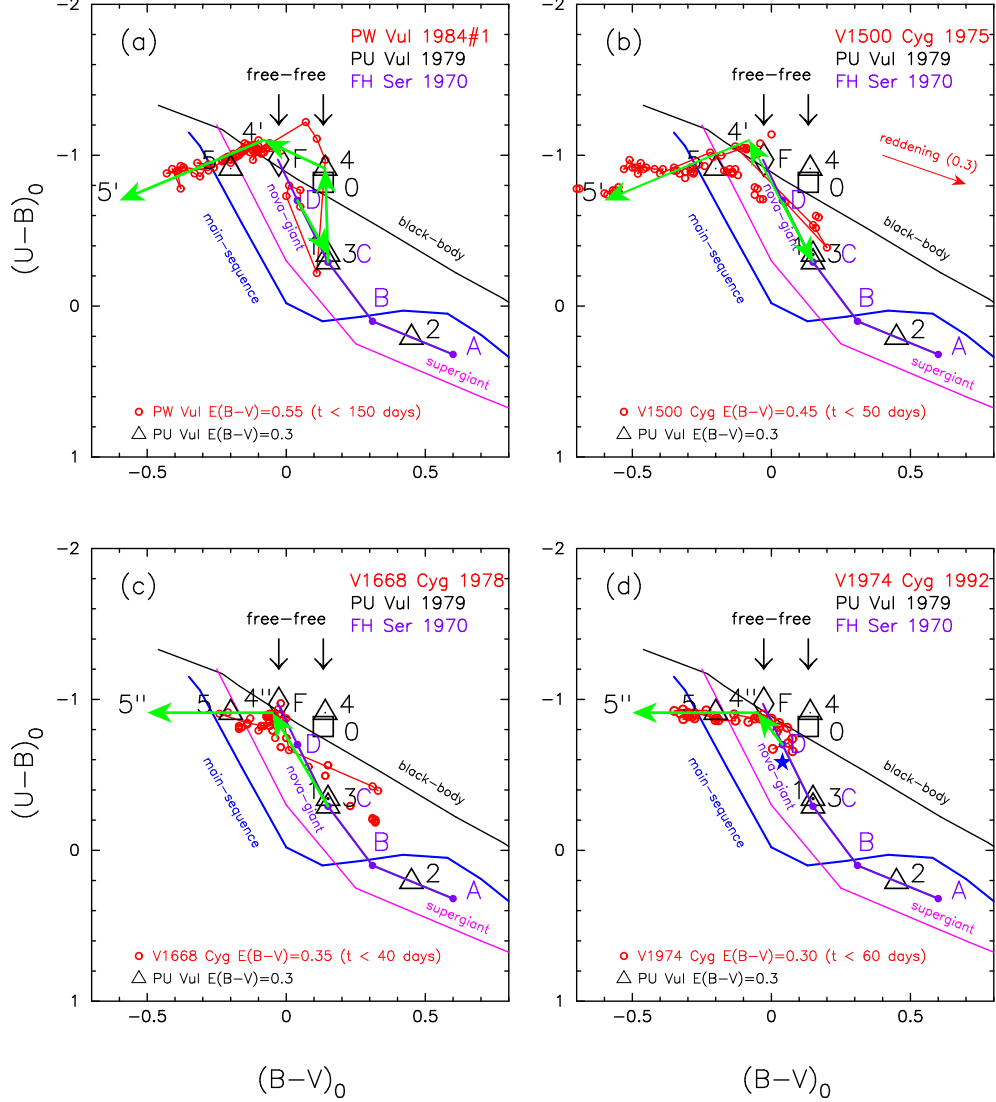


FIG. 8.— Color-color evolution of four classical novae in the intrinsic  $(B-V)_0$  vs.  $(U-B)_0$  diagram. (a) PW Vul 1984#1, (b) V1500 Cyg 1975, (c) V1668 Cyg 1978, and (d) V1974 Cyg 1992. Color data for each nova are denoted by red open circles. Purple solid line indicates the nova-giant sequence of FH Ser, and green arrows indicate the path of each nova. Blue filled star symbol in (d) denotes a datum in the pre-maximum phase of V1974 Cyg. Other various symbols and lines have the same meanings as in Figure 4. We add 10 points, 0, 1, 2, 3, 4, 5, 4', 5', 4'', and 5'', and their data are listed in Table 1. See text for more details.

which are tabulated in Table 1. We specify a template for the color-color evolution of PW Vul by a green arrow from point D to point C (=3) and then by three green arrows from point 3 to point 4, from point 4 to point 4', and from point 4' to point 5' (“PW Vul template”). The data for the PW Vul template are also tabulated in Table 1.

### 3.2. Free-Free Emission Phase

In this way, the evolutionary path of PW Vul first follows the nova-giant sequence from point D to point C. Then it departs from the nova-giant sequence and jumps up to points 4, and 4', and then to point 5' in the color-color diagram. This jump to point 4' is mainly due to free-free emission.

We can interpret this transition from point C to 4' as follows: in the early expanding phase, from point D to C, we observed the photospheric emission (A–F type supergiants), as schematically illustrated in Figures 5(a) and (b). The nova-giant sequence is much redder than that of the blackbody sequence in the  $(U-B)_0$  color because of a large contribution from the Balmer jump. When the photosphere shrinks leav-

ing the ejecta behind, or winds begin to blow, the configuration of the envelope changes from that in Figure 5(b) to that in Figure 5(c). Then the Balmer jump absorption becomes shallower and is eventually filled with emission lines. The resultant  $(U-B)_0$  color becomes bluer to approach that of a black-body (or free-free emission). This type of spectral change was well documented by Belyakina et al. (1989) for PU Vul (see their Figure 6), which will be mentioned later in Section 4.1.

To understand this property, we analyze the spectral energy distribution (SED) of PW Vul 64 days after the outburst, that is, when PW Vul stayed between point 4' and point 5', as shown in Figure 6 (denoted by “SED”). We assume that the spectrum is approximated by a summation of the black-body emission at the photospheric temperature  $T_{\text{ph}} = T_{\text{BB}}$  and optically-thick free-free emission at the electron temperature of  $T_e$ , i.e.,

$$F_\nu = f_1 B_\nu(T_{\text{ph}}) + f_2 S_\nu(T_e), \quad (5)$$

where  $B_\nu(T_{\text{ph}})$  is the Planckian at  $T_{\text{ph}}$ , and  $S_\nu(T_e)$  is the free-free spectrum at  $T_e$ , and  $f_1$  and  $f_2$  are numeric constants (e.g., Nishimaki et al. 2008). Nishimaki et al. adopted this formu-

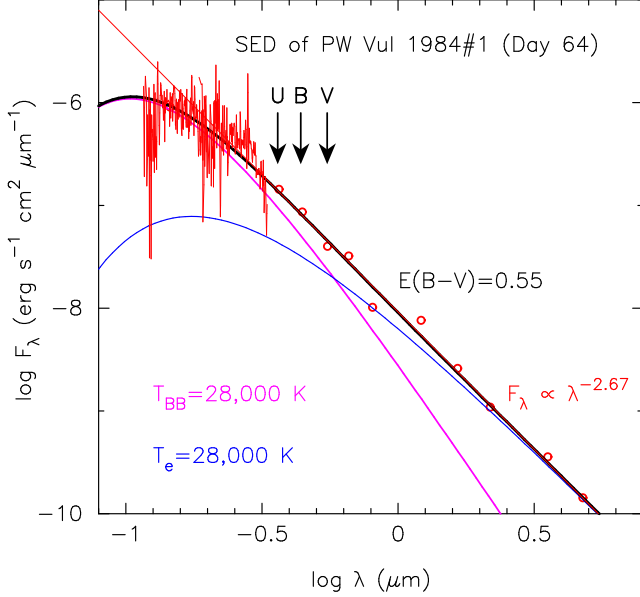


FIG. 9.— Dereddened spectrum of PW Vul 1984#1 64 days after the outburst (September 30). Red solid line: *IUE* spectra, SWP24088 and LWP04458, are taken from the INES data archive server. Open red circles: *UBVRI* data from Robb & Scarfe (1995) and *JHKLM* data from Gehrz et al. (1988). All data are dereddened with  $E(B-V) = 0.55$ . Global features of spectrum can be fitted with combination (thick black solid line) of blackbody with temperature of  $T_{BB} = 28,000$  K (thick magenta line) and optically-thick, free-free emission with electron temperature of  $T_e = 28,000$  K (thick blue line). We also add a red thin solid straight line of  $F_\lambda \propto \lambda^{-2.67}$  (corresponding to point F in Figure 8) as the limiting case of optically-thick free-free emission for  $T_e = \infty$ .

lation to analyze the spectra of Wolf-Rayet (WR) stars. The optically-thick free-free spectrum of  $S_\nu(T_e)$  was obtained by Wright & Barlow (1975) as

$$S_\nu(T_e) = B_\nu(T_e) K_\nu^{2/3}(T_e), \quad (6)$$

where the linear free-free absorption coefficient  $K_\nu(T_e)$  is given by

$$K_\nu(T_e) = 3.7 \times 10^8 \left[ 1 - \exp\left(-\frac{h\nu}{kT_e}\right) \right] Z^2 g_\nu(T_e) T_e^{-1/2} \nu^{-3}, \quad (7)$$

in cgs units (Wright & Barlow 1975), and  $g_\nu(T_e)$  is the Gaunt factor. The Gaunt factor generally depends weakly on the frequency and temperature, and we simply assume that it is unity in this paper. Thus, we have four fitting parameters in this expression, i.e.,  $f_1$ ,  $f_2$ ,  $T_{ph}$ , and  $T_e$ . In the radio and IR regions of the spectrum where  $h\nu \ll kT$ , Equation (6) can be expressed in a simple form as

$$S_\nu \propto \nu^{2/3}. \quad (8)$$

Figure 9 shows the broadband spectrum of PW Vul, a combination of *IUE* spectra from Short Wavelength Prime (SWP)24088 and Long Wavelength Prime (LWP)04458 taken from the INES archive data server<sup>2</sup>, and the *UBVRI* data from Robb & Scarfe (1995) and the *JHKLM* data from Gehrz et al. (1988). All the data were dereddened with  $E(B-V) = 0.55$ . Assuming that  $T_{ph} = T_e$ , we varied  $T_{ph}$  in 500 K steps and obtained a temperature of  $T_{ph} = T_e = 28,000$  K. The global features of the SED is approximated well by a combination (black solid line) of the blackbody (thick magenta line) and free-free emission (thick blue line) spectra. The slope of

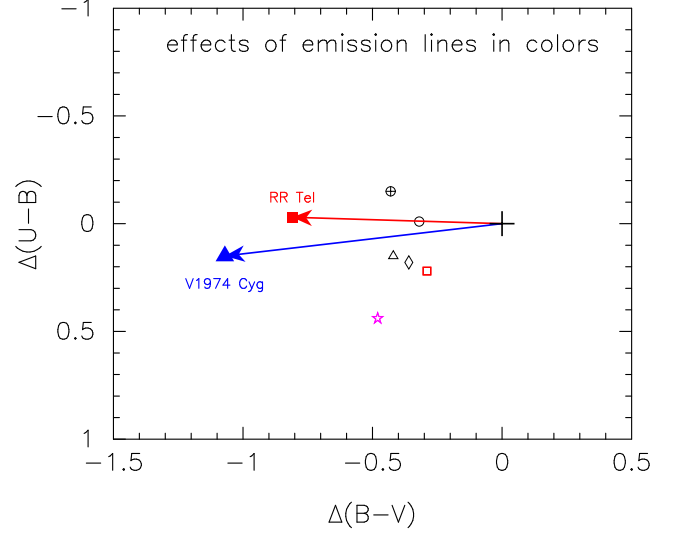


FIG. 10.— Effects of emission lines in the color-color diagram for seven stars. Here,  $\Delta(B-V)$  and  $\Delta(U-B)$  are the excesses due to emission lines. Compiling the data in Skopal (2007), we plot AG Peg (red open square), Z And (open diamond), AR Pav (open triangle), AX Per in eclipse (open circle), AX Per out of eclipse (open circle with a plus sign), RR Tel (red filled square), V1016 Cyg (magenta open star symbol), and V1974 Cyg (blue filled triangle). RR Tel and V1974 Cyg show large and almost horizontal blueward excursions from the origin (black plus sign) because of the effects of emission lines. See text for more details.

the combined spectrum at the *UBV* bands is very close to that of optically-thick free-free emission ( $F_\lambda \propto \lambda^{-8/3} \approx \lambda^{-2.67}$ ), where  $F_\lambda$  is the energy flux at the wavelength  $\lambda$ . This explains why the position of stage 4' is close to both the blackbody sequence and optically-thick free-free emission, i.e., point F in Figure 8(a).

PW Vul stayed at point 4' (near point F) for a while during the free-free emission phase, and moved gradually from point 4' to point 5', as shown in Figures 6 and 8(a). In the color-color diagrams of Figure 8, the other three novae also do not stay only at or near point F but evolve blueward from point 4' to 5' (or 4'' to 5'') while maintaining an almost constant  $(U-B)_0$ . From point 4' to 5', optically-thick free-free emission dominates the spectrum in the optical and IR region, as shown in Figure 9. Then, the optical light curve almost follows the universal decline law (Hachisu & Kato 2006) and its  $(B-V)_0$  and  $(U-B)_0$  colors should be  $-0.03$  and  $-0.97$ , respectively. We added a free-free emission light curve and  $(B-V)_0$  and  $(U-B)_0$  colors in Figure 6 (magenta solid lines). These light and color curves roughly reproduce the trends of the observed data except for the gradual deviation of the  $(B-V)_0$  color after point 4' (or 4''). This supports the fact that free-free emission dominates the spectrum during the phase between 4' and 5' (or 4'' and 5'').

### 3.3. Effects of Strong Emission Lines

Figure 10 shows the excesses of  $B-V$  and  $U-B$  colors due to emission lines for several classical and symbiotic novae and symbiotic stars. Here, the excesses due to emission lines in the  $U$ ,  $B$ , and  $V$  magnitudes are defined as  $\Delta U$ ,  $\Delta B$ , and  $\Delta V$ , respectively, and the data for them are taken from Skopal (2007). In the classical nova V1974 Cyg (blue filled triangle) and symbiotic nova RR Tel (red filled square),  $\Delta U$  and  $\Delta B$  are much brighter than  $\Delta V$ , but  $\Delta U$  is as large as  $\Delta B$ , so the resultant  $\Delta(U-B)$  color changes very little even if  $\Delta(B-V)$  takes a long blueward journey. Unfortunately, PW Vul is not included in Skopal's analysis. Instead, we show the blueward

<sup>2</sup> <http://sdc.cab.inta-csic.es/ines/index2.html>

excursions of the fast nova V1974 Cyg about 210 days after light maximum. The length of the blueward excursion is significant; i.e.,  $\Delta(B-V) \approx -1.1$ . Thus, we conclude that the gradual blueward trip from point 4' to 5' (or from point 4'' to 5'') is mainly due to the growth of strong emission lines, especially in the  $U$  and  $B$  bands.

In this work, we stop following the color evolution when the  $V$  magnitude drops by 3 mag from the maximum because strong emission lines make an increasingly large contribution to the  $(U-B)_0$  and  $(B-V)_0$  colors, and their effects cloud the general evolution of colors.

### 3.4. V1500 Cyg

V1500 Cyg is an extremely fast nova, exhibiting probably the fastest and largest eruption among novae. The light curve is shown in Figure 1 on a linear timescale and the  $V$  light curve and  $(B-V)_0$  and  $(U-B)_0$  color curves are plotted in Figures 6 and 7 on a logarithmic timescale. It rose to the maximum,  $m_V = 1.85$ , on 1975 August 31 from a pre-outburst brightness of  $m_V > 21$  (Young et al. 1976). The distance of  $1.2 \pm 0.2$  kpc (Lance et al. 1988) and interstellar extinction of  $E(B-V) = 0.5 \pm 0.05$  (Ferland 1977) suggest a peak absolute luminosity of  $M_V = -10.0 \pm 0.3$ , which is about 4 mag brighter than the Eddington luminosity. An extensive summary of the observational results and modelings can be found in the review by Ferland et al. (1986).

Gallagher & Ney (1976) obtained the magnitudes of the three optical bands ( $V$ ,  $R$ , and  $I$ ) and the eight IR bands (1.2, 1.6, 2.2, 3.6, 4.8, 8.5, 10.6, and 12.5  $\mu\text{m}$ ) during the 50 days following the discovery. They estimated the outburst day to be UT August 28.9 from the angular expansion of the photosphere. They concluded that the SED was approximately that of a blackbody during the first 3 days, whereas it is close to  $F_\nu = \text{constant}$  after the 4th day. These  $F_\nu \propto \nu^0$  (constant) spectra resemble those usually ascribed to optically-thin, free-free emission.

On the basis of the IR photometry from 1 to 20  $\mu\text{m}$ , Ennis et al. (1977) also concluded that the nova's spectrum changed from blackbody to bremsstrahlung emission at day  $\sim 4-5$ , that is, from Rayleigh-Jeans,  $F_\nu \propto \nu^2$ , to thermal bremsstrahlung,  $F_\nu \propto \nu^0$ . Thus we regard that the nova enters a free-free emission phase about 5 days after the outburst. They also obtained an outburst date of JD 2442653.0  $\pm$  0.5 from an analysis of the photospheric expansion similar to that of Gallagher & Ney (1976). Thus, we adopted the outburst day of V1500 Cyg as  $t_{\text{OB}} = \text{JD } 2442653.0$  (defined as  $t = 0$ ).

The distance to V1500 Cyg has been discussed by many authors. Young et al. (1976) estimated the distance to be  $1.4 \pm 0.1$  kpc for  $E(B-V) = 0.45$  (Tomkin et al. 1976) from the reddening-distance law toward the nova. A firm upper limit to the apparent distance modulus was obtained as  $(m-M)_V \leq 12.5$  by Ando & Yamashita (1976) from the galactic rotational velocities of interstellar H and K absorption lines. The nebular expansion parallax method is a different way to estimate the distance. Becker & Duerbeck (1980) first imaged an expanding nebula ( $0''.25 \text{ yr}^{-1}$ ) of V1500 Cyg and estimated a distance of 1350 pc assuming the expansion velocity of  $v_{\text{exp}} = 1600 \text{ km s}^{-1}$ . However, Wade et al. (1991) resolved an expanding nebula and obtained a much lower expansion rate of  $0''.16 \text{ yr}^{-1}$ ; they estimated the distance to be 1.56 kpc, with a much smaller expansion velocity of  $v_{\text{exp}} = 1180 \text{ km s}^{-1}$  observed by Cohen (1985). Slavin et al. (1995) obtained a similar expanding angular velocity of the

nebula ( $0''.16 \text{ yr}^{-1}$ ) and obtained a distance of 1550 pc assuming  $v_{\text{exp}} = 1180 \text{ km s}^{-1}$ . Here, we adopted a distance of  $d = 1.5$  kpc and a reddening of  $E(B-V) = 0.45$ . Thus, the distance modulus is  $(m-M)_V = 12.3$ , and the maximum brightness is  $M_{V,\text{max}} = m_{V,\text{max}} - (m-M)_V = 1.85 - 12.3 = -10.45$ .

The dereddened color-color diagram is plotted in Figure 8(b), where the  $UBV$  magnitudes are taken from Pfau (1976), Arkhipova & Zaitseva (1976), Duerbeck & Wolf (1977), and Contadakis (1980). In the figure we connect only the data set of Duerbeck & Wolf (1977) with a red, thin, solid line to show the development of the colors. V1500 Cyg follows the nova-giant sequence in the pre-maximum stage, i.e., starting from point D and reaching point C (=3) at optical light maximum. It did not reach point B, point 2, or point A. In the post-maximum phase, it returns from point C (=3) and reaches point 4' (near point F) along the nova-giant sequence.

As introduced in the previous Sections 3.1 and 3.2, optically-thick, free-free emission dominates the spectrum in the optical and IR region from point 4' to 5' (Figure 9). When the continuum of free-free emission dominates the spectrum, the optical light curve follows the universal decline law (Hachisu & Kato 2006), and its  $(B-V)_0$  and  $(U-B)_0$  colors remain at point F, i.e.,  $(B-V)_0 = -0.03$  and  $(U-B)_0 = -0.97$  (magenta solid lines in Figures 6 and 7). When strong emission lines contribute to the  $UBV$  broadband, the light curves deviate from these values. We specify a template ("V1500 Cyg template") consisting of the four points in Figure 8(b) to illustrate the track of color-color evolution, from point D to C (=3), 4', and then to 5'. We tabulate each position of the V1500 Cyg template in Table 1.

### 3.5. V1668 Cyg

V1668 Cyg was discovered on UT 1978 September 10.24 (Morrison et al. 1978), two days before its optical maximum of  $m_{V,\text{max}} = 6.04$ . The light curve of V1668 Cyg is plotted in Figure 1 on a linear timescale and in Figures 7 and 11 on a logarithmic timescale. The distance-reddening law in the direction of V1668 Cyg was obtained by Slovak & Vogt (1979), as shown in Figure 12 (large red filled circles), although the number of stars is small and the data are scattered for  $d > 1$  kpc. They also obtained a reddening of  $E(B-V) = 0.38$  from the interstellar feature of K I (7699  $\text{\AA}$ ) and thus a distance of  $d = 3.3$  kpc. Duerbeck et al. (1980) criticized Slovak & Vogt's work and proposed a distance of  $d = 2.3$  kpc from their newly obtained distance-reddening law and  $E(B-V) = 0.35$ , using the same stars as those in Slovak & Vogt (1979). These distance-reddening laws, however, rely on only three stars beyond 1 kpc (Slovak & Vogt 1979), so we cannot judge these two different estimates. Assuming that the optical maximum is the Eddington luminosity, Stickland et al. (1981) estimated the distance to be  $d = 2.2$  kpc, together with their  $E(B-V) = 0.40$  from the 2200  $\text{\AA}$  feature. However, we have no evidence that the maximum luminosity of V1668 Cyg is just the Eddington limit.

The distance to the nova can also be estimated from the MMRD relation. Klare et al. (1980) obtained  $M_{V,\text{max}} = -8.0 \pm 0.2$  from Schmidt-Kaler's (Schmidt 1957) relation together with  $t_3 = 24.3$  days (Mallama & Skillman 1979). This gives a distance modulus of  $(m-M)_V = 14.04$  and a distance of  $d = 3.7$  kpc, together with  $m_{V,\text{max}} = 6.04$  and  $A_V = 3.1E(B-V) = 3.1 \times 0.40 = 1.24$ .

Using the model light curves of free-free emission, Hachisu & Kato (2010) analyzed the multiwavelength light



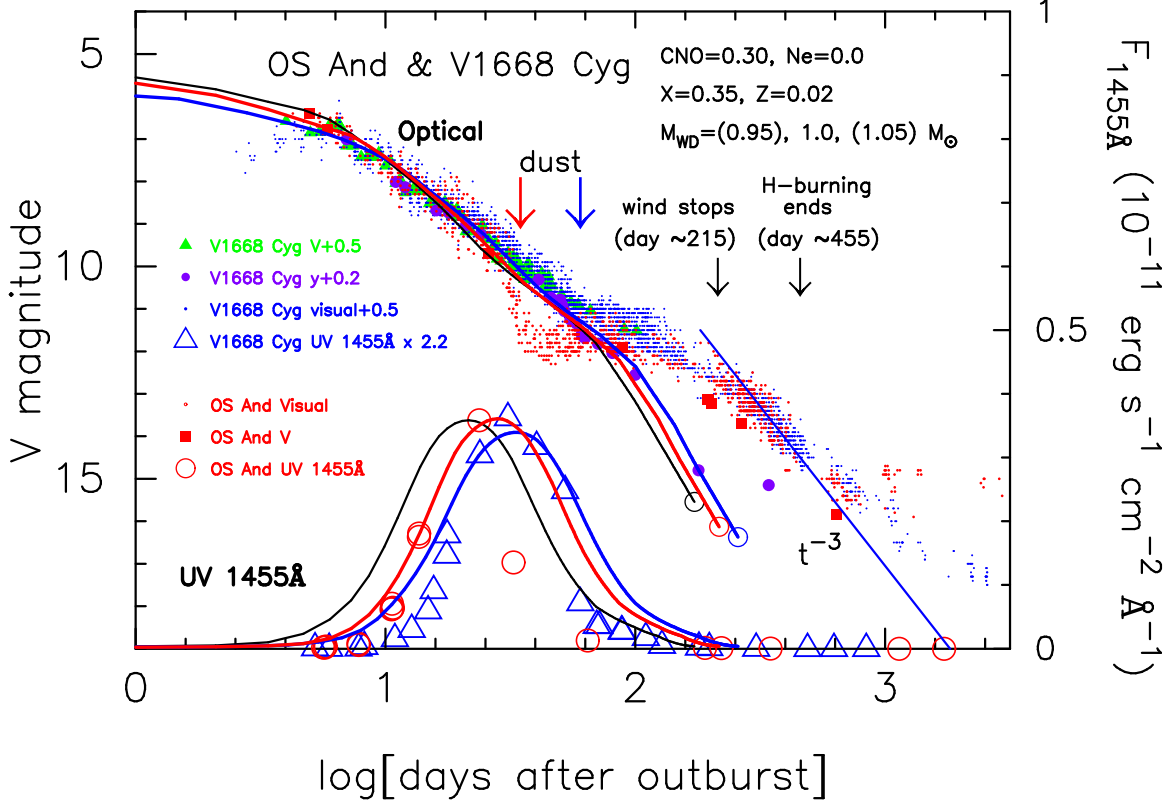


FIG. 11.— Optical/UV 1455Å light curves of OS And 1986 and V1668 Cyg 1978. The UV 1455Å data of OS And are taken from Cassatella et al. (2002). The optical/UV 1455Å data for V1668 Cyg are the same as those in Figure 16 of Hachisu & Kato (2006). The optical V data (red filled squares) of OS And were taken from Kikuchi et al. (1988), Ohmori & Kaga (1987), and IAU Circular Nos. 4282, 4293, 4306, 4342, and 4452. Visual data (red small dots) of OS And are from the AAVSO archive. We also add our model free-free emission light curves and UV 1455Å model fluxes for both OS And and V1668 Cyg. The best fit model of OS And is a  $1.0 M_{\odot}$  WD among three WDs with  $0.95$  (blue solid line),  $1.0$  (red solid), and  $1.05$  (black solid)  $M_{\odot}$  and an assumed chemical composition of  $X = 0.35$ ,  $Y = 0.33$ ,  $Z = 0.02$ , and  $X_{C+O} = 0.30$ . On the other hand, the best fit model of V1668 Cyg is a  $0.95 M_{\odot}$  WD. The sudden drops in the UV flux of OS And on day  $\sim 30$  and of V1668 Cyg on day  $\sim 60$  are caused by the formation of an optically-thick/thin dust shell (denoted by arrows with “dust”).

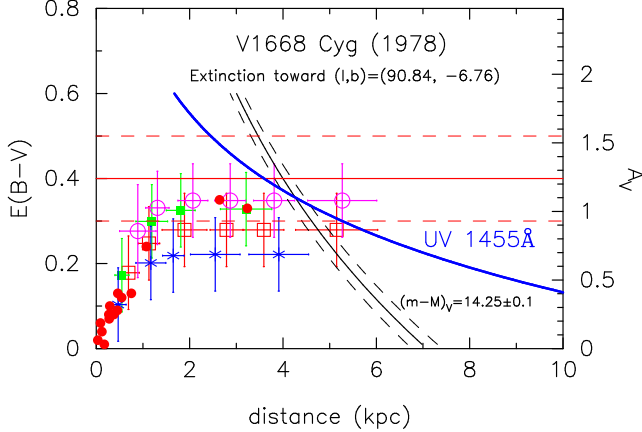


FIG. 12.— Distance-reddening relation toward V1668 Cyg. Blue thick solid line denotes the distance-reddening relation for UV 1455Å flux fitting. Red horizontal solid line flanked by red dashed lines show the reddening of  $E(B-V) = 0.4 \pm 0.1$  determined from the 2200Å feature (Stickland et al. 1981). Black solid line flanked by dashed lines corresponds to a distance modulus of  $(m-M)_V = 14.25 \pm 0.1$ . Red filled circles represent distance-reddening relation data from Slovak & Vogt (1979). Four sets of data with error bars show distance-reddening relations in four directions close to V1668 Cyg:  $(l, b) = (90^{\circ}75', -6^{\circ}75')$  (red open squares),  $(91^{\circ}00', -6^{\circ}75')$  (green filled squares),  $(90^{\circ}75', -7^{\circ}00')$  (blue asterisks), and  $(91^{\circ}00', -7^{\circ}00')$  (magenta open circles); data were taken from Marshall et al. (2006). These trends/lines cross at  $d \approx 4.3$  kpc and  $E(B-V) \approx 0.35$ .

curves of V1668 Cyg and V1974 Cyg. They calibrated the absolute magnitudes of the model light curves for various

WD masses and tabulated them in their Tables 2 and 3. If we use these calibrated model light curves, the absolute magnitudes of nova light curves are determined by fitting. In the following, we show an example of this fitting. We plot the light curves of V1668 Cyg (and OS And, see Section 6.12) in Figure 11 with the free-free emission model light curves taken from Hachisu & Kato (2010). This figure also shows the UV 1455Å light curves corresponding to each optical light curve model. This narrowband flux represents well the evolution of the photospheric temperature of novae (e.g., Cassatella et al. 2002; Hachisu & Kato 2006; Hachisu et al. 2008). In the figure, we shift down the V and visual magnitudes by 0.5 mag and the y magnitudes of V1668 Cyg by 0.2 mag so that they overlap with the V light curve of OS And. The UV 1455Å fluxes of V1668 Cyg are also scaled up by a factor of 2.2. The  $0.95 M_{\odot}$  WD (blue solid line) model shows the best fit with both the observed *IUE* fluxes and optical V light curve of V1668 Cyg when we increase the WD mass in  $0.05 M_{\odot}$  steps. Here, we assumed a chemical composition of  $X = 0.35$ ,  $Y = 0.33$ ,  $Z = 0.02$ ,  $X_{C+O} = 0.30$ . From the optical light curve fitting, we obtained the distance modulus of V1668 Cyg as

$$(m-M)_V = m_w - M_w = (16.35 - 0.5) - (+1.6) = 14.25, \quad (9)$$

where  $m_w = 16.35$  is read directly from the end point of the free-free emission model light curve (large, open circle at the bottom of the line) in Figure 11 and  $M_w$  is taken from

Table 2 of Hachisu & Kato (2010) as  $M_w = +1.6$  for the  $M_{WD} = 0.95 M_\odot$  model. Thus, we obtain a distance modulus of  $(m-M)_V = 14.25 \pm 0.1$ , where  $\pm 0.1$  is the possible fitting error.

Hachisu & Kato (2010) also proposed another distance-reddening relation calculated from the UV 1455Å flux fitting as

$$2.5 \log(F_\lambda^{\text{obs}}/F_\lambda^{\text{mod}}) = 8.3E(B-V) + 5 \log\left(\frac{d}{10 \text{ kpc}}\right), \quad (10)$$

where, as shown in Figure 11,  $F_\lambda^{\text{mod}}$  is the model flux (blue solid line) at the distance of 10 kpc without absorption,  $F_\lambda^{\text{obs}}$  is the observed flux (blue large open triangles), and the absorption is calculated from  $A_\lambda = 8.3E(B-V)$  for  $\lambda = 1455\text{\AA}$  (Seaton 1979).

Figure 12 shows various distance-reddening relations toward V1668 Cyg. Here, we omit the MMRD relation mentioned above because it is not very reliable. The first is the distance reddening relation given by Equation (2) together with the distance modulus of  $(m-M)_V = 14.25 \pm 0.1$  calculated above from the calibrated model light curve. The second is the distance-reddening relation given by Equation (10) for fitting UV 1455Å. The third is an estimated value of  $E(B-V) = 0.4 \pm 0.1$  from the 2200 Å feature (Stickland et al. 1981). The fourth is a relation given by Marshall et al. (2006), where the galactic coordinates of V1668 Cyg are  $(l, b) = (90^\circ 83' 73'', -6^\circ 75' 98'')$ . The four sets of data with error bars show the distance-reddening relations in four directions close to V1668 Cyg:  $(l, b) = (90^\circ 75', -6^\circ 75')$  (red open squares),  $(91^\circ 00', -6^\circ 75')$  (green filled squares),  $(90^\circ 75', -7^\circ 00')$  (blue asterisks), and  $(91^\circ 00', -7^\circ 00')$  (magenta open circles). These trends/lines cross at  $d \approx 4.3$  kpc and  $E(B-V) \approx 0.35$ . We adopted  $d = 4.3$  kpc and  $E(B-V) = 0.35$  in this paper. Then, the maximum magnitude is  $M_{V, \text{max}} = m_{V, \text{max}} - (m-M)_V = 6.04 - 14.25 \approx -8.2$ .

Figure 8(c) shows the dereddened color-color diagram of V1668 Cyg, where the *UBV* data are taken from deRoux (1978), Duerbeck et al. (1980), and Kolotilov (1980). It started from somewhere on or near the nova-giant sequence (probably point D), although we did not find data on the pre-maximum (rising) phase of V1668 Cyg. Then, it reached near point C (=3). The nova quickly evolved to point 4" (near point F) along the nova-giant sequence and stayed at point 4" for a while. Optically-thick free-free emission dominates the spectrum in the optical and IR region from point 4" to 5", as denoted by magenta solid lines in Figure 7. Then the nova moved horizontally (blueward in  $(B-V)_0$  toward point 5" but was almost constant in  $(U-B)_0$ ). In the figure we only connect the points observed by deRoux (1978) to follow the early color evolution. We do not connect other data observed by Duerbeck et al. (1980) and Kolotilov (1980) to avoid a confusing presentation of many line-connections. Thus, we specify a template for V1668 Cyg ("V1668 Cyg template") by three points, that is, (probably from point D to point C), from point C to point 4", and then from point 4" to 5". These points are tabulated in Table 1.

### 3.6. V1974 Cyg

V1974 Cyg was discovered at  $m_V \sim 6.8$  on UT 1992 February 19.07 (JD 2448671.57; Collins 1992) on the way to its optical maximum of  $m_{V, \text{max}} \approx 4.2$  around February 22 (JD 2448674.5). This is the first nova ever observed in all the

wavelengths from gamma-ray to radio, and was especially well-observed by an X-ray satellite *ROSAT* and a UV satellite *IUE*. The light curve and color curves of V1974 Cyg are plotted in Figure 7 and the UV 1455Å and X-ray light curves are shown in Figure 13 both on a logarithmic timescale. *ROSAT* first detected the beginning and end of supersoft X-ray emission from classical novae (e.g., Krautter et al. 1996; Balman et al. 1998).

To determine the reddening toward V1974 Cyg, we plot the distance-reddening relation in Figure 14. The distance to V1974 Cyg was carefully determined by Chochol et al. (1997) to be  $d = 1.77 \pm 0.11$  kpc using an expansion parallax method. Here we adopted Chochol et al.'s distance value of  $d = 1.8 \pm 0.1$  kpc (black vertical solid line flanked by thin, dashed lines). The galactic coordinates of V1974 Cyg are  $(l, b) = (89^\circ 13' 38'', 7^\circ 8' 19'')$ . The four sets of data points with error bars show the distance-reddening relations in four directions close to V1974 Cyg:  $(l, b) = (89^\circ 00', 7^\circ 75')$  (red open squares),  $(89^\circ 25', 7^\circ 75')$  (green filled squares),  $(89^\circ 00', 8^\circ 00')$  (blue asterisks), and  $(89^\circ 25', 8^\circ 00')$  (magenta open circles); the data are taken from Marshall et al. (2006). The closest one is that denoted by green filled squares, which crosses the  $d = 1.8$  kpc line at  $E(B-V) = 0.25 \pm 0.05$ . The reddening was also estimated by many researchers. Chochol et al. (1997) presented their mean value of  $E(B-V) = 0.26 \pm 0.03$  from various estimates based mainly on the MMRD relations. Austin et al. (1996) obtained the reddening toward V1974 Cyg mainly on the basis of the UV and optical line ratios for days 200 through 500, i.e.,  $E(B-V) = 0.36 \pm 0.04$ . The NASA/IPAC galactic dust absorption map gives  $E(B-V) = 0.35 \pm 0.01$  in the direction toward V1974 Cyg. Here we adopted the mean value of these four estimates, i.e.,  $E(B-V) = 0.3 \pm 0.1$  and plot this in Figure 14 (horizontal, red, solid line flanked by thin, dashed lines).

The distance-reddening relation is also obtained from the UV 1455Å flux fitting in Figure 13. Comparing the model flux of  $1.05 M_\odot$  WD and the observed ones, we obtain the relation in Equation (10) for V1974 Cyg, which is plotted by a magenta thick solid line in Figure 14. We also plot the distance-reddening relation, i.e., Equation (2), using the distance modulus of  $(m-M)_V = 12.2 \pm 0.1$  from the free-free model light curve fitting, i.e.,  $(m-M)_V = m_w - M_w = 13.8 - (+1.6) = 12.2$  in Figure 13. These trends/lines consistently cross at  $d \approx 1.8$  kpc and  $E(B-V) \approx 0.30$ . Therefore, we confidently adopt  $d = 1.8$  kpc and  $E(B-V) = 0.30$  for V1974 Cyg.

Using  $E(B-V) = 0.30$ , we dereddened the color-color evolution of V1974 Cyg in Figure 8(d), where the *UBV* data are taken from IAU Circulars and Chochol et al. (1993). It started from a position near point D in the color-color diagram before an iron curtain developed in the UV wavelength region. This point is highlighted by a blue filled star symbol because it is only the data in the pre-maximum phase (Kosai et al. 1992). The blue star symbol is located on the nova-giant sequence. This starting point is very similar to that of PW Vul and corresponds to the so-called fireball stage. Then, the nova ascended to point 4" (near point F) along the nova-giant sequence. After the nova reached point 4", it stayed at or near point 4" for 10–20 days. Then it gradually moved horizontally leftward, as shown in Figures 7 and 8(d). This track is almost the same as that of V1668 Cyg. We specify it by points D, 4", and 5" ("V1974 Cyg template"). These positions are tabulated in Table 1.

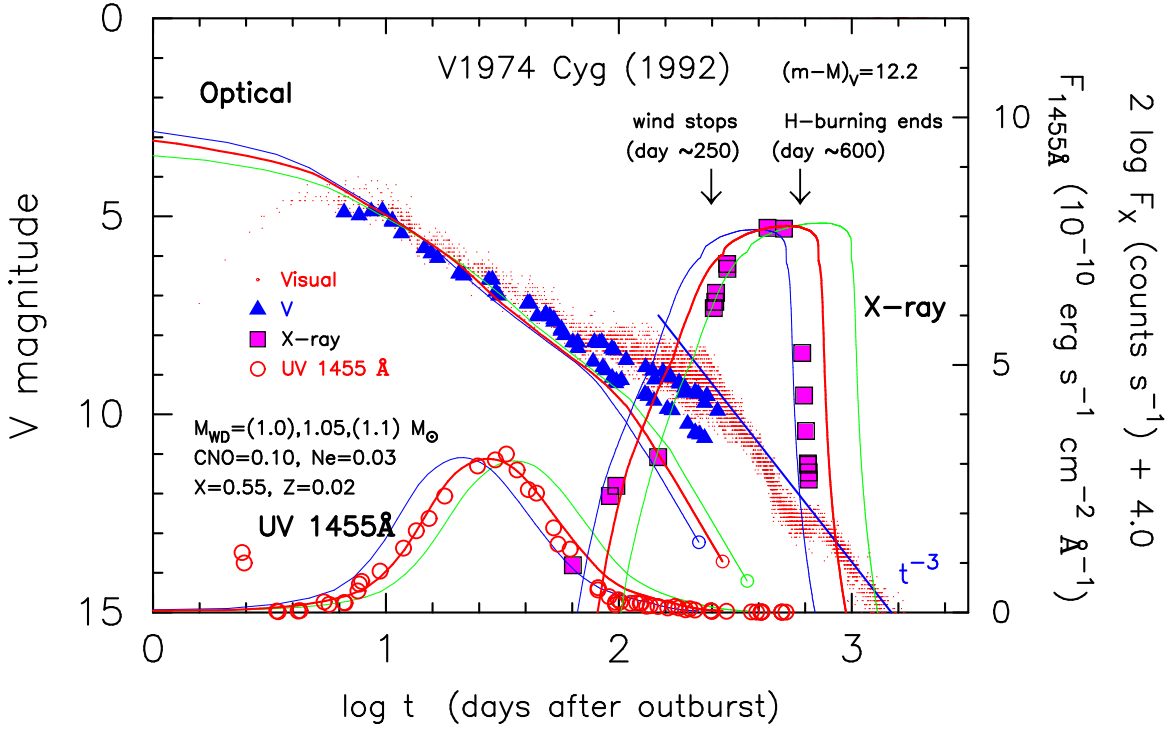


FIG. 13.— Optical/UV 1455Å /X-ray light curves of V1974 Cyg. The optical/UV 1455Å /X-ray data for V1974 Cyg are the same as those in Figure 19 of Hachisu & Kato (2006). The best fit model is a  $1.05 M_{\odot}$  WD among three WDs with  $1.0$  (green solid line),  $1.05$  (red thick solid line), and  $1.1$  (blue solid line)  $M_{\odot}$  WDs and an assumed chemical composition of  $X = 0.55$ ,  $Y = 0.30$ ,  $Z = 0.02$ ,  $X_{\text{C+O}} = 0.10$ , and  $X_{\text{Ne}} = 0.03$ .

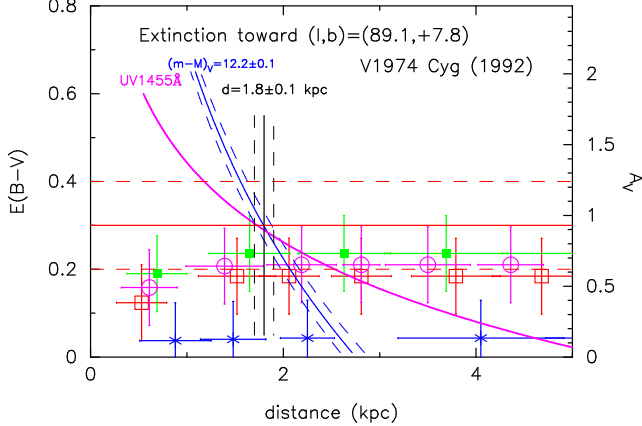


FIG. 14.— Same as Figure 12, but for V1974 Cyg. Magenta thick solid line denotes the distance-reddening relation for UV 1455Å flux (see Figure 19 of Hachisu & Kato 2006). Red horizontal solid line flanked by red dashed lines shows reddening of  $E(B-V) = 0.3 \pm 0.1$ . Blue solid line flanked by dashed lines corresponds to  $(m-M)_V = 12.2 \pm 0.1$ . Black vertical solid line flanked by dashed lines corresponds to the distance  $d = 1.8 \pm 0.1$  kpc. Four sets of data with error bars show distance-reddening relations in four directions close to V1974 Cyg:  $(l, b) = (89^{\circ}00, 7^{\circ}75)$  (red open squares),  $(89^{\circ}25, 7^{\circ}75)$  (green filled squares),  $(89^{\circ}00, 8^{\circ}00)$  (blue asterisks), and  $(89^{\circ}25, 8^{\circ}00)$  (magenta open circles); data are taken from Marshall et al. (2006). These trends/lines cross at  $d \approx 1.8$  kpc and  $E(B-V) \approx 0.30$ .

Note that V1974 Cyg did not make a long journey toward point C ( $\approx 3$ ). It did not reach point C whereas the other three novae, PW Vul, V1500 Cyg, and V1668 Cyg, did. This behavior is very consistent with the development of the UV1455Å continuum flux (see Figure 13). In V1974 Cyg the UV flux was relatively high a few days before optical maximum and then almost vanished near optical maximum, followed by a quick rise just after the optical maximum. On the other hand, V1668 Cyg maintained

almost zero UV1455Å flux for a relatively long time (10–20 days) before and after optical maximum, followed by a quick rise with a timescale similar to that of V1974 Cyg (Cassatella et al. 2002; Kato & Hachisu 2007), although  $t_3$  is shorter in V1668 Cyg (26 days) than in V1974 Cyg (42 days). This fact simply means that the photospheric temperature at the optical maximum in V1974 Cyg is much higher than that of V1668 Cyg. This is why the excursion toward point C is much shorter in V1974 Cyg than in V1668 Cyg. From the viewpoint of nova theory, this suggests a much lower envelope mass in V1974 Cyg than in V1668 Cyg.

In this way, we found that the five well-observed novae follow a similar path in the color-color diagram. Our new finding of the nova-giant sequence is a characteristic property near and around optical maximum that is common among these novae.

#### 4. COLOR EVOLUTION OF SYMBIOTIC NOVA PU VUL

Our next example is the symbiotic nova PU Vul, because there are many  $UBV$  color data (e.g., Shugarov et al. 2012) during the long lasting outburst. It is an eclipsing binary with an orbital period of  $\sim 4900$  days (13.4 yr) (Kolotilov et al. 1995; Nussbaumer & Vogel 1996; Garnavich 1996; Shugarov et al. 2012). It exhibited an outburst in 1978 (see e.g. Belyakina et al. 1989), and its very slow evolution provides us with dense optical spectroscopic/photometric data as well as *IUE/Hubble Space Telescope (HST)* UV observations. The  $V$  light curve of PU Vul is plotted in Figure 15, together with the light curve of the very slow nova V723 Cas, which we discuss later in Section 5. PU Vul consists of a mass-accreting WD and a mass-donating, semi-regularly pulsating M6 red giant (RG). Kato et al. (2011, 2012) obtained  $\sim 0.6 M_{\odot}$  for the WD and  $\sim 0.8 M_{\odot}$  for the RG.

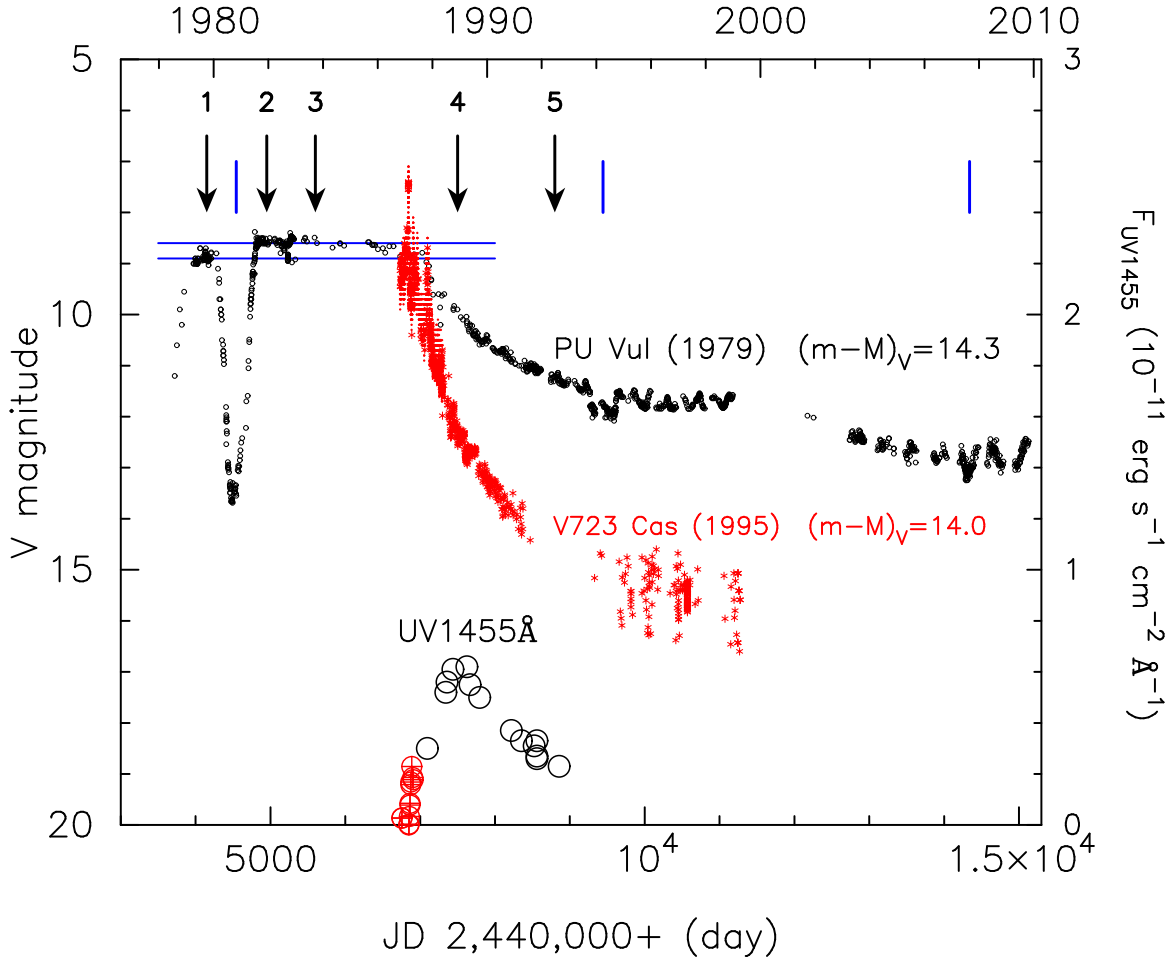


FIG. 15.— Optical and UV 1455 Å light curves of PU Vul (black symbols) and V723 Cas (red symbols). Small open black circles:  $V$  magnitudes of PU Vul. Large open black circles:  $IUE$  UV 1455 Å flux of PU Vul. All data for PU Vul are those in Kato et al. (2011, 2012). Three blue vertical lines indicate the central times of eclipses in 1980, 1994, and 2007. Five downward arrows denote five stages of color evolution of PU Vul as defined in Section 4. Two horizontal solid lines denote absolute magnitudes of  $M_V = -5.4$  and  $-5.7$  in the flat peak of PU Vul in 1979 and 1981–1983, respectively. Red asterisks and dots show  $V$  and visual magnitudes of V723 Cas, which are taken from Chochol & Pribulla (1997, 1998) and the AAVSO archive, respectively. Large open red circles with a plus sign inside:  $IUE$  UV 1455 Å flux of V723 Cas, the values of which are multiplied by ten. Light curves of V723 Cas are shifted by about 8 yr leftward to match the start of the UV 1455 Å outburst of these two novae;  $V$  and visual light curves of V723 Cas are shifted by 0.3 mag upward to match the absolute magnitudes of these two novae.

Kato et al. (2012) carefully analyzed the available data for PU Vul and obtained a reddening of  $E(B-V) = 0.30$  with a possible systematic error of 0.05 and a distance of  $d = 4.7$  kpc from four combinations of three independent methods. The NASA/IPAC galactic dust absorption map gives  $E(B-V) = 0.29 \pm 0.01$  in the direction of PU Vul, whose galactic coordinates are  $(l, b) = (62^\circ 57' 53'', -8^\circ 53' 17'')$ ; this is perfectly consistent with Kato et al.’s reddening estimate. Therefore, we adopted  $E(B-V) = 0.30$  and  $d = 4.7$  kpc in this paper. Thus, the distance modulus in the  $V$  band is  $(m-M)_V = A_V + 5 \log(d/10 \text{ pc}) = 3.1 \times 0.3 + 5 \log(470) = 14.3$ .

To follow the color evolution, we chose five epochs that represent typical evolutionary stages of PU Vul, as indicated by downward arrows in Figure 15. These stages were chosen to avoid the three total eclipses in 1980, 1994, and 2007, which are indicated by three, blue, vertical lines in Figure 15, because the hot component (the WD) is totally occulted by the cool component (the RG) during the eclipses. We briefly summarize the features of each stage in the  $V$  magnitude as follows:

stage 1: Pre-maximum phase, 0.3 mag below the maximum.  
stage 2: Optical maximum.

stage 3: Post-maximum flat peak before the nebular phase.  
stage 4: Onset of the nebular phase,  $\sim 1.5$  mag decayed from the maximum.  
stage 5: Mid nebular phase,  $\sim 2.5$  mag decayed from the maximum.

For each stage, we took a mean value of the magnitudes in Figure 3 of Shugarov et al. (2012), which shows many color data with a small scatter around the mean value. Using the 1979–1993 data of Shugarov et al. (2012), we show the color-color evolution of PU Vul in Figure 16 for the pre-maximum phase (from stage 1 to 2) and in Figure 17 for the post-maximum phase (from stage 2 to stages 3, 4, and 5).

#### 4.1. Nova-giant Sequence: Stages 1–3

During the flat peak (stages 1 – 3), PU Vul evolved from point 1 to 2 in Figure 16 and from point 2 to 3 in Figure 17. Kanamitsu (1991) reported pure absorption spectra for F-type supergiants, which we attribute to the photospheric emission of PU Vul. The paths from points 1 to 2 through point B and from points 2 to 3 through point B are parallel to, but  $\Delta(U-B) \approx -0.2$  mag bluer than, the supergiant sequence,

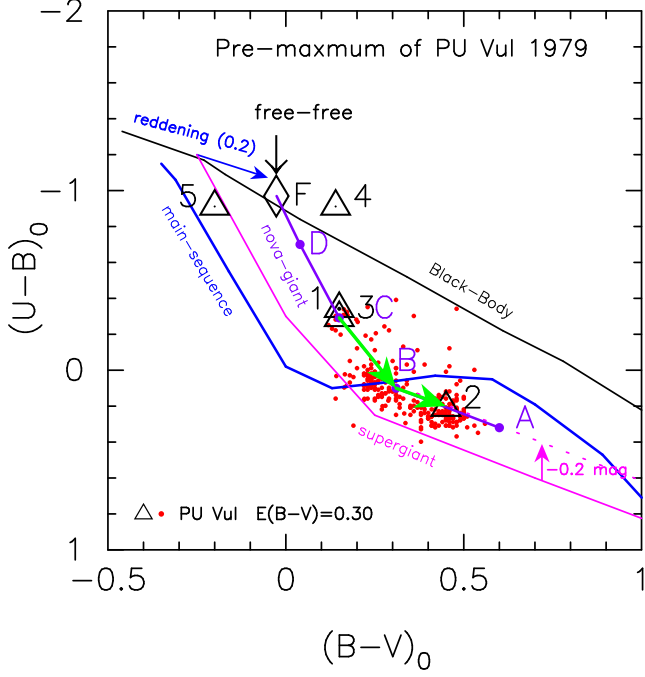


FIG. 16.— Same as Figure 4, but for PU Vul (denoted by red filled circles) in the pre-maximum phase. The data are taken from Shugarov et al. (2012). Five evolutionary epochs of PU Vul in Figure 15 are indicated by open triangles with numbers. A landmark of optically-thick, free-free emission spectra is added, i.e., point F denoted by an open diamond. The track of PU Vul (green arrows) almost coincides with the nova-giant sequence (from point 1 to 2 through point B), which is located at about  $\Delta(U-B) \approx -0.2$  mag bluer than the supergiant sequence. The reddening direction is shown at the top of the supergiant sequence by a blue arrow, the length of which corresponds to  $E(B-V) = 0.2$ . See text for more details.

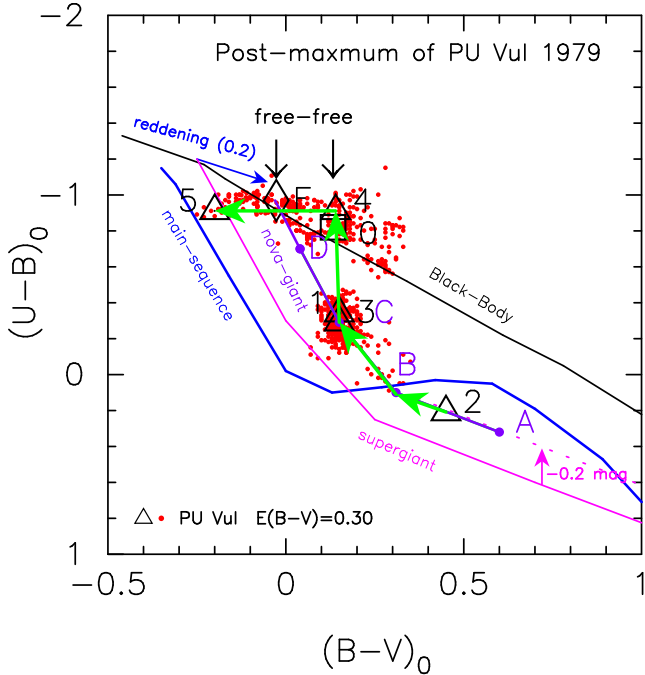


FIG. 17.— Same as Figure 16, but in the post-maximum phase (from points 2, 3, 4, and 5). Two landmarks of free-free emission spectra are added: optically-thin (open square denoted by 0) and optically-thick (open diamond denoted by F).

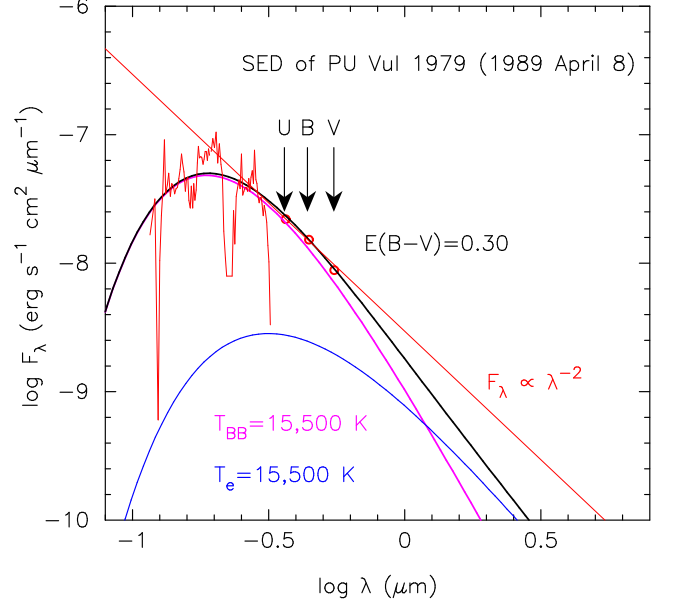


FIG. 18.— Same as Figure 9, but for PU Vul about 11 yr after the outburst. Open red circles:  $U$ ,  $B$ , and  $V$  band fluxes (taken from Kolotilov et al. 1995), which are denoted by three black downward arrows. Red solid line: UV fluxes (*IUE* SWP35966 and LWP15323). All fluxes are dereddened with  $E(B-V) = 0.30$ . Global features of spectrum can be fitted with combination (black solid line) of blackbody with temperature  $T_{BB} = 15,500$  K (magenta solid line) and optically-thick, free-free emission with electron temperature  $T_e = 15,500$  K (blue solid line). We also plot an optically-thin, free-free emission spectrum of  $F_\nu \propto \nu^0$ , that is,  $F_\lambda \propto \lambda^{-2}$  (red thin straight solid line). In the  $UBV$  bands, the spectral energy distribution (SED) is close enough to that of optically-thin, free-free emission of  $F_\lambda \propto \lambda^{-2}$ .

as shown in Figures 16 and 17. This part of the track coincides perfectly with the nova-giant sequence defined by the FH Ser data in Section 2. This bluer position can be seen in the spectra of PU Vul obtained by Belyakina et al. (1989, p. 123), who reported, “There is a good agreement of the energy distribution of PU Vul and normal supergiants in the spectrum region from  $3000\text{\AA}$  to  $7000\text{\AA}$ . In the region from  $3200\text{\AA}$  to  $3800\text{\AA}$ , the UV excess is clearly seen. The amount of this excess in 1983 agrees well with the photometric estimate  $\Delta(U-B) = -0.2$  mag.” (See the spectrum in Figure 6 of Belyakina et al. (1989) for more details.) We will show below in Sections 5 and 6 that this nova-giant sequence is common among many novae.

#### 4.2. Wind phase: stage 4

The optical spectrum of PU Vul changed to that of a Wolf-Rayet (WR) star in 1987 (Iijima 1989), indicating a transition to the nebular phase (see also Belyakina et al. 1989; Tomov et al. 1991). Vogel & Nussbaumer (1992) and Sion et al. (1993) also reported that *IUE* spectra changed to that of a WR type wind. These changes are consistent with Kato et al.’s (2012) UV light curve analysis that optically-thin winds with a mass-loss rate of several times  $10^{-7} M_\odot \text{ yr}^{-1}$  started in 1987. At this epoch, PU Vul quickly ascends in the color-color diagram almost vertically to point 4 (at stage 4) above the blackbody sequence. Point 4 is very close to point 0, which is denoted by an open square in Figure 17, corresponding to the position of optically-thin free-free emission ( $F_\nu \propto \nu^0$ ), i.e.,  $(B-V)_0 = +0.13$  and  $(U-B)_0 = -0.82$ .

We can interpret this transition from stage 3 to 4 as follows: in the early expanding phase, PU Vul moved along the nova-giant sequence from stage 1 to 2 and then returned to



3. We observed the photospheric emission (pure absorption feature of F-supergiants) during stages 1 – 3, as schematically illustrated in Figure 5(b). The nova-giant sequence is much redder than the blackbody sequence in the  $(U - B)_0$  color because of the large contribution from the Balmer jump. When winds began to blow, the configuration of the envelope changed from that in Figure 5(b) to that in Figure 5(c). Then, the Balmer jump became shallower (see the spectrum in Figure 6 of Belyakina et al. 1989) and was filled with emission lines. Thus, the spectrum is approaching that of a blackbody or free-free emission. The resultant  $(U - B)_0$  color becomes bluer to approach that of a blackbody or free-free emission.

To understand this property, we analyze the nova spectra from UT 1989 April 8, in the nebular phase (stage 4). We assume that the spectrum is a summation of the blackbody emission at the photospheric temperature  $T_{\text{ph}} = T_{\text{BB}}$  and optically thick free-free emission at the electron temperature of  $T_e$ , i.e., Equation (5). Figure 18 shows the broad band spectrum of PU Vul, a combination of *IUE* spectra of SWP35966 and LWP15323 taken from the INES archive data server and optical *UBV* fluxes observed on UT 1989 April 8 (Kolotilov et al. 1995). Assuming that  $T_{\text{ph}} = T_e$ , we changed  $T_{\text{ph}}$  in 500 K steps and obtained a temperature of  $T_{\text{ph}} = T_e = 15500$  K. This is roughly consistent with the photospheric temperature of  $T_{\text{ph}} \sim 20000$  K theoretically calculated by Kato et al. (2012). As shown in Figure 18, we need a free-free emission component to fit the spectrum although its contribution is rather small at the *UBV* bands. The slope of the resultant spectrum at the *UBV* bands is very close to that of optically-thin free-free emission ( $F_{\lambda} \propto \lambda^{-2}$ ). This explains why the position of stage 4 is close to both the blackbody sequence and optically-thin, free-free emission, i.e., point 0 in Figure 17.

#### 4.3. Effects of Strong Emission Lines: Stage 5

In the color-color diagram of Figure 17, PU Vul further evolves blueward from point 4 to 5 (stage 4 to 5) while maintaining an almost constant  $(U - B)_0$ . This blueward change is mainly due to the growth of strong emission lines, especially in the *U* and *B* bands, as already explained in Section 3.3.

Figure 10 shows the effect of strong emission lines, i.e.,  $\Delta(B - V)$  and  $\Delta(U - B)$ , in the color-color diagram. Among the seven stars in Figure 10, six are symbiotic stars and three are symbiotic novae. Symbiotic novae can be divided into two groups according to their spectral evolution. The first group exhibits a long (several years) “supergiant phase,” in which they resemble an A–F supergiant while the star undergoes a nova outburst. In the second group, a nebular phase begins almost immediately after optical maximum, and a “supergiant phase,” if there is one, has a very short duration (Mürset & Nussbaumer 1994). The first group includes PU Vul, RR Tel, AG Peg, and RT Ser. The second group includes V1016 Cyg, HBV 475, and HM Sge. Because PU Vul is not included in Skopal (2007), we highlight RR Tel in Figure 10 because it belongs to the same group as PU Vul and its spectral evolution is similar to that of PU Vul. It is very clear that the blueward excursion in the color-color diagram is due to emission lines, because the position moves almost horizontally by  $\Delta(B - V) \approx -0.8$ .

Thus, we specify the color-color evolution of PU Vul by points 1, 2, 3, 4, and 5 (“PU Vul template”). These points are tabulated in Table 1. Here we stop following the color evolution when the *V* magnitude drops by about 3 mag from the maximum because strong emission lines make increasingly large contributions to the colors, and their effects cloud the

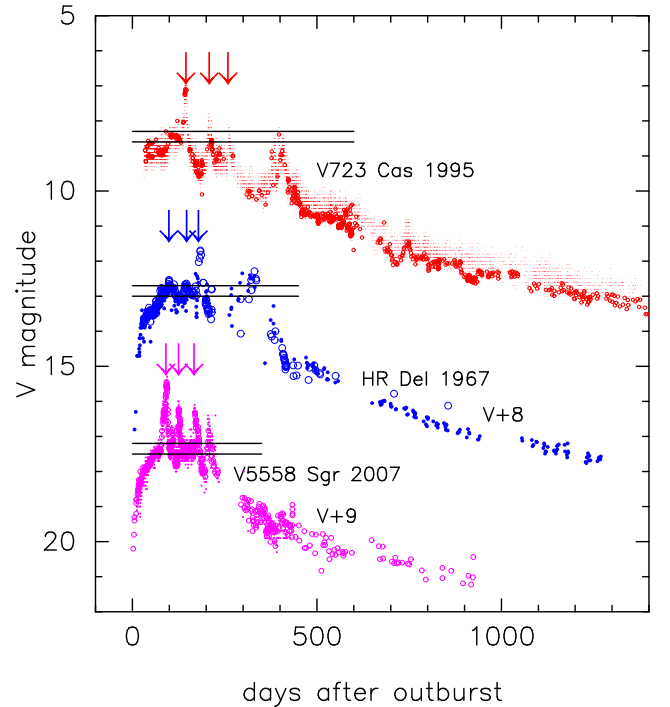


FIG. 19.— Optical light curves of three very slow novae, V723 Cas (red), HR Del (blue), and V5558 Sgr (magenta), from top to bottom. V723 Cas: small red dots are visual magnitudes taken from the AAVSO archive; red open circles are *V* magnitudes taken from Chochol & Pribulla (1997). HR Del: blue small filled circles are photographic magnitudes ( $m_{\text{pg}}$ ) taken from Terzan (1968); blue large open circles are *V* magnitudes taken from Mollerus (1969), Mannery (1970), Barnes & Evans (1970), Onderlíčka & Vetešník (1968), and Drechsel et al. (1977). V5558 Sgr: magenta dots are visual magnitudes taken from the AAVSO archive; magenta open circles are *V* magnitudes taken from the AAVSO and Variable Star Observers League in Japan (VSOLJ) archives. Two horizontal solid lines denote absolute magnitudes of  $M_V = -5.4$  and  $-5.7$ , which correspond to the flat peaks of PU Vul in 1979 and 1981–1983, respectively. First three flaring peaks are denoted by downward arrows for each nova.

overall color evolution.

It may be surprising that the color-color evolution of PU Vul follows almost the same tracks as those of slow/moderately fast/fast novae. This is because the physics of emission (Figure 5) is common among these novae regardless of the speed class or light curve shape. In a classical nova, the evolution is very fast, and it quickly passes stages (a) and (b) in Figure 5 and enters the optically thick wind phase (c). On the other hand, in PU Vul, the optically-thick winds were not accelerated and it slowly evolved from stages (a) to (b) and then entered the optically-thin wind phase. In the next section, we further show that very slow novae also follow this common track in color-color evolution.

#### 5. COLOR EVOLUTION OF VERY SLOW NOVAE, HR DEL, V723 CAS, AND V5558 SGR

In this section, we examine the color evolutions of three very slow novae, HR Del, V723 Cas, and V5558 Sgr. They have similar light curves (see Figure 19) and spectral evolutions (e.g., Friedjung 1992; Friedjung & Iijima 2002; Evans et al. 2003; Munari et al. 2007).

##### 5.1. The Nature of Outbursts: Transition from Static to Wind Evolution

HR Del, V723 Cas, and V5558 Sgr show multiple peaks in their light curves, as shown in Figure 19, whereas PU Vul shows a smooth light curve with a flat maximum phase except

for the eclipses. Kato & Hachisu (2009) proposed the concept of multiple solutions of novae as an explanation for such multipeak structures in the optical light curves. They pointed out that there are two different types of nova evolution; one is evolution with optically-thick winds for  $M_{\text{WD}} \gtrsim 0.5 M_{\odot}$  (e.g., Kato & Hachisu 1994) and the other is that without them for  $M_{\text{WD}} \lesssim 0.7 M_{\odot}$ . Both types can be realized in slow novae in a certain range of WD masses,  $0.5 M_{\odot} \lesssim M_{\text{WD}} \lesssim 0.7 M_{\odot}$ . For example, the evolution of GQ Mus 1983 is explained by a sequence of optically-thick wind solutions on a  $\sim 0.7 M_{\odot}$  WD (Hachisu et al. 2008), whereas the evolution of PU Vul 1979 is described by a sequence of hydrostatic solutions on a  $\sim 0.6 M_{\odot}$  WD (Kato et al. 2011). These two evolutions show a remarkable difference in the optical light curves. In a wind-type nova, massive optically-thick winds carry away a large part of the envelope, producing a quick decay of the light curve. Thus, the optical light curve of the nova shows a sharp peak. On the other hand, in low mass WDs no optically-thick winds are accelerated, so the nova evolves very slowly and retains an extended photosphere with low temperatures for a long time, which produces a long lasting flat optical peak before the magnitude slowly decays as in PU Vul.

Kato & Hachisu (2011) explained theoretically that the transition from static evolution to wind evolution could occur during an outburst. In such a case, the nova shows a flat optical peak with no indication of strong mass loss in the early phase of the outburst, like PU Vul, followed by a quick decay phase, as in normal novae with strong optically-thick winds. They further suggested that such a transition from a static to a wind structure is accompanied by behavior such as oscillations in the brightness, because the internal structures of the static/wind solutions differ greatly, and a relaxation process in the transition should induce some oscillatory features. They suggested that the light curve behaviors of HR Del, V723 Cas, and V5558 Sgr in Figure 19 correspond to this type of transition.

Kato & Hachisu (2011) proposed the following transition mechanism: The static evolution itself is stable, as seen in the 8-yr flat peak of PU Vul (Figures 1 and 15). In close binaries, however, the envelope structures are affected because of the effect of a companion star's gravity, which may trigger the transition. For PU Vul ( $P_{\text{orb}} = 4900$  days), however, the transition was not triggered because its companion star is far outside the photosphere of the bloated WD envelope. For HR Del ( $P_{\text{orb}} = 0.214$  days), V723 Cas ( $P_{\text{orb}} = 0.692$  days), and V5558 Sgr ( $P_{\text{orb}} = \text{unknown}$ ), their outbursts started as static evolution, but their transitions were triggered a few hundred days after the outburst, owing to the effect of the companion located deep in the nova envelope. If this is the case, these three novae should exhibit not only similar light curve evolution but also similar color evolution. In this section we first examine the distances and absorptions of these three novae to obtain the dereddened colors and then discuss the color evolution of these three very slow novae.

### 5.2. Absolute magnitude at pre-maximum halt in slow novae

First, we examine the absolute magnitude of these very slow novae. As already explained in Section 5.1, Kato & Hachisu (2011) modeled the pre-maximum phase of these very slow novae with a static evolution followed by the transition from a static to a wind structure. They predicted that this transition occurs in a narrow range of WD masses,  $0.5 M_{\odot} \lesssim M_{\text{WD}} \lesssim 0.7 M_{\odot}$ . Thus, the brightness at the pre-maximum phase is similar to that of PU Vul ( $\sim 0.6 M_{\odot}$ ), i.e.,

$M_V = -5.4$  in stage 1 and  $M_V = -5.7$  in stage 2. We apply these two absolute magnitudes of PU Vul to the  $V$  light curves of the three novae. Because these light curves show oscillatory behavior, it is not easy to define the stages corresponding to stages 1 and 2 in PU Vul. However, we finally found reasonable fittings, as shown in Figure 19. Thus, we obtained a distance modulus of  $(m-M)_V = 10.4, 14.0,$  and  $13.9$  for HR Del, V723 Cas, and V5558 Sgr, respectively.

We confirmed and calibrated the distance moduli of these three novae obtained above by comparing their light curves with that of RR Pic, because the distance to RR Pic was recently obtained using trigonometric parallax, i.e.,  $d = 521^{+54}_{-45}$  pc (Harrison et al. 2013). The distance modulus of RR Pic is calculated to be  $(m-M)_V = 5 \log 521^{+54}_{-45} / 10 + 0.13 = 8.7 \pm 0.2$ , where we used  $A_V = 0.13$  after Harrison et al. (2013). The  $V$  light curve of RR Pic is plotted in Figure 20 on a linear timescale and in Figure 21 on a logarithmic timescale with those of HR Del, V723 Cas, and V5558 Sgr. We shifted the  $V$  light curves of RR Pic, V5558 Sgr, and HR Del vertically so that they overlap that of V723 Cas. The light curve of RR Pic is very similar to those of these three novae, so RR Pic belongs to the same type of novae as HR Del, V723 Cas, and V5558 Sgr, although the very early (rising) phase of RR Pic was not observed. Because these four novae have almost the same timescale of decline, we simply assumed that their brightnesses are all the same. The difference in  $V$  magnitude compared to V723 Cas is  $-5.3$  for RR Pic,  $-3.6$  for HR Del, and  $-0.1$  for V5558 Sgr. Therefore, the difference  $\Delta V$  from RR Pic is calculated as  $\Delta V = -3.6 + 5.3$  for HR Del,  $\Delta V = -0.0 + 5.3$  for V723 Cas, and  $\Delta V = -0.1 + 5.3$  for V5558 Sgr. The distance moduli of these three novae are  $(m-M)_{V, \text{HR Del}} = 10.4$ ,  $(m-M)_{V, \text{V723 Cas}} = 14.0$ , and  $(m-M)_{V, \text{V5558 Sgr}} = 13.9$ . Thus we have

$$\begin{aligned} (m-M)_{V, \text{RR Pic}} &= 8.7 \pm 0.2 \\ &= (m-M)_{V, \text{HR Del}} - \Delta V \\ &= 10.4 - (-3.6 + 5.3) = 8.7 \\ &= (m-M)_{V, \text{V723 Cas}} - \Delta V \\ &= 14.0 - (-0.0 + 5.3) = 8.7 \\ &= (m-M)_{V, \text{V5558 Sgr}} - \Delta V \\ &= 13.9 - (-0.1 + 5.3) = 8.7. \end{aligned} \quad (11)$$

These values are very consistent with each other.

### 5.3. HR Del 1967

The very slow nova HR Del was discovered by Alcock (Candy et al. 1967) at  $m_v = 5.0$  on UT 1967 July 8.9 (JD 2439680.4). The light curve of HR Del is plotted in Figures 19, 20, and 21. It reached 4.7 mag at optical maximum. Since the outburst day is not known, we adopted UT 1967 June 8.5 as the outburst day, i.e.,  $t_{\text{OB}} = \text{JD } 2439653.0$ , from the figure of Robinson & Ashbrook (1968). Verbunt (1987) obtained  $E(B-V) = 0.15 \pm 0.03$  for the extinction toward HR Del. The NASA/IPAC galactic dust absorption map gives  $E(B-V) = 0.11 \pm 0.006$  in the direction of HR Del, whose galactic coordinates are  $(l, b) = (63^\circ.4304, -13^\circ.9721)$ ; this is roughly consistent with Verbunt's value. Downes & Duerbeck (2000) obtained a distance of  $d = 0.76 \pm 0.13$  kpc to HR Del from the nebular expansion parallax. More recently, Harman & O'Brien (2003) obtained a new value of the distance,  $d = 0.97 \pm 0.07$  kpc, also from the expansion parallax method using *HST* imaging. Other, older, estimates are all between the above two estimates, i.e.,  $d = 0.940 \pm 0.155$  kpc from various expansion par-

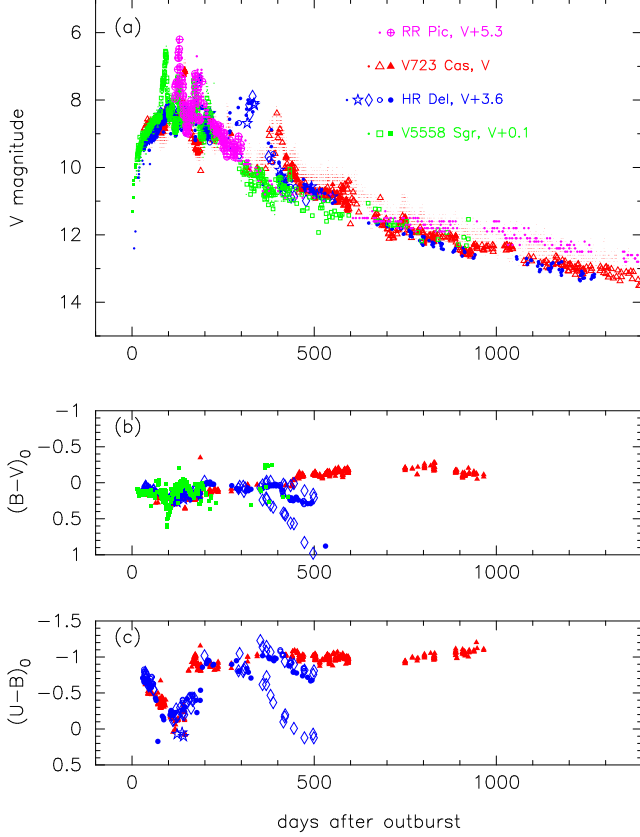


FIG. 20.— Light curves in (a)  $V$  band, and color evolution in (b)  $(B-V)_0$  and (c)  $(U-B)_0$  for RR Pic (magenta open circles with a plus sign), HR Del (blue symbols), V723 Cas (red triangles), and V5558 Sgr (green squares). To overlap them for as long as possible, we shifted the  $V$  magnitudes of RR Pic, HR Del, and V5558 Sgr downward by 5.3, 3.6, and 0.1 mag, respectively, and arranged the origin of the time of each nova against those of V723 Cas. The visual and photometric data for RR Pic are taken from the AAVSO archive and Dawson (1926), respectively.

allax methods (Malakpur 1975; Kohoutek 1981; Duerbeck 1981; Solf 1983; Cohen & Rosenthal 1983; Slavin et al. 1994, 1995) or  $d = 0.835 \pm 0.092$  kpc from other techniques (Drechsel et al. 1977). If we adopted the new distance estimate of  $d = 0.97$  kpc (Harman & O’Brien 2003) and the extinction of  $E(B-V) = 0.15$  (Verbunt 1987), the distance modulus is  $(m-M)_V = 5 \log 970/10 + 3.1 \times 0.15 = 10.4$ , which is perfectly consistent with the value in Equation (11). Therefore, we used  $E(B-V) = 0.15$  and  $d = 0.97$  kpc for HR Del.

#### 5.4. V723 Cas 1995

V723 Cas is also a very slow nova; it was discovered at mag 9.2 on UT 1995 August 24.57 (JD 2449954.07). Munari et al. (1996) proposed UT July 20.5 as the outburst day, i.e.,  $t_{OB} = \text{JD } 2449919.0$ , so we adopted this day in this paper. The interstellar extinction and distance toward V723 Cas were estimated by many authors. Chochol & Pribyla (1997) obtained  $(m-M)_V = 13.8$ ,  $E(B-V) = 0.57$ , and  $d = 2.38$  kpc from various MMRD relations as well as the  $V_{15}$  and  $B_{15}$  brightnesses (absolute  $M_V$  and  $M_B$  15 days after the maximum, respectively) of novae. Iijima et al. (1998) gave  $(m-M)_V = 13.2$ ,  $A_V = 0.88$  ( $E(B-V) = A_V/3.1 = 0.28$ ), and  $d = 3$  kpc from the interstellar absorption, but Iijima (2006) revised the value to  $(m-M)_V = 14.0$  for  $E(B-V) = 0.57 \pm 0.05$  and  $d = 2.8$  kpc. Evans et al. (2003) obtained  $(m-M)_V = 14.9$ ,  $A_V = 1.9$  ( $E(B-V) = A_V/3.1 = 0.61$ ), and  $d = 4$  kpc using the MMRD relation and the Eddington limit of a  $0.67 M_\odot$  WD

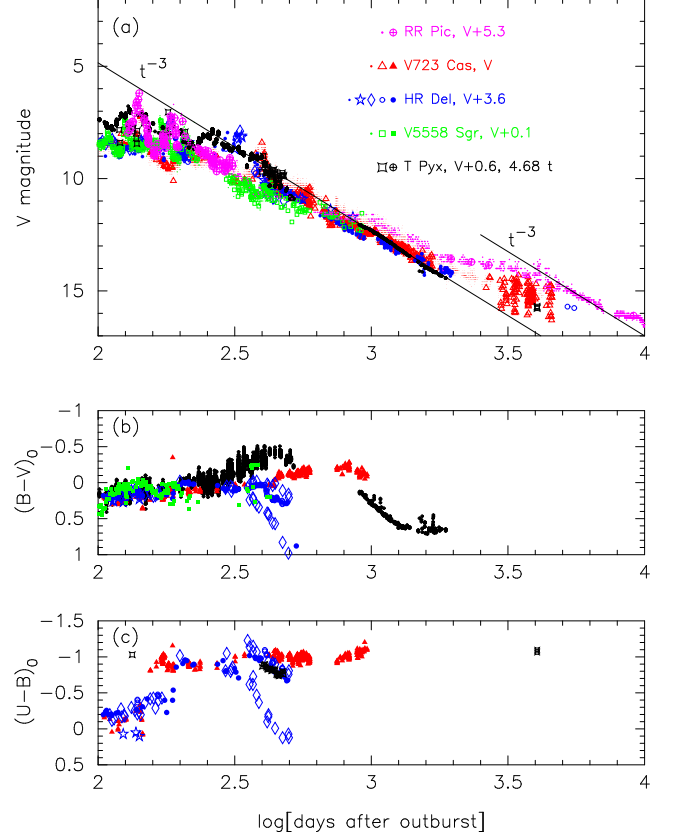


FIG. 21.— Same as Figure 20, but on a logarithmic timescale. Data for T Pyx (black symbols) are added for comparison (see Section 6.5). The data for T Pyx are taken from the AAVSO archive. We stretched the light curve of T Pyx by 4.68 and shifted the magnitudes down by 0.6 mag against that of V723 Cas. The late phase  $V$  light curves of these novae follow a  $t^{-3}$  law for a uniform expansion of constant nebular mass.

( $M_V = -6.59$ ), together with the apparent flat peak magnitude of  $m_V = 8.25$ . However, their assumed absolute magnitude of  $M_V = -6.59$  is too bright for a nova on a low-mass WD (see, e.g., Equations (3) and (4) of Hachisu & Kato 2004). As a result, their obtained value of  $(m-M)_V = 14.9$  is too large. If we adopt  $M_V = -5.3$  (Hachisu & Kato 2004) for a low-mass WD and  $m_V = 8.25$  above, the distance modulus becomes  $(m-M)_V = 13.6$ , which is much smaller than  $(m-M)_V = 14.9$  and roughly consistent with the other values mentioned above.

Ness et al. (2008) criticized the application of the MMRD relations to very irregular light curves. Instead, they assumed that the absolute magnitude of V723 Cas is the same as that of HR Del, because they are similar types of novae. They obtained  $(m-M)_V = 13.7$ ,  $E(B-V) = 0.5 \pm 0.1$ , and  $d = 2.7^{+0.4}_{-0.3}$  kpc. Hachisu & Kato (2004) obtained the distance modulus of  $(m-M)_V = 13.9$  for a  $0.59 M_\odot$  WD with a solar composition envelope, by comparing their blackbody light curves with observations. Hachisu & Kato could not specify  $E(B-V)$  but proposed  $d = 2.5$  kpc for  $E(B-V) = 0.6$  and  $d = 4.0$  kpc for  $E(B-V) = 0.3$ . Thus, the resultant distance modulus to V723 Cas was not very scattered and fell in a relatively narrow range of  $(m-M)_V = 13.6-14.0$ .

The interstellar extinction toward V723 Cas was also estimated by many authors, but their values are quite scattered. In increasing order, Rudy et al. (2002) obtained  $E(B-V) = 0.20 \pm 0.12$  in 1999 August and  $0.25 \pm 0.1$  in 2000 July from the Paschen and Brackett lines. Iijima et al. (1998) obtained  $E(B-V) = 0.29$  from the reddening of field stars near the lo-

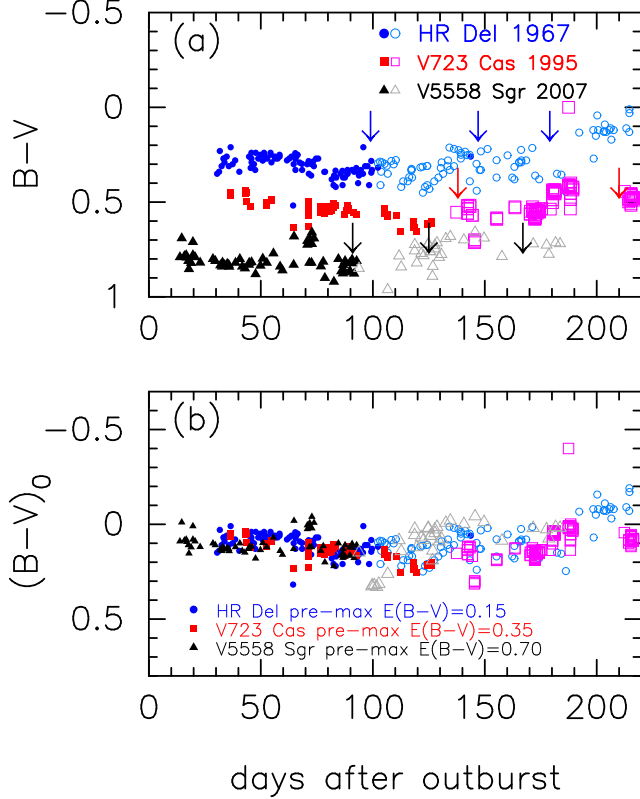


FIG. 22.— (a) Observed  $B-V$  colors of three novae, HR Del, V723 Cas, and V5558 Sgr. Downward arrows indicate first three flaring peaks of novae, which are the same as those in Figure 19. We use filled and open symbols to denote data before and after the first flaring peak, respectively. The data for HR Del are taken from O’Connell (1968), Mannery (1970), Barnes & Evans (1970), and Onderlička & Vetešník (1968). The data for V723 Cas are taken from Chochol & Pribulla (1997). The data for V5558 Sgr are taken from the AAVSO and VSOLJ archives. (b) Intrinsic  $(B-V)_0$  colors of the three novae. We estimated the interstellar extinctions by assuming that the colors of these three novae are the same in the pre-maximum phase. Here we fix the extinction of HR Del to be  $E(B-V) = 0.15$ . The obtained extinctions are  $E(B-V) = 0.35$  for V723 Cas and  $E(B-V) = 0.70$  for V5558 Sgr.

cation of V723 Cas. Munari et al. (1996) obtained  $E(B-V) = 0.45$  from interstellar Na I D double lines. Ness et al. (2008) estimated the extinction to be  $E(B-V) = 0.5 \pm 0.1$  from various values in the literature and their  $N_H$  value from X-ray spectrum model fits. Chochol & Pribulla (1997) obtained  $E(B-V) = 0.57$  from the intrinsic colors at maximum and at two magnitude below maximum. González-Riestra et al. (1996) gave  $E(B-V) = 0.60$  from the 2200Å dust absorption feature. Evans et al. (2003) derived  $E(B-V) = 0.78 \pm 0.15$  from the IR H I recombination lines.

The galactic extinction is  $E(B-V) = 0.39$  in the direction of V723 Cas from the dust map of Schlegel et al. (1998), where the galactic coordinates of V723 Cas are  $(l, b) = (124^\circ 96' 06'', -8^\circ 80' 68'')$ . The HEASARC  $N_H$  tool yields  $N_H = 2.1 \times 10^{21}$  for LAB (Leiden/Argentine/Bonn; Kalberla et al. 2005) and  $2.4 \times 10^{21} \text{ cm}^{-2}$  for DL (Dickey & Lockman 1990), respectively. If we use the relation of  $E(B-V) = N_H / 5.8 \times 10^{21} \text{ cm}^{-2}$  (Bohlin et al. 1978) (or the recent relation of  $E(B-V) = N_H / 8.3 \times 10^{21} \text{ cm}^{-2}$  (Liszt 2014)), the extinction is  $E(B-V) = 0.4$  (or  $E(B-V) = 0.29$ ). The recent NASA/IPAC dust map gives  $E(B-V) = 0.34 \pm 0.01$ . Therefore, the extinction could be around  $E(B-V) \sim 0.35$  if the circumstellar absorption is negligible.

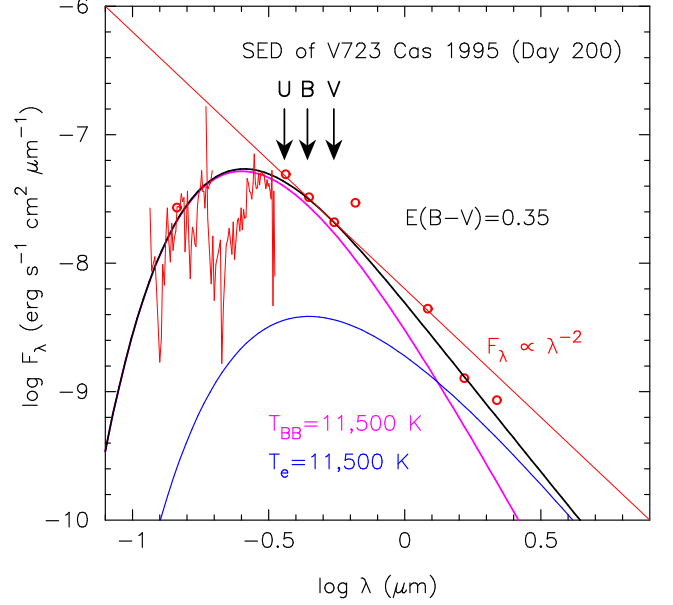


FIG. 23.— Same as Figure 18, but for V723 Cas about 200 days after the outburst. Observed  $UBV$  fluxes are taken from Chochol & Pribulla (1997) and  $JHK$  fluxes are taken from Kamath & Ashok (1999).  $IUE$  UV spectra (SWP56799 and LWP31977) are taken from the INES archive data server. We also plot the UV1455Å flux. All fluxes denoted by red open circles and red thin solid lines are dereddened with  $E(B-V) = 0.35$ . Global features of spectrum can be fitted with combination (black solid line) of blackbody with temperature  $T_{BB} = 15,500 \text{ K}$  (magenta solid line) and optically-thick, free-free emission with electron temperature  $T_e = 15,500 \text{ K}$  (blue solid line). In the region of the  $UBV$  bands, the SED is close to that of optically-thin, free-free emission of  $F_\lambda \propto \lambda^{-2}$  (red thin solid line).

González-Riestra et al. (1996) obtained a large value of  $E(B-V) = 0.6$  on the basis of the strength of the 2175 Å absorption feature in the  $IUE$  spectra taken in 1996 January, approximately 150 days after the outburst. This value must be taken as an upper limit, because it was obtained from spectra taken while the nova was still in an optically-thick state, and may have been affected by an additional circumstellar absorption. To confirm this effect, R. González-Riestra (2012, private communication) examined  $IUE$  spectra taken later in the outburst, and obtained color excess values of 0.34, 0.33, and 0.25 for days 160, 172, and 176 after the outburst, respectively, all with an uncertainty of  $\pm 0.05$ . These values are much smaller than that of 0.60 obtained 150 days after the outburst. Therefore, she concluded that the reddening toward V723 Cas is  $E(B-V) = 0.30 \pm 0.05$ .

The reddening can be estimated by another method based on the similarity of the three novae, HR Del, V723 Cas, and V5558 Sgr. Figure 22(a) shows the  $B-V$  color evolution of these three novae during the first 200 days, that is, in the flat pre- and post-maximum phase. The positions of flaring pulses are indicated by downward arrows. Figure 22(b) shows HR Del dereddened with  $E(B-V) = 0.15$  (see Section 5.3). We also plot the data for V723 Cas and V5558 Sgr shifted upward by 0.35 and 0.70, respectively, to match their data with those of HR Del. In our fitting process, we changed the  $E(B-V)$  value by steps of 0.05, so the possible systematic error is 0.05. If the intrinsic colors  $(B-V)_0$  of these three very slow novae are the same in the pre-maximum phase,  $E(B-V)$  is about 0.35 for V723 Cas, which is consistent with the new estimates by González-Riestra and the value in the dust map on the NASA/IPAC web site.

Recently, Lyke & Campbell (2009) obtained a distance



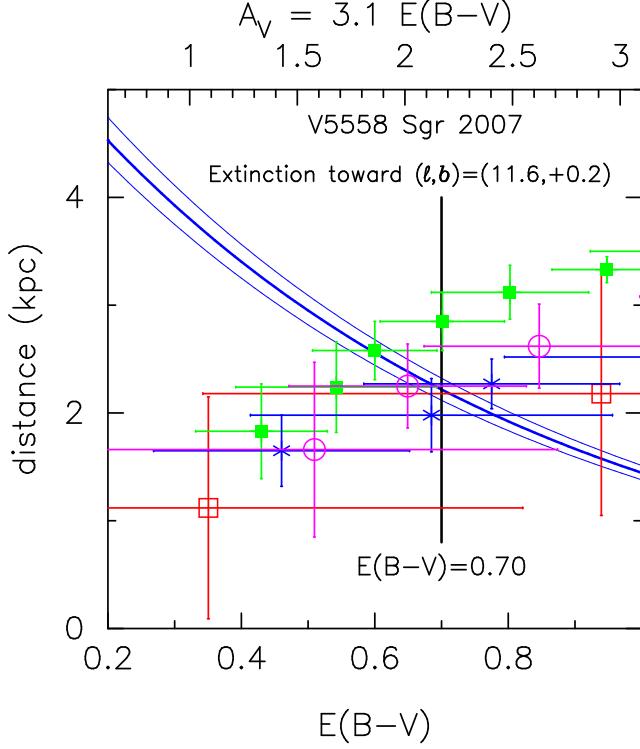


FIG. 24.— Distance-reddening relation toward V5558 Sgr. Blue thick solid line flanked by blue thin solid lines denotes the distance-reddening relation of  $(m-M)_V = 13.9 \pm 0.1$ . Four sets of data with error bars show distance-reddening relations in four directions close to V5558 Sgr:  $(l, b) = (11.5, +0.0)$  (red open squares),  $(11.75, +0.0)$  (green filled squares),  $(11.5, +0.25)$  (blue asterisks), and  $(11.75, +0.25)$  (magenta open circles); data are taken from Marshall et al. (2006). Vertical black solid line represents color excess  $E(B-V) = 0.70$ .

of  $d = 3.85^{+0.23}_{-0.21}$  kpc to V723 Cas from the expansion parallax method. If we adopt this distance and reddening  $E(B-V) = 0.35$ , we obtain the distance modulus  $(m-M)_V = 5 \log 3850/10 + 3.1 \times 0.35 = 14.0$ , which is perfectly consistent with Equation (11). Therefore, we use  $d = 3.85$  kpc and  $E(B-V) = 0.35$  for V723 Cas.

Figure 23 shows the dereddened spectrum of V723 Cas about 200 days after the outburst. The broadband spectrum can be reproduced by a combination of a blackbody ( $T_{BB} = 11,500$  K) and free-free ( $T_e = 11,500$  K) emission, as introduced in the previous section. The *UBV* magnitudes are closely fitted with only a blackbody of  $T_{BB} = 11,500$  K and, at the same time, are fitted with the spectrum of optically-thin free-free emission ( $F_\nu \propto \nu^0$  or  $F_\lambda \propto \lambda^{-2}$  represented by a red thin solid line). Therefore, its position is close to point 0 in the color-color diagram. We discuss the color-color evolution of V723 Cas in Section 5.6 below.

### 5.5. V5558 Sgr 2007

V5558 Sgr was discovered by Sakurai (Nakano et al. 2007) at mag 10.3 on UT 2007 April 14.777. Sakurai also reported that nothing is visible on an image taken on UT April 9.8 (limiting mag 11.4). The star was also detected by Haseda (Yamaoka et al. 2007) at mag 11.2 on UT April 11.792. Because the outburst day is not known, we adopted UT 2007 April 8.5 as the outburst day, i.e.,  $t_{OB} = \text{JD } 2454199.0$ . The optical light curve and color evolution are shown in Figures 19, 20, 21, and 22.

We found in the literature two different estimates for the reddening: one  $E(B-V) = 0.36$  was obtained by Munari et al.

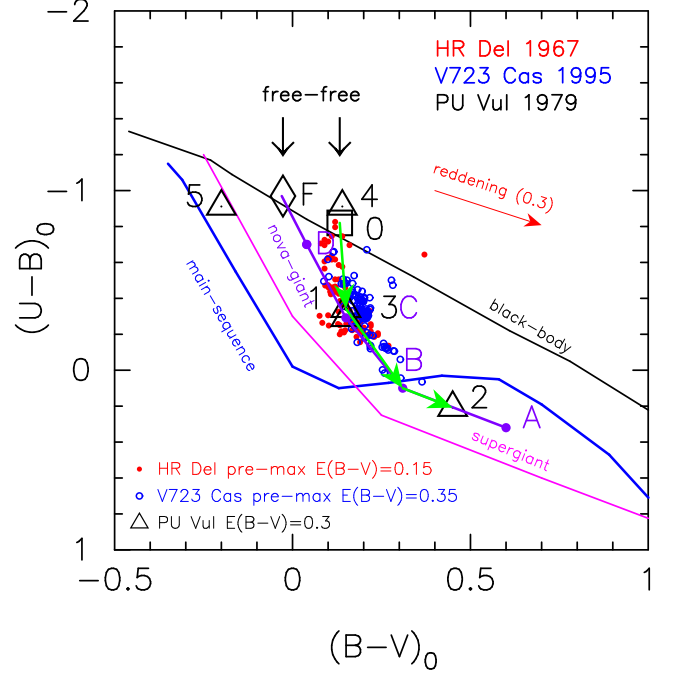


FIG. 25.— Same as Figure 16, but for the pre-maximum phases of HR Del (red filled circles) and V723 Cas (blue open circles). Large open square denotes stage 0 for the  $F_\nu \propto \nu^0$  optically-thin, free-free emission. Green arrows indicate evolutionary paths of HR Del and V723 Cas. It seems that both HR Del and V723 Cas started at stage 0 and then moved to 1, B, and 2. We indicated the direction of reddening by a red arrow, the length of which corresponds to  $E(B-V) = 0.3$ .

(2007) from the Na I D lines, and the other  $E(B-V) = 0.8$  was obtained by Rudy et al. (2007) from the O I lines. Our estimate in the previous subsection,  $E(B-V) = 0.70$ , is consistent with Rudy et al.'s value but much larger than Munari et al.'s. Because these two values are very different, we further examine  $E(B-V)$  from a different point of view. In the previous subsections, we showed the similarity of the absolute magnitudes of HR Del, V723 Cas, and PU Vul in the pre-maximum phase (see Figure 19). Thus, we derived  $(m-M)_{V, V5558 \text{ Sgr}} = 13.9$ , assuming that V5558 Sgr has the same absolute magnitude in the pre-maximum phase. This distance modulus was confirmed and calibrated using the similarity of the light curves to that of RR Pic (see Equation (11)). Using this distance modulus in the *V* band, we derived a distance-reddening relation, i.e.,  $(m-M)_V = 13.9 \pm 0.1$ , together with Equation (2). Figure 24 shows this distance-reddening relation as a blue thick solid line flanked with two blue thin solid lines, which correspond to  $\pm 0.1$  mag error.

This figure also shows the distance-reddening relations for four directions near V5558 Sgr, whose galactic coordinates are  $(l, b) = (11.6107, +0.2067)$ . The closest distance-reddening relation, which is denoted by blue asterisks, crosses the blue thick line at or near the vertical black solid straight line of  $E(B-V) = 0.70$ . Thus, we use  $E(B-V) = 0.70$  and  $d = 2.2$  kpc in this paper.

The distance to V5558 Sgr was also estimated by Poggiani (2010). Using various MMRD relations, she obtained a distance modulus of  $(m-M)_V = 12.4\text{--}12.8$ , which is much smaller than our value of  $(m-M)_V = 13.9$ . This suggests that the MMRD relations are problematic in calculating the absolute magnitude of very slow novae such as V5558 Sgr.



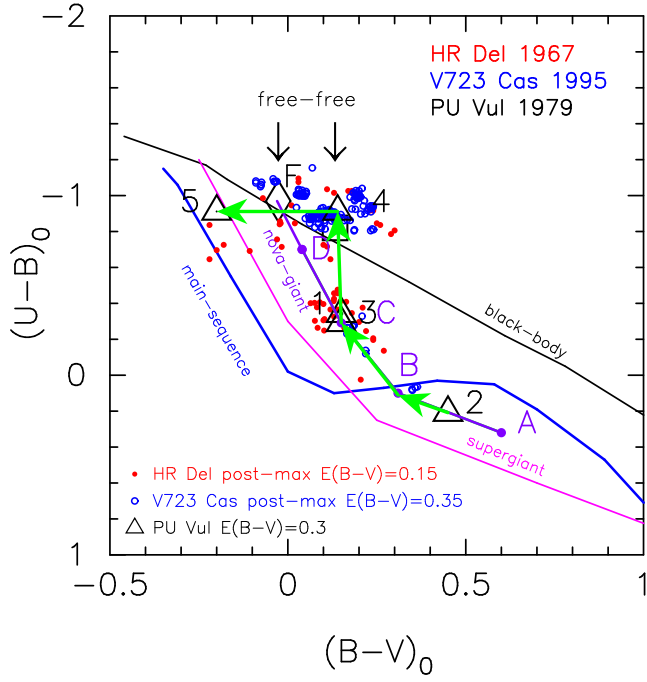


FIG. 26.— Same as Figure 25, but for the post-maximum phases of HR Del (red filled circles) and V723 Cas (blue open circles).

### 5.6. Color-color Evolution of Very Slow Novae HR Del and V723 Cas

Many authors have discussed the resemblance between HR Del and V723 Cas in their light curves and spectral evolution (e.g., Friedjung & Iijima 2002; Evans et al. 2003). We noted another resemblance in the color evolution of HR Del and V723 Cas in the pre-maximum phase. Figure 25 depicts the color-color evolution of V723 Cas (blue open circles) and HR Del (red filled circles) in the pre-maximum phase. These novae follow almost the same track as PU Vul (large, black, open triangles). Unfortunately, no  $U$ -band data are available for V5558 Sgr, but we expect that this nova also shows a similar evolution in the color-color diagram.

The only difference with respect to PU Vul is that HR Del and V723 Cas started their very early evolutions from point 0, which represents the position of optically-thin, free-free emission. This is because they had optically-thin winds in the very early phase of their outbursts. Iijima et al. (1998) reported prominent emission lines of H I and Fe II with a P-Cygni profile in an early stage of the pre-maximum phase of V723 Cas. We regard this early pre-maximum phase with winds as stage 0 (see Figure 25). Similar winds in the very early pre-maximum phase were also reported for HR Del (Rafanelli & Rosino 1978) and V5558 Sgr (Tanaka et al. 2011). Iijima et al. (1998) observed that the emission lines of V723 Cas gradually weakened with time as absorption components developed. Then, the pure absorption spectra of F-type supergiants appeared near optical maximum. Similar spectral features were also observed in HR Del (Rafanelli & Rosino 1978) and V5558 Sgr (Tanaka et al. 2011). We regard this late, pre-maximum phase with virtually no winds as stage 1, point B, and stage 2 (Figure 25). This is consistent with our interpretation that the pre-maximum evolution of V723 Cas is represented essentially by a static evolution with virtually no wind mass loss, like that of in PU Vul.

Figure 26 shows the color-color diagram in the post-maximum phase of V723 Cas and HR Del. In

Kato & Hachisu (2011), the nova entered the optically thick wind phase after the transition from a static to a wind configuration, i.e., after the relaxation oscillation. V723 Cas moved from stages 3 to 4 (near stage 0) after optical maximum (and the relaxation oscillation). The position of stage 4 is close to point 0 (optically-thin, free-free emission), because the wind mass-loss rate is relatively small and the free-free emission makes a small contribution to the  $UBV$  band region, as shown in Figures 18 and 23. The blueward excursion in  $(B-V)_0$  from stages 4 to 5 is mainly due to the effects of strong emission lines, as already discussed in the previous section. In this way, we found that V723 Cas evolved from stage 0 to stages 1, 2, 3, 4, and 5.

The evolution of HR Del is also plotted in Figures 25 and 26. It also started at stage 0 and moved to 1 and then went to a midway point with respect to 2; it then returned to 3, jumped up to 4 and finally moved to 5. Even in the post-maximum phase, the color evolutions of HR Del, V723 Cas, and PU Vul almost overlap each other (Figure 26). In PU Vul, the phase from 3 to 4 corresponds to the epoch in which optically-thin winds began to blow. In HR Del and V723 Cas, this phase corresponds to the phase after the transition from a static to a wind configuration. In much less massive WDs ( $\sim 0.6 M_\odot$ ), optically-thick winds are relatively weak so the wind mass-loss rate is not as large as in fast novae, as already described in Section 3. As a result, these very slow novae evolve to point 4, which is very close to point 0, which corresponds to optically-thin, free-free emission. This is why the evolutionary paths resemble that of PU Vul.

Figure 27 shows a schematic illustration of the evolution of these very slow novae. In the very early stage of the pre-maximum phase, optically-thin winds are accelerated because the photospheric temperature is high. In very slow novae, the rising phase lasts long enough to be spectroscopically observed. This stage corresponds to stage 0 on the color-color diagram (e.g., Figure 25) and in Figure 27(a). The position of point 0 is defined by the spectrum of optically-thin free-free emission ( $F_\nu \propto \nu^0$ ) but it happens to be close to the black-body sequence. The spectra of slow novae at this early stage are close to that of a blackbody in the  $UBV$  wavelength region because prominent emission lines of H I and Fe II dominate and fill the Balmer jump so the resultant  $U-B$  color is close to that of a blackbody. The emission lines gradually weakened with time, and absorption components developed as the photospheric temperature decreased. The optically-thin winds virtually stop. The absorption spectra of F-type supergiants appeared at this optical maximum stage. The nova enters stages 1, 2, and then 3 in Figures 25, 26, and in Figure 27(b). During these stages, we directly observe the photospheric emission of an F-type supergiant. Therefore, the nova evolves along the nova-giant sequence. After the transition from a static to a wind configuration, the nova entered the wind phase, in which optically-thick winds are accelerated and the mass-loss rate is much higher than in the early rising phase. Then the position in the color-color diagram returns again to the wind phase at point 4 slightly above point 0. This stage is illustrated in Figure 27(c), and the spectrum of V723 Cas is plotted in Figure 23. The spectrum in the  $UBV$  region is very close to that of optically-thin free-free emission, i.e.,  $F_\nu \propto \nu^0$  or  $F_\lambda \propto \lambda^{-2}$  (thin red line). The final excursion from stages 4 to 5 is mainly due to the development of strong emission lines in the nebula (winds), as discussed in the previous sections.

## (a) very early phase (b) pre-maximum (c) post-maximum

stage 0

stage 1,2,3

stage 4,5

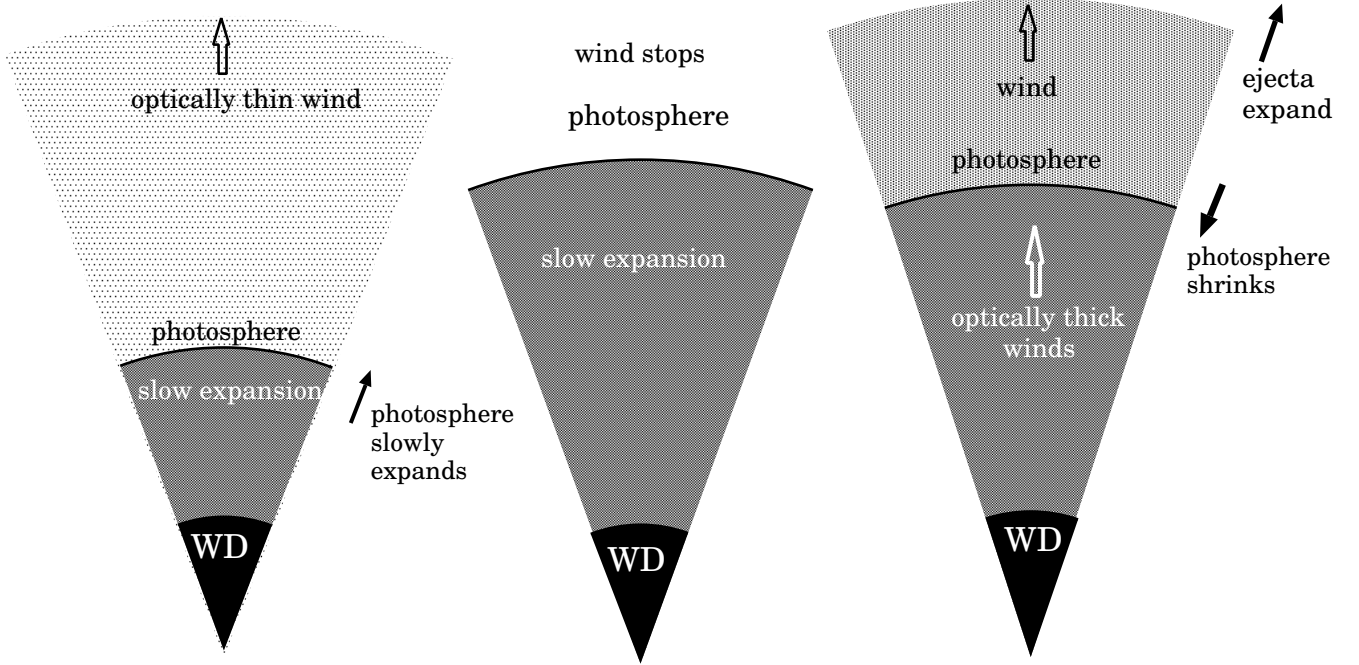


FIG. 27.— Schematic illustration of envelope structures in very slow novae such as HR Del, V723 Cas, and V5558 Sgr. (a) Optically-thin winds blow in the very early (rising) phase, which corresponds to stage 0 in Figure 25. The photospheric temperature is high enough to blow optically-thin winds in the rising phase of the novae. Here the term “optically-thin wind” means that winds are accelerated outside the photosphere, i.e., in the optically-thin region. The WD envelope is close to a static configuration, so the wind velocity is much higher than that of the photospheric expansion. (b) Emission lines gradually weaken with time, and absorption components develop. The optically-thin winds virtually stop. Near optical maximum, the nova spectra resemble the absorption spectra of F-type supergiants. We regard this phase as stage 1, 2, or 3. (c) After the transition from a static to a wind configuration, the nova entered the optically-thick wind phase. Here the term “optically-thick wind” means that winds are accelerated deep inside the photosphere, i.e., in the optically-thick region. The position in the color-color diagram returns again to the wind phase (stage 4 near stage 0). Final excursion from stage 4 to 5 is mainly due to the development of strong emission lines.

In this way, these very slow novae follow essentially the same path on the color-color diagram as that deduced from FH Ser and other traditional novae. The small difference comes from the difference in the wind mass-loss rates, that is, optically-thin/thick winds (Figure 27). Thus, the color-color evolutions are almost the same among these novae, because the physics involved is the same.

## 6. ESTIMATES OF EXTINCTION TOWARD VARIOUS NOVAE

### 6.1. General Course of UBV Color-Color Evolution

We studied the color-color evolution of novae in the  $(B-V)_0 - (U-B)_0$  diagram and showed that well-observed novae follow very similar evolutionary courses in the intrinsic color-color diagram. There are slight differences among them, and we summarize these differences in Figure 28. Here, we specified four templates, (1) the moderately fast nova FH Ser, a prototype of the nova-giant sequence, (2) the slow nova PW Vul and the very fast nova V1500 Cyg, (3) the fast novae V1668 Cyg and V1974 Cyg, and (4) the symbiotic nova PU Vul and the very slow novae V723 Cas and HR Del. The tracks are characterized by several specified points (A, B, C, D, F, 0, 1, ..., 5, 4', 5', 4'', and 5'''; see Table 1 for their values). Figure 29(a) shows the templates of these eight well-observed novae. It is again remarkable that these different types of no-

vae follow similar tracks in the color-color diagram. Because these eight well-observed novae follow the templates in Figure 29(a), we expect that many other novae also follow the same path. In other words, if all the novae follow this template, we can determine the color excess of a target nova by directly comparing its track in the color-color diagram with our general track in Figure 29(a). This is a new method for obtaining the color excesses of classical novae.

In this section, we determine the color excesses of various novae using our general color-evolution tracks found in this work. We collected as many novae from the literature as possible that have sufficient data points (usually more than 10). We assume that all the novae follow the color-color evolution tracks in Figure 29(a). (Compare specifically one of the tracks in Figure 28.) To obtain  $E(B-V)$ , we changed  $E(B-V)$  by steps of 0.05 to fit the observed track of a target nova with our general tracks in Figure 28. Thus, the possible error of the resultant  $E(B-V)$  is  $\pm 0.05$ . In what follows, we will show our target 19 novae in the order of discovery. Their color-color diagrams are summarized in Figures 29 — 33 and the distance-reddening relations toward the target novae are shown in Figures 34 — 37.

### 6.2. RS Oph 1958

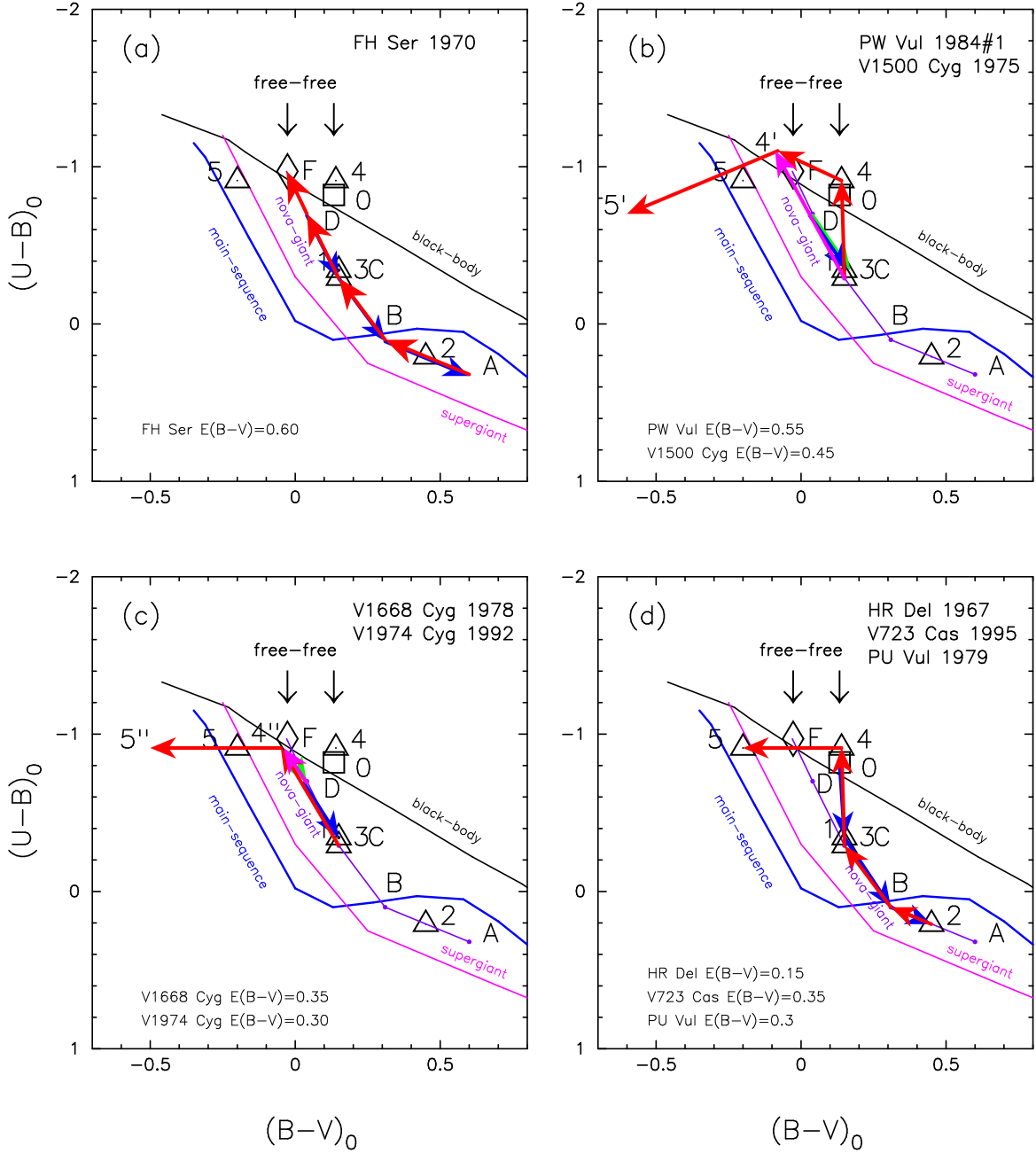


FIG. 28.— Typical templates for novae in the intrinsic  $(B-V)_0$  vs.  $(U-B)_0$  color-color diagram. (a) FH Ser, (b) PW Vul (blue/red) and V1500 Cyg (green/magenta), (c) V1668 Cyg (blue/red) and V1974 Cyg (green/magenta), (d) PU Vul, HR Del, and V723 Cas. Various symbols and lines have the same meanings as in Figures 4 and 17. Blue/green arrows show rising phase of novae; red/magenta arrows indicate declining phase. See text for more details.

RS Oph is a recurrent nova with six recorded outbursts, in 1898, 1933, 1958, 1967, 1985, and 2006. We plot the  $V$  light curve,  $(B-V)_0$  and  $(U-B)_0$  color evolution of RS Oph outbursts in the Appendix (Figure 42) and the color-color evolution of the 1958 outburst in Figure 29(b), where the  $UBV$  data are taken from Connelley & Sandage (1970). We obtained  $E(B-V) = 0.65 \pm 0.05$  by fitting. This value is roughly consistent with those obtained by Snijders (1987), i.e.,  $E(B-V) = 0.73 \pm 0.06$  from the He II line ratio of 1640Å and 3203Å, and  $E(B-V) = 0.73 \pm 0.10$  from the 2715Å interstellar dust absorption feature.

We examine the distance-reddening relation using the data given by Marshall et al. (2006) as shown in Figure 34(a). The galactic coordinates of RS Oph are  $(l, b) =$

$(19^\circ 7995, +10^\circ 3721)$ . In the figure, we plot two relations in the direction close to RS Oph. These two different directions are  $(l, b) = (19^\circ 75, 10^\circ 00)$  (red open squares) and  $(20^\circ 0, 10^\circ 00)$  (green filled squares), both with error bars. Here we also plot the distance modulus of RS Oph,  $(m-M)_V = 12.8$  (blue solid line), which was calculated using the time-stretching method in the Appendix (Figure 42). We also obtained another distance-reddening relation by UV 1455Å fitting (magenta solid line) in Figure 34(a).

In Figure 34(a), four trends,  $E(B-V) = 0.65$  (vertical black solid line),  $(m-M)_V = 12.8$  (blue solid line), UV 1455Å fitting (magenta solid line), and distance-reddening relation of Marshall et al. (2006), consistently cross at  $E(B-V) \sim 0.65$  and  $d \sim 1.4$  kpc. If we adopt  $d \sim 1.4$  kpc, the galactic

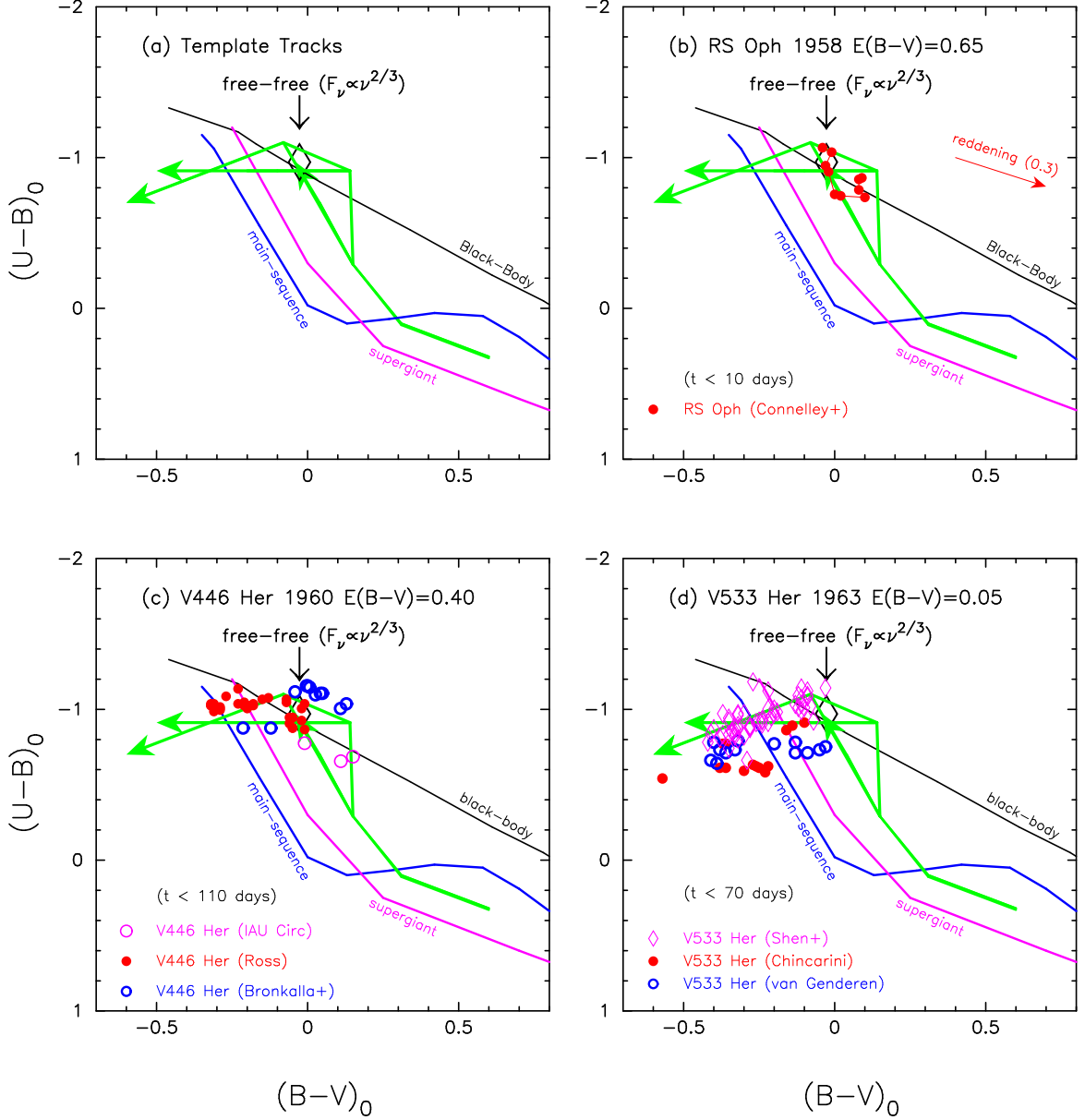


FIG. 29.— Same as Figure 8, but for (a) typical templates of tracks, (b) RS Oph 1958, (c) V446 Her 1960, and (d) V533 Her 1963. Green lines with an arrow indicate several general tracks of nova color-color evolution, as shown in Figure 28. We obtained the following color excesses for these three novae: (b)  $E(B-V) = 0.65$  for RS Oph, (c)  $E(B-V) = 0.40$  for V446 Her, and (d)  $E(B-V) = 0.05$  for V533 Her. The  $UBV$  data are taken from the literature as noted in each figure.

height of RS Oph is  $z \sim 260$  pc, much above the scale height of the galactic matter distribution ( $\sim 125$  pc, Marshall et al. 2006). The NASA/IPAC galactic dust absorption map gives  $E(B-V) = 0.64 \pm 0.03$  in the direction toward RS Oph, which is also consistent with our value of  $E(B-V) = 0.65 \pm 0.05$  if circumstellar absorption is negligible.

### 6.3. V446 Her 1960

V446 Her was discovered by Olaf Hassel at fifth magnitude on UT 1960 March 7, a few days past maximum (Cragg 1960; Mayall 1963). We plot the  $V$  light curve,  $(B-V)_0$  and  $(U-B)_0$  color evolution of V446 Her in the Appendix (Figure 42). Its maximum magnitude was  $m_V \sim 2.75$  (Mayall 1963; Cohen 1985). Then it rapidly and smoothly declined with  $t_2 = 5$  days (e.g., Cohen 1985) and  $t_3 = 16$  days (e.g., Duerbeck 1981). We plot the color-color evolution of V446 Her in Figure 29(c),

where the  $UBV$  data are taken mainly from Ross (1960) and Bronkalla & Notni (1961). These observations started after the nova had already decayed to  $m_V = 5.5$ , so we missed the early evolution of this nova. We also add three data points (magenta open circles) from IAU Circular No. 1730, which start at about 2.5 mag below the maximum. The observed color evolution started from point 4' (or point F) and reached point 5', as shown in Figure 29(c). We obtained a reddening of  $E(B-V) = 0.40 \pm 0.05$  mainly from the data of Ross (1960), because their data follow the track from point 4' to 5'. The color evolution is very similar to that of PW Vul.

The reddening toward V446 Her was determined to be  $E(B-V) = 0.45 \pm 0.1$  from the galactic absorption (Bronkalla & Notni 1961),  $E(B-V) = A_V/3.1 = (1.7 \pm 0.5)/3.1 = 0.55 \pm 0.15$  from the galactic absorption (Duerbeck 1981),  $E(B-V) = A_V/3.1 = (1.44 \pm 0.12)/3.1 =$

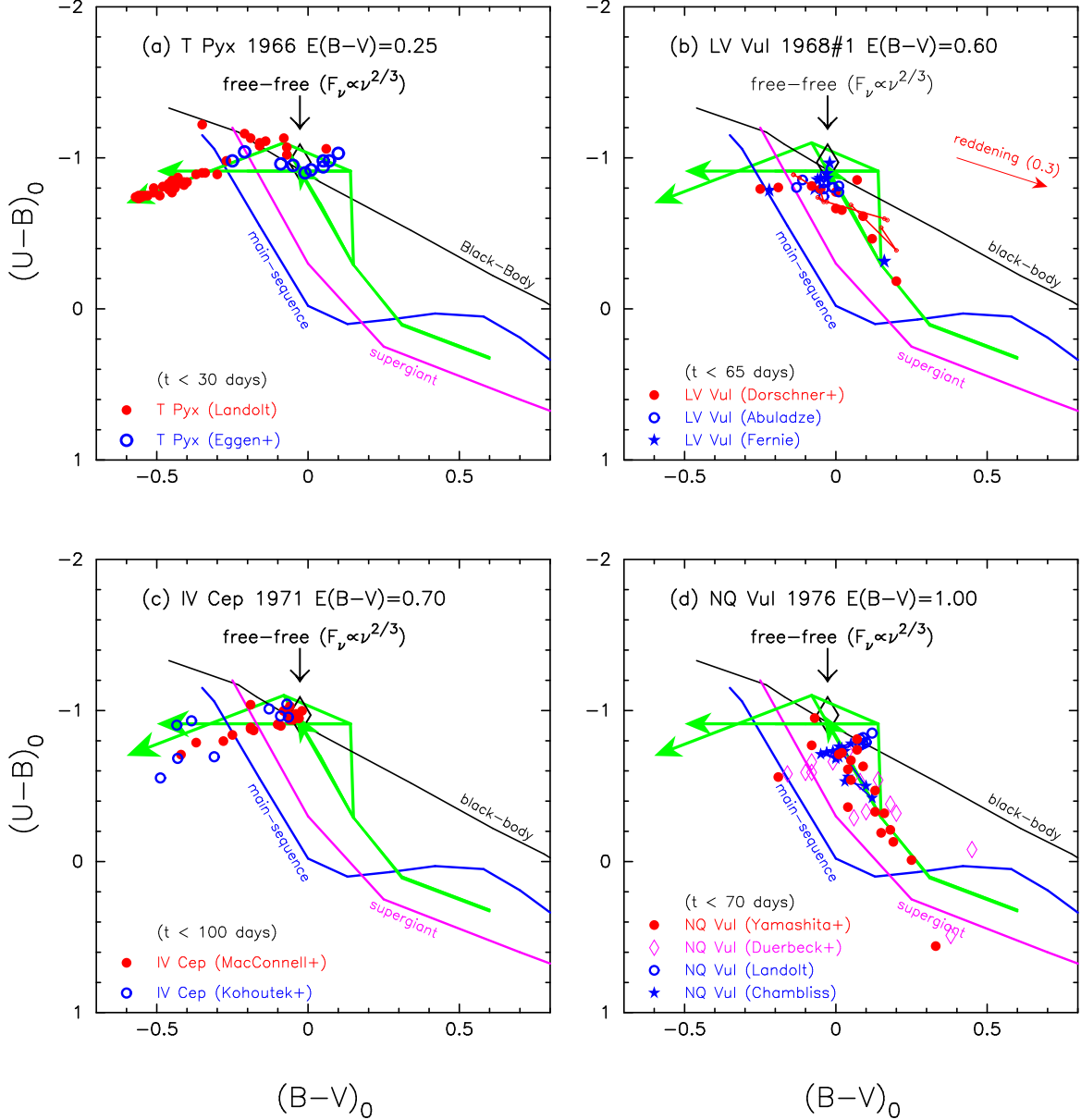


FIG. 30.— Same as Figure 29, but for (a) T Pyx 1966, (b) LV Vul 1968#1, where we add loci of V1500 Cyg (thin red solid lines) only for the very early phase, (c) IV Cep 1971, and (d) NQ Vul 1976.

$0.46 \pm 0.04$  from the value at the stabilization stage (Miroshnichenko 1988),  $E(B-V) = A_V/3.1 = 1.12/3.2 = 0.35$  from the  $2200\text{\AA}$  feature (Gilmozzi et al. 1994),  $E(B-V) = 0.25$  from the depth of the interstellar bump at  $2175\text{\AA}$  (Selvelli 2004). These reddening estimates range from 0.25 to 0.55 and we obtained a simple average of  $E(B-V) = 0.41 \pm 0.15$ , which is consistent with our value.

We further analyzed the distance-reddening relation based on the data given by Marshall et al. (2006), as shown in Figure 34(b). The galactic coordinates of V446 Her are  $(l, b) = (45^\circ 40' 92'', +4^\circ 70' 75'')$ . In the figure, we plot four relations in directions close to V446 Her:  $(l, b) = (45^\circ 25', 4^\circ 50')$  (red open squares),  $(45^\circ 50', 4^\circ 50')$  (green filled squares),  $(45^\circ 25', 4^\circ 75')$  (blue asterisks), and  $(45^\circ 50', 4^\circ 75')$  (magenta open circles), all with error bars. The last magenta open circles correspond to the closest direction. We also plot the distance modulus of V446 Her,  $(m-M)_V = 11.7$  (blue solid line), which was calculated using the time-stretching method in the Ap-

pendix (Figure 42). Three trends,  $E(B-V) = 0.40$  (vertical black solid line),  $(m-M)_V = 11.7$  (blue solid line), and the distance-reddening relation of Marshall et al. (2006), consistently cross at  $E(B-V) \sim 0.40$  and  $d \sim 1.2$  kpc.

#### 6.4. V533 Her 1963

V533 Her was discovered by Leslie Peltier at fourth magnitude on UT 1963 February 6 (Mayall 1963; van Genderen 1963). We plot the  $V$  light curve, and the  $(B-V)_0$  and  $(U-B)_0$  color evolution of V533 Her in the Appendix (Figure 41). It reached third magnitude at maximum on UT January 31 (Mayall 1963; van Genderen 1963). Then it gradually declined with  $t_2 = 22$  days and  $t_3 = 46$  days (e.g., Downes & Duerbeck 2000). We plot the color-color evolution of V533 Her in Figure 29(d), where the  $UBV$  data are taken from van Genderen (1963), Chincarini (1964) and Shen et al. (1964). These three observations started after the nova had already decayed to  $m_V \sim 4.8$ , so we missed its early



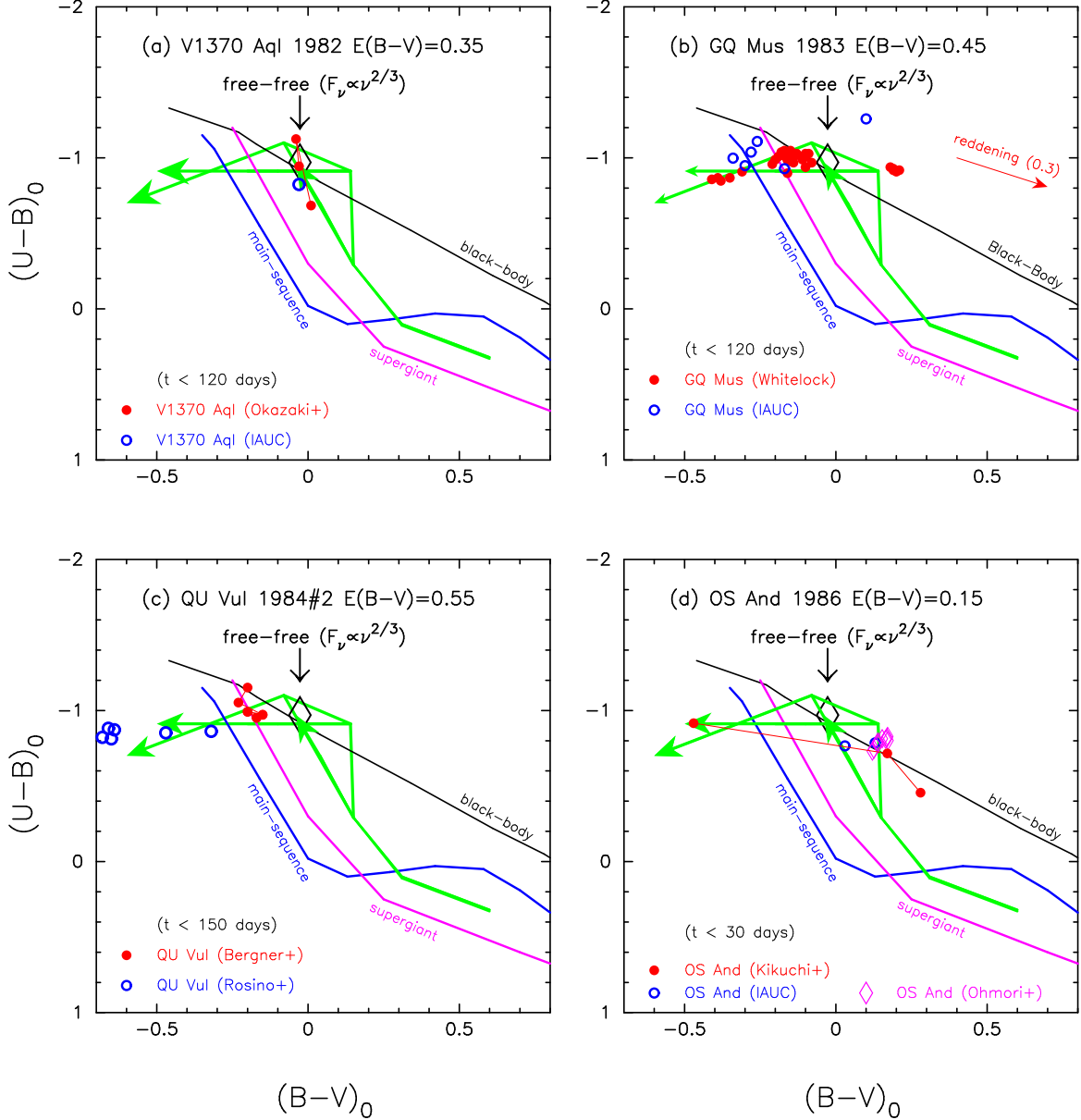


FIG. 31.— Same as Figure 29, but for (a) V1370 Aql 1982, (b) GQ Mus 1983, (c) QU Vul 1984#2, and (d) OS And 1986.

evolution. The observed color evolution started at point 4' (near point F) and reached point 5', as shown in Figure 29(d). We obtained a reddening value of  $E(B-V) = 0.05 \pm 0.05$ , mainly from the early phase data of Shen et al. (1964), because these data (magenta open diamonds) follow the track from point 4' to 5'.

The reddening toward V533 Her was determined to be  $E(B-V) \sim 0.0$  (Verbunt 1987),  $E(B-V) = A_V/3.1 \sim 0.0$  (Gilmozzi et al. 1994), both from the 2200Å feature, and  $E(B-V) = A_V/3.1 = 0.16/3.1 \sim 0.05$  from the value at the stabilization stage (Miroschnichenko 1988). The NASA/IPAC galactic dust absorption map gives  $E(B-V) = 0.038 \pm 0.002$  in the direction toward V533 Her, whose galactic coordinates are  $(l, b) = (69^\circ 1887, +24^\circ 2733)$ . Our value of  $E(B-V) = 0.05 \pm 0.05$  is consistent with these estimates.

### 6.5. T Pyx 1966

T Pyx is a recurrent nova with known outbursts in 1890, 1902, 1920, 1944, 1966, and 2011. We plot the color evo-

lution of the 1966 outburst in Figure 30(a), the *UBV* data of which are taken from Landolt (1970) and Eggen et al. (1967). We obtained  $E(B-V) = 0.25 \pm 0.05$  by fitting. Gilmozzi & Selvelli (2007) also obtained  $E(B-V) = 0.25 \pm 0.02$  from the 2175Å interstellar absorption feature in the *IUE* spectra of T Pyx, which is consistent with our estimate.

The galactic coordinates of T Pyx are  $(l, b) = (257^\circ 2072, +9^\circ 7067)$ . If we assume a distance of  $\sim 4.8$  kpc (Sokoloski et al. 2013), its galactic height is  $z \sim 800$  pc, which is much above the galactic matter distribution of  $\sim 125$  pc. The NASA/IPAC galactic dust absorption map gives  $E(B-V) = 0.24 \pm 0.01$  in the direction toward T Pyx. This value is consistent with our estimate of  $E(B-V) = 0.25 \pm 0.05$  but inconsistent with the value of  $E(B-V) = 0.5 \pm 0.1$  recently estimated by Shore et al. (2011) from the diffuse interstellar band (DIB) features of the 2011 outburst. We think that there is a large scatter in the  $E(B-V)$  versus  $W_\lambda$  (5780Å) relation near  $W_\lambda = 300\text{mÅ}$  that Shore et

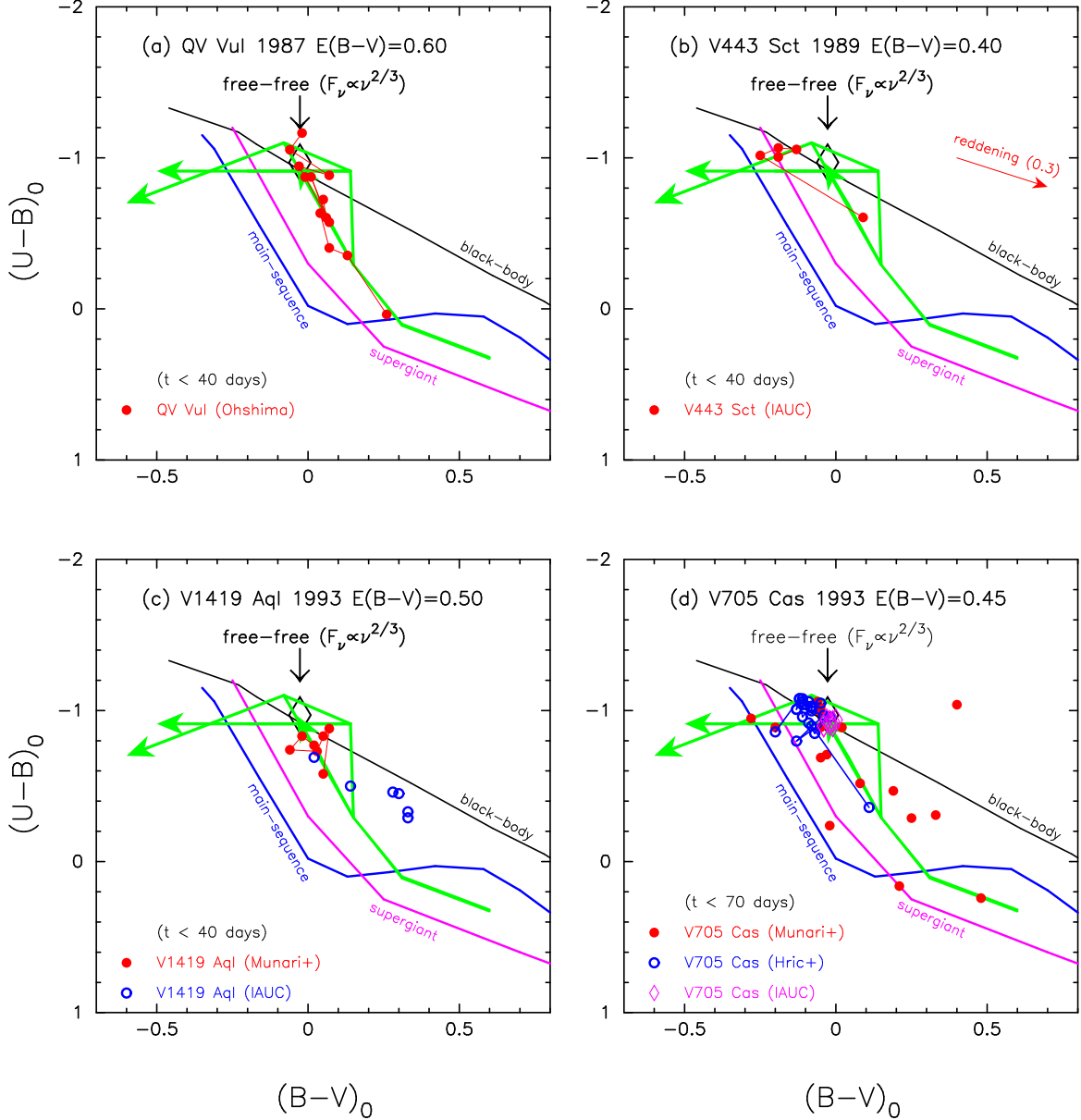


FIG. 32.— Same as Figure 29, but for (a) QV Vul 1987, (b) V443 Sct 1989, (c) V1419 Aql 1993, and (d) V705 Cas 1993.

al. used, where  $W_\lambda(5780\text{\AA})$  is the equivalent width of the 5780Å DIB in units of mÅ (see Figure 4 of Friedman et al. 2011). Therefore, we consider that this empirical relation for the 5780Å DIB does not accurately determine the individual extinctions at least for a range of  $E(B-V) = 0.2-0.8$ .

#### 6.6. LV Vul 1968 No.1

LV Vul was discovered by Alcock (1968) on UT 1968 April 15. We plot the  $V$  light curve and the  $(B-V)_0$  and  $(U-B)_0$  colors of LV Vul in the Appendix (Figure 44). It reached its optical maximum at  $m_V = 4.7$  on April 17. LV Vul has  $t_2 = 20.2$  days and  $t_3 = 37$  days (Tempesti 1972) so it belongs to the class of fast novae. Andrillat et al. (1986) took a spectrum at the pre-maximum phase that showed an F-type spectrum. Therefore, we expect that the early color evolution of LV Vul follows the nova-giant sequence in the color-color diagram. Figure 30(b) shows the color-color evolution, where the  $UBV$  data are taken from Abuladze (1969),

Dorschner et al. (1969), and Fernie (1969). The color-color evolution of LV Vul resembles those of V1500 Cyg and V1668 Cyg. We obtained  $E(B-V) = 0.60 \pm 0.05$  by fitting.

Fernie (1969) determined the reddening toward LV Vul to be  $E(B-V) = 0.6 \pm 0.2$  from the color excesses of 14 B stars near the line of sight, which is consistent with our value. Tempesti (1972) obtained  $E(B-V) = 0.55$  from the color at optical maximum; i.e.,  $E(B-V) = (B-V)_{\text{max}} - (B-V)_{0,\text{max}} = 0.9 - 0.35 = 0.55$ . He adopted  $(B-V)_{0,\text{max}} = +0.35$  (Schmidt 1957) instead of  $(B-V)_{0,\text{max}} = +0.23$  (van den Bergh & Younger 1987).

Using  $E(B-V) = 0.60$  together with the distance modulus  $(m-M)_{V,\text{LV Vul}} = 11.9$  calculated by the time-stretching method in the Appendix (Equation (A7)), we obtain a distance of  $d = 1.0$  kpc. This is consistent with the value of  $d = 0.92 \pm 0.08$  kpc obtained by Slavin et al. (1995) by the expansion parallax method. We compare our results with the distance-reddening relation proposed by Marshall et al. (2006) as shown in Figure 34(c). Four distance-reddening

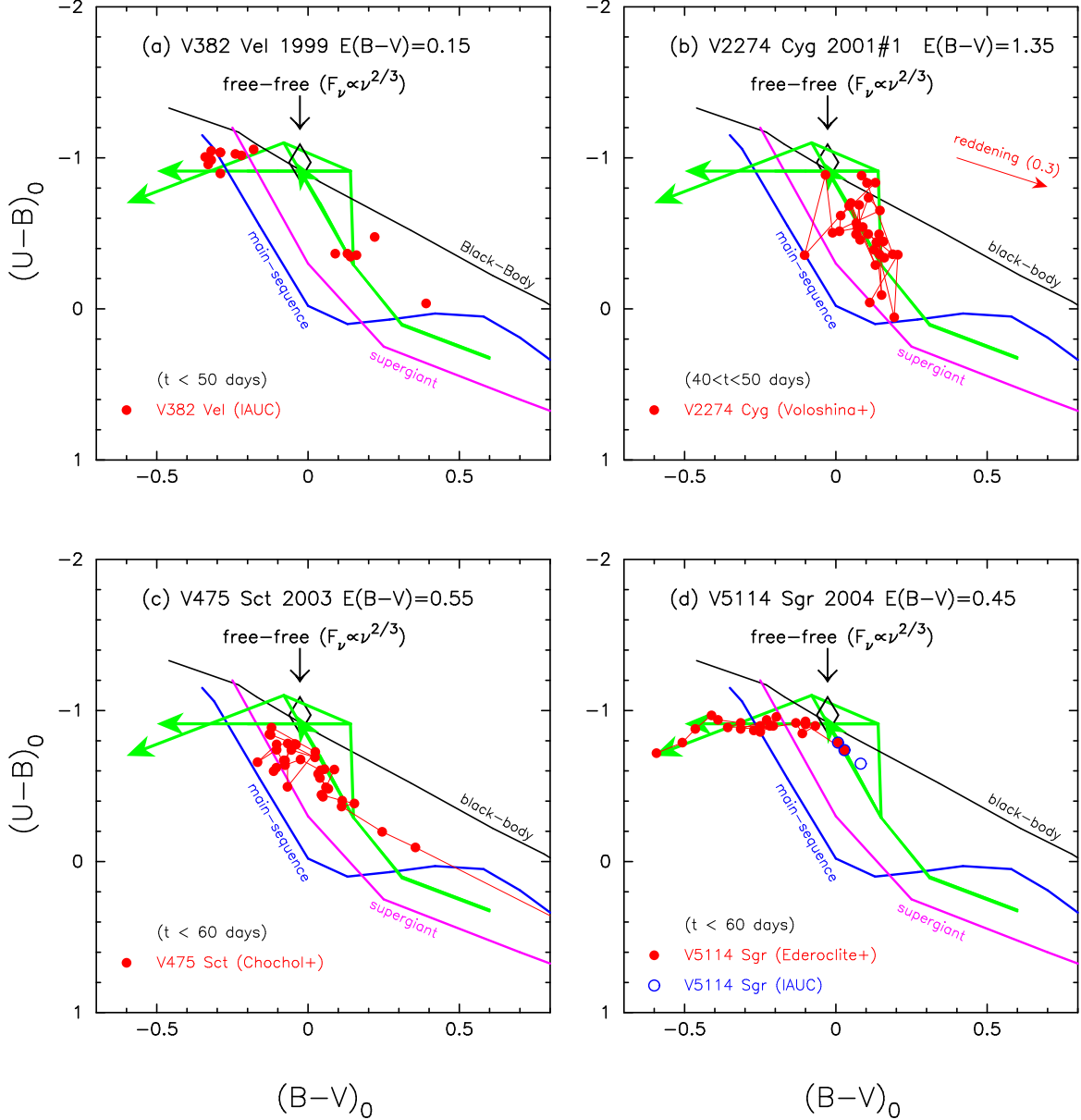


FIG. 33.— Same as Figure 29, but for (a) V382 Vel 1999, (b) V2274 Cyg 2001#1, (c) V475 Sct 2003, and (d) V5114 Sgr 2004.

relations are plotted: toward  $(l, b) = (63^\circ 25, 0^\circ 75)$  (red open squares), toward  $(l, b) = (63^\circ 50, 0^\circ 75)$  (green filled squares), toward  $(l, b) = (63^\circ 25, 1^\circ 00)$  (blue asterisks), toward  $(l, b) = (63^\circ 50, 1^\circ 00)$  (magenta open circles). The closest direction is that denoted by red open squares because the galactic coordinates of LV Vul are  $(l, b) = (63^\circ 3030, +0^\circ 8464)$ . Marshall et al.'s relation gives  $d \sim 3.0$  kpc at  $E(B-V) = 0.60$ . This is not consistent with our estimate of  $d = 1.0$  kpc. On the other hand, Downes & Duerbeck (2000) obtained  $E(B-V) = 0.56 \pm 0.14 = A_V/3.1 = (1.75 \pm 0.42)/3.1$  using the galactic extinction model of Hakkila et al. (1997). Thus, we plot the distance-reddening relation calculated using the model of Hakkila et al. (1997), as shown in Figure 34(c) (black open triangles). This model is consistent with our estimate.

#### 6.7. IV Cep 1971

IV Cep was discovered by Kuwano on UT 1971 July 10 with  $m_V = 8.0$  (Kuwano et al. 1971) a few days after its optical maximum of  $m_{V,\max} = 7.5$  (e.g., Sato et al. 1973;

Rosino 1975). The  $V$  light curve and the  $(B-V)_0$  and  $(U-B)_0$  color evolution of IV Cep are shown in the Appendix (Figures 44, 46, and 47), and the color-color evolution is plotted in Figure 30(c), where the  $UBV$  data are taken from MacConnell & Thomas (1972) (red filled circles) and Kohoutek & Klawitter (1973) (open blue circles). We obtained  $E(B-V) = 0.70 \pm 0.05$  by fitting the cluster of red points with point F (or point 4"). All the  $UBV$  data were obtained after the optical maximum, so the nova had already reached point 4" (near point F) in Figure 28(c). It then moved gradually leftward, like V1974 Cyg, owing to the effects of emission lines. If we use the distance modulus of  $(m-M)_V = 14.7$  calculated by the time-stretching method in the Appendix (Equation (A9)), we obtain a distance of  $d = 3.2$  kpc.

The reddening toward IV Cep was estimated to be  $E(B-V) = 0.8$  (Sato et al. 1973) from the interstellar absorption in the Cepheus region, and  $E(B-V) = A_V/3.1 = 1.8/3.1 = 0.58$  (Thomas et al. 1973) and  $E(B-V) = A_V/3.1 = 1.7/3.1 = 0.55$

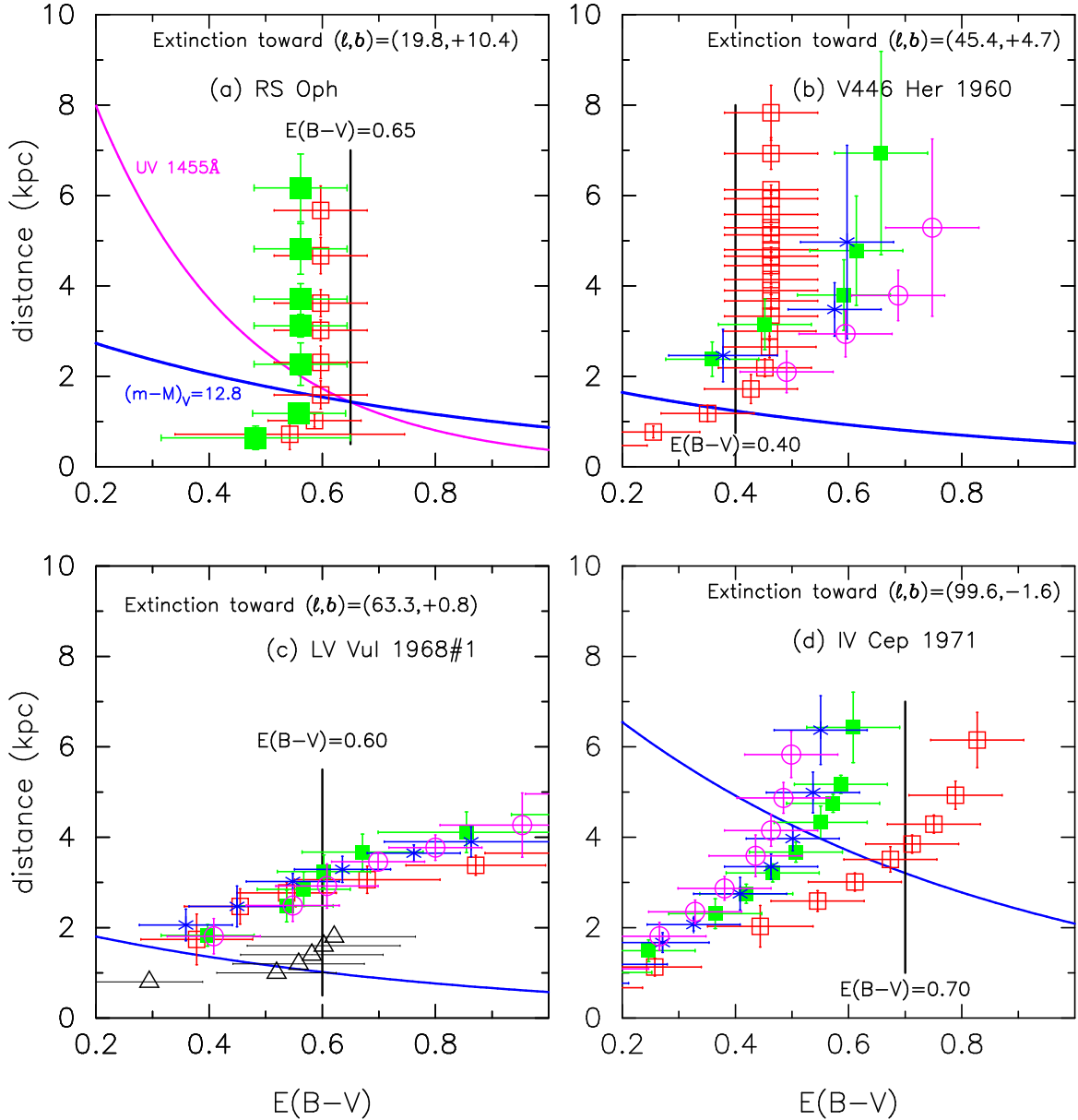


FIG. 34.— Same as Figure 3, but for (a) RS Oph, (b) V446 Her, (c) LV Vul, and (d) IV Cep. Blue solid lines indicate relations (a)  $(m-M)_V = -5 + 3.1E(B-V) + 5 \log d = 12.8$ , (b)  $(m-M)_V = 11.7$ , (c)  $(m-M)_V = 11.9$ , where black open triangles indicate the galactic extinction model of Hakkila et al. (1997), and (d)  $(m-M)_V = 14.7$ . Magenta solid line in (a) denotes the distance-reddening relation of UV 1455Å fitting calculated in the Appendix (Figure 42).

(Kohoutek & Klawitter 1973), both from the absorption-distance relation given by Neckel (1967). We reanalyzed the data using a new distance-reddening relation given by Marshall et al. (2006), as shown in Figure 34(d). We plot four relations in directions close to IV Cep,  $(l, b) = (99.6137, -1.6381)$ :  $(l, b) = (99.5, -1.5)$  (red open squares),  $(99.75, -1.5)$  (green filled squares),  $(99.5, -1.75)$  (blue asterisks), and  $(99.75, -1.75)$  (magenta open circles). The closest direction is that denoted by red open squares. The two trends, i.e., the distance modulus of  $(m-M)_V = 14.7$  (blue thick solid line) and the distance-reddening relation denoted by red open circles, cross consistently at or near  $E(B-V) \approx 0.70$  and  $d \approx 3.2$  kpc. This supports our estimate of  $E(B-V) = 0.70 \pm 0.05$  from the general tracks.

#### 6.8. NQ Vul 1976

NQ Vul was discovered by G. E. D. Alcock (Milbourn et al. 1976) on UT 1976 October 21.7 near optical maximum (Milbourn et al. 1976). It then rose to  $m_V \approx 6.0$  at maximum on UT November 2. We plot the  $V$  light curve and the  $(B-V)_0$  and  $(U-B)_0$  color evolution of NQ Vul in the Appendix (Figures 43 and 48), where the  $UBV$  data are taken from Yamashita et al. (1977), Landolt (1977), Chambliss (1977), and Duerbeck & Seitter (1979). We also plot the  $V$  and visual magnitudes taken from di Paolantonio & Patriarca (1978) and the archive of the American Association of Variable Star Observers (AAVSO), respectively. The  $V$  magnitude of Yamashita et al. (1977) is systematically brighter by 0.2 mag than the other data, so we shifted them down by 0.2 mag. In addition the  $B-V$  and  $U-B$  colors of Yamashita et al. (1977) are systematically bluer by 0.05 and 0.2 mag, respectively, than the other data. Therefore, we shift them down by 0.05 and 0.2 mag,

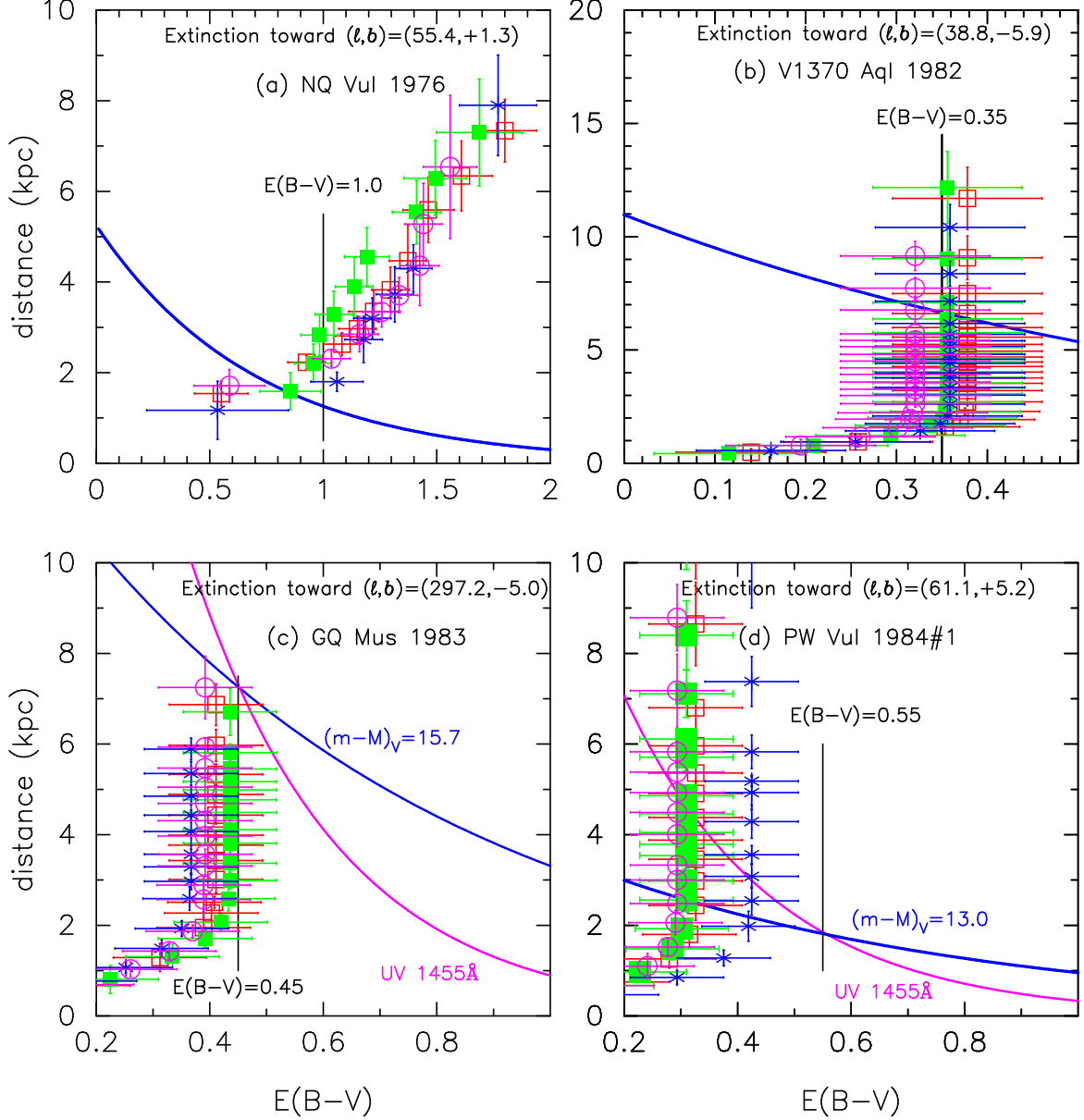


FIG. 35.— Same as Figure 34, but for (a) NQ Vul, (b) V1370 Aql, (c) GQ Mus, and (d) PW Vul. Blue solid lines indicate relations (a)  $(m-M)_V = 13.6$ , (b)  $(m-M)_V = 15.2$ , (c)  $(m-M)_V = 15.7$ , and (d)  $(m-M)_V = 13.0$ . Magenta solid lines in (c) and (d) denote distance-reddening relations of UV 1455Å fitting for GQ Mus and PW Vul, respectively, calculated in the Appendix (Figure 50).

respectively. Figure 30(d) shows the color-color evolution of NQ Vul. We obtained  $E(B-V) = 1.00 \pm 0.05$  by fitting, mainly from Chambliss' data because they have less scatter.

The overall distribution of the observational data points is in reasonable agreement with our general tracks in the color-color diagram. Yamashita et al. (1977) wrote that the absorption spectrum on October 22 closely resembled those of F5Ia supergiants. This suggests that the early data follow the nova-giant sequence, at least in the pre-maximum phase. The color-color data of NQ Vul in Figure 30(d) start from near point 2, i.e.,  $(B-V)_0 \approx +0.4$ , and then run along the nova-giant sequence up to near point D and remain there for a while. The nova then darkened suddenly owing to dust formation, and we stop following the color evolution.

Using  $E(B-V) = 1.00$  and the distance modulus of  $(m-M)_V = 13.6$  calculated in the Appendix (Equation (A6)), we obtain a distance of  $d = 1.25$  kpc to NQ Vul. The distance

to NQ Vul was estimated by Downes & Duerbeck (2000) to be  $d = 1.16$  kpc from an expansion parallax method, which is consistent with our estimate.

The following values for reddening toward NQ Vul were obtained, in increasing order of  $E(B-V)$ :  $E(B-V) = 0.7 \pm 0.2$  (Younger 1980) from the equivalent width of the interstellar band at 6614Å,  $E(B-V) = 0.8$  (Yamashita et al. 1977) from the color of spectral type F5Ia on October 22,  $E(B-V) = 0.9 \pm 0.3$  (Martin & Maza 1977) from the interstellar polarization, and  $E(B-V) = 1.2 \pm 0.2$  (Carney 1977) from the interstellar CH and CH<sup>+</sup> equivalent widths. The simple arithmetic mean of these values is  $E(B-V) = 0.9 \pm 0.2$ , which is consistent with our value of  $E(B-V) = 1.00 \pm 0.05$ .

The galactic coordinates of NQ Vul are  $(l, b) = (55.3549, +1.2904)$ . We plot the distance-reddening relation toward NQ Vul in Figure 35(a), the data for which are taken from Marshall et al. (2006). The data show four directions:



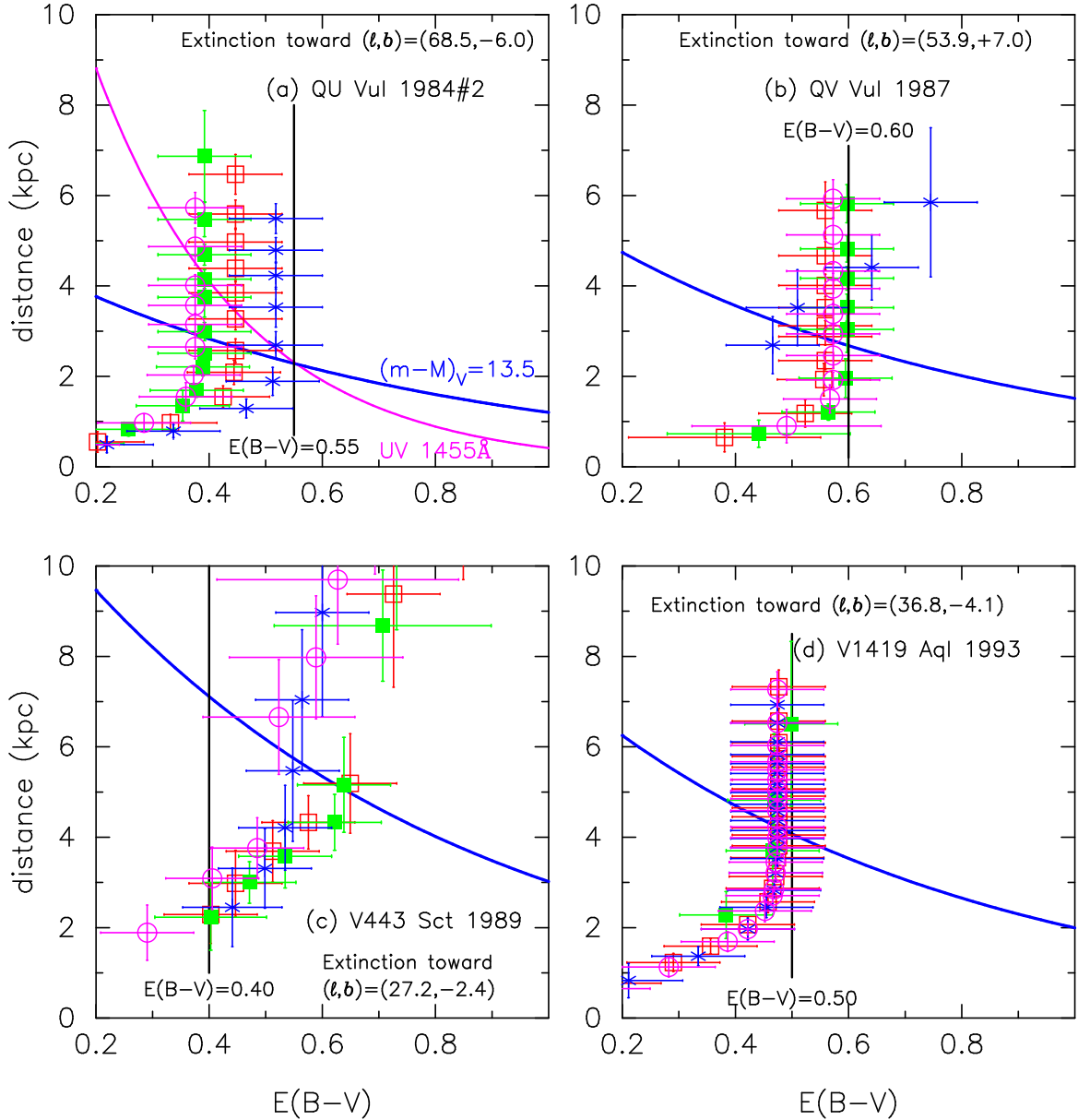


FIG. 36.— Same as Figure 34, but for (a) QU Vul, (b) QV Vul, (c) V443 Sct, and (d) V1419 Aql. Blue solid lines indicate relations (a)  $(m-M)_V = 13.5$ , (b)  $(m-M)_V = 14.0$ , (c)  $(m-M)_V = 15.5$ , and (d)  $(m-M)_V = 14.6$ . Magenta solid line in (a) denotes distance-reddening relation of UV 1455Å fitting for QU Vul calculated in the Appendix (Figure 50).

$(55^\circ 25, 1^\circ 25)$  (red open squares),  $(55^\circ 50, 1^\circ 25)$  (green filled squares),  $(55^\circ 25, 1^\circ 50)$  (blue asterisks),  $(55^\circ 50, 1^\circ 50)$  (magenta open circles). Our estimates of  $E(B-V) = 1.00 \pm 0.05$  and a distance of  $d \sim 1.25$  kpc are roughly consistent with Marshall et al.'s distance-reddening relation.

#### 6.9. V1370 Aql 1982

V1370 Aql was discovered by Honda on UT 1982 January 27.85 at about 6–7 mag (Kosai et al. 1982). The  $V$  light and  $(B-V)_0$  and  $(U-B)_0$  color curves of V1370 Aql are plotted in the Appendix (Figure 49). It rapidly decayed to  $m_V = 11.2$  on UT April 2 and entered a shallow dust blackout phase (e.g., Rosino et al. 1983). Then it came back to the usual decline of classical novae about 90 days after the outburst. We plot the color-color evolution of V1370 Aql in Figure 31(a), where the  $UBV$  data are taken from Okazaki & Yamasaki (1986) and IAU Circular No. 3689. Only a few observational points are

available, but we were able to obtain a reddening of  $E(B-V) = 0.35 \pm 0.05$ . The novae stayed at or around point F (or point 4' or point 4''), as shown in Figure 31(a).

The following values of the reddening toward V1370 Aql were obtained:  $E(B-V) = 0.55 \pm 0.15$  (Snijders et al. 1982) from the 2175Å feature,  $E(B-V) = A_V/3.1 \sim 3.0/3.1 \sim 1.0$  (Williams & Longmore 1984) from the assumed spectral type of O8–9 and from the nearby cluster NGC 6755 ( $l = 38^\circ 6, b = -1^\circ 7$ ). These two values are much larger than our estimate of  $E(B-V) = 0.35 \pm 0.05$ .

Figure 35(b) shows the distance-reddening relation toward V1370 Aql, whose galactic coordinates are  $(l, b) = (38^\circ 8126, -5^\circ 9465)$ . Here we plot four nearby directions using data from Marshall et al. (2006):  $(l, b) = (38^\circ 75, -5^\circ 75)$  (red open squares),  $(39^\circ 00, -5^\circ 75)$  (green filled squares),  $(38^\circ 75, -6^\circ 00)$  (blue asterisks), and  $(39^\circ 00, -6^\circ 00)$  (magenta open circles). The closest one is that denoted by blue aster-

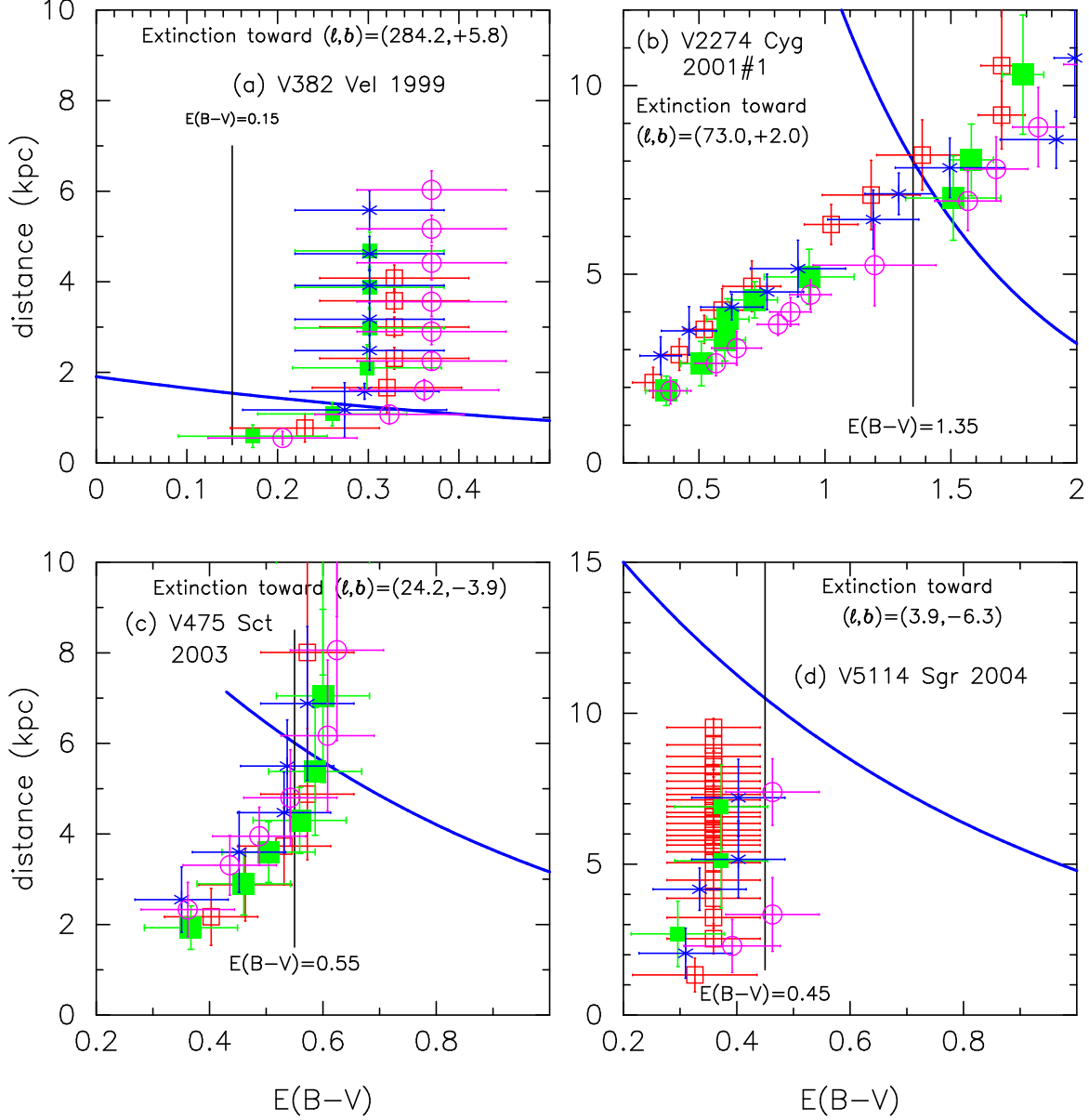


FIG. 37.— Same as Figure 34, but for (a) V382 Vel, (b) V2274 Cyg, (c) V475 Sct, and (d) V5114 Sgr. Blue solid lines indicate distance-reddening relations (a)  $(m-M)_V = 11.4$ , (b)  $(m-M)_V = 18.7$ , (c)  $(m-M)_V = 15.6$ , and (d)  $(m-M)_V = 16.5$ .

isks. We also plot the distance-reddening relation based on the distance modulus of  $(m-M)_V = 15.2$  (blue thick solid line), which is calculated by the time-stretching method in the Appendix (Equation(A12)). Our estimate of  $E(B-V) = 0.35$  is consistent with the distance-reddening relation, which gives a set of  $d \sim 6.7$  kpc and  $E(B-V) \approx 0.35$  for V1370 Aql. The NASA/IPAC galactic dust absorption map gives  $E(B-V) = 0.41 \pm 0.02$  in the direction toward V1370 Aql, which is also consistent with our estimate.

#### 6.10. GQ Mus 1983

GQ Mus is a fast nova with  $t_2 \sim 17$  days (Warner 1995). Although its peak was missed, Krautter et al. (1984) estimated the peak brightness to be  $m_{V,\max} \approx 7.0$  (or  $m_{V,\max} < 7.3$ ). In this paper, we adopt  $m_{V,\max} \approx 7.2$  after Hachisu et al. (2008). We plot the  $V$  light curve and  $(B-V)_0$  and  $(U-B)_0$  color evolution in the Appendix (Figure 50). The  $UBV$  data for GQ Mus are taken from Budding (1983)

and Whitelock et al. (1984) whereas the visual (or  $V$ ) data are from the Fine Error Sensor monitor on board *IUE* and the visual photometric data collected by the Royal Astronomical Society of New Zealand and by the AAVSO (see Hachisu et al. 2008, for more details).

We plot the color-color diagram of GQ Mus in Figure 31(b). It seems that these data started a few days after optical maximum (e.g., Hachisu et al. 2008) and its color-color evolution is consistent with the path from point 4 to point 5. We adopted  $E(B-V) = 0.45 \pm 0.05$  by fitting our general tracks to that of GQ Mus.

The color excess of GQ Mus was also determined to be  $E(B-V) = 0.43$  (de Freitas Pacheco & Codina 1985) and  $E(B-V) = 0.50 \pm 0.05$  (Péquignot et al. 1993) both from the hydrogen Balmer lines. Similar values were reported by Krautter et al. (1984) and Hassall et al. (1990), who found  $E(B-V) = 0.45$  and  $0.50$ , respectively, on the basis of the 2175 Å feature in the early *IUE* spectra. Hachisu et al. (2008) ob-

TABLE 2  
EXTINCTIONS AND DISTANCES OF SELECTED NOVAE

Object	Year	Present <sup>a</sup> $E(B-V)$	V&Y(1987) <sup>b</sup> $E(B-V)$	M(1988) <sup>c</sup> $E(B-V)$	Present ( $m-M$ ) <sub>V</sub>
OS And	1986	0.15	(0.21/0.27) <sup>d</sup>	(0.34) <sup>e</sup>	14.7
V1370 Aql	1982	0.35	...	...	15.2
V1419 Aql	1993	0.50	(0.5/0.6)	(0.62)	14.6
V705 Cas	1993	0.45	(0.33/0.36)	(0.43)	13.4
V723 Cas	1995	0.35	(0.48/-)	(0.57)	14.0
IV Cep	1971	0.70	0.66	0.75	14.7
V1500 Cyg	1975	0.45	0.37	0.47	12.3
V1668 Cyg	1978	0.35	0.31	0.36	14.25
V1974 Cyg	1992	0.30	(0.17/0.27)	(0.35)	12.2
V2274 Cyg	2001#1	1.35	...	...	18.7
HR Del	1967	0.15	(0.24/-)	(0.24)	10.4
V446 Her	1960	0.40	0.27	0.46	11.7
V533 Her	1963	0.05	0.0	0.05	11.1
GQ Mus	1983	0.45	(-/0.37)	0.42	15.7
RS Oph	1958	0.65	(0.67/0.65)	(0.75)	12.8
T Pyx	1966	0.25	(0.16/0.20)	(0.33)	13.8
V443 Sct	1989	0.40	(-/0.25)	...	15.5
V475 Sct	2003	0.55	(0.71/0.47)	(0.72)	15.6
FH Ser	1970	0.60	0.61	0.79	11.7
V5114 Sgr	2004	0.45	(0.43/0.40)	(0.55)	16.5
V5558 Sgr	2007	0.70	(0.63/-)	(0.83)	13.9
V382 Vel	1999	0.15	(0.08/-)	...	11.4
LV Vul	1968#1	0.60	0.58	0.70	11.9
NQ Vul	1976	1.00	1.0	1.2	13.6
PU Vul	1979	0.30	(0.52/0.29)	(0.55)	14.3
PW Vul	1984#1	0.55	0.39	0.51	13.0
QU Vul	1984#2	0.55	(-/0.42)	...	13.5
QV Vul	1987	0.60	(1.0/0.70)	(0.75)	14.0

<sup>a</sup> Estimated from color-color diagram fit.

<sup>b</sup> Taken from van den Bergh & Younger (1987).

<sup>c</sup> Taken from Miroshnichenko (1988).

<sup>d</sup> Parentheses indicate values of  $E(B-V)$  estimated by other authors from intrinsic colors at maximum/ $t_2$ -time proposed by van den Bergh & Younger (1987). See Section 7.2 for details.

<sup>e</sup> Parentheses indicate values estimated by other authors using the method proposed by Miroshnichenko (1988). See Section 7.1 for details.

tained  $E(B-V) = 0.55 \pm 0.05$  on the basis of the 2175Å feature and various line ratios. These estimates are all consistent with our estimate of  $E(B-V) = 0.45 \pm 0.05$ .

Its distance was estimated to be  $d \sim 5$  kpc by Krautter et al. (1984), Whitelock et al. (1984), and Hachisu et al. (2008). Using  $E(B-V) = 0.45$  and the distance modulus of  $(m-M)_V = 15.7$  calculated from the time-stretching method in the Appendix (Equation(A13)), we obtained a distance to GQ Mus of 7.3 kpc. The galactic coordinates of GQ Mus are  $(l, b) = (297^\circ 21'18'', -4^\circ 9'59'')$ . Thus, its height is  $z \sim -630$  pc below the galactic plane, which is much larger than the scale height  $\sim 125$  pc of the galactic matter distribution. The NASA/IPAC galactic dust absorption map gives  $E(B-V) = 0.42 \pm 0.01$  in the direction toward GQ Mus, which is consistent with our estimated value. We also obtained another distance-reddening relation by UV 1455Å fitting (magenta solid line) in Figure 35(c), which is calculated in the Appendix (Figure 50(a)).

We also plot four distance-reddening relations close to GQ Mus, as shown in Figure 35(c), the data for which are taken from Marshall et al. (2006):  $(l, b) = (297^\circ 00', -4^\circ 75')$  (red open squares),  $(297^\circ 25', -4^\circ 75')$  (green filled squares),  $(297^\circ 00', -5^\circ 00')$  (blue asterisks), and  $(297^\circ 25', -5^\circ 00')$  (magenta open circles). The closest one is that denoted by magenta open circles. Four trends,  $E(B-V) = 0.45$  (vertical black solid line),  $(m-M)_V = 15.7$  (blue solid line), UV 1455Å fitting (magenta solid line), and distance-reddening relation of Marshall et al. (2006), consistently cross at  $E(B-V) \sim 0.45$  and  $d \sim 7.3$  kpc.

### 6.11. QU Vul 1984 No.2

QU Vul was discovered by Collins et al. on UT 1984 December 22.13 at about 6.8 mag (Collins et al. 1984). We plot the  $V$  light curve and  $(B-V)_0$  and  $(U-B)_0$  color evolution in the Appendix (Figure 50). The  $UBV$  data for QU Vul are taken from IAU Circular No. 4033, Kolotilov (1988), Bergner et al. (1988), Rosino et al. (1992), and the AAVSO archive. It rose to  $m_V \approx 5.5$  at maximum on UT December 27 (e.g., Rosino et al. 1992). Then it gradually declined with  $t_2 = 22$  days and  $t_3 = 49$  days (e.g., Downes & Duerbeck 2000). The nova is a fast neon nova (Gehrz et al. 1985).

Figure 31(c) shows the color-color evolution of QU Vul. The color evolution started near point F (or point 4'') and then moved leftward to point 5''. We obtained  $E(B-V) = 0.55 \pm 0.05$  by fitting.

The following values were obtained for the reddening toward QU Vul:  $E(B-V) = A_V/3.1 \sim 1.0/3.1 = 0.3$  (Gehrz et al. 1986) from the galactic absorption toward  $b = -6^\circ$ ;  $E(B-V) = 0.5$  (Rosino et al. 1992) from the difference between the F2–F5 spectral types of the nova at maximum, which correspond to  $(B-V)_0 = 0.35$  and the observed one  $B-V = 0.8$ ; and  $E(B-V) = 0.61 \pm 0.1$  (Saizar et al. 1992) from the He II 1640/4686Å ratio in the nebular phase and from the 2200Å UV spectral feature. della Valle et al. (1997) adopted  $E(B-V) = A_V/3.1 \sim 1.7/3.1 = 0.55$  for dereddening the spectra. Schwarz (2002) used Saizar et al.'s  $E(B-V) = 0.61$  for obtaining UV fluxes that were consistent with the optical fluxes. These values are roughly consistent with our estimate of  $E(B-V) = 0.55 \pm 0.05$ .

To further examine the reddening, we plot the distance-reddening relation toward QU Vul in Figure 36(a). The galactic coordinates of QU Vul are  $(l, b) = (68^\circ 51'08'', -6^\circ 02'63'')$ . Here we plot four nearby directions using data from Marshall et al. (2006):  $(l, b) = (68^\circ 50', -6^\circ 00')$  (red open squares),  $(68^\circ 75', -6^\circ 00')$  (green filled squares),  $(68^\circ 50', -6^\circ 25')$  (blue asterisks), and  $(68^\circ 75', -6^\circ 25')$  (magenta open circles). The closest one is that denoted by red open squares.

We also plot the distance-reddening relation of  $(m-M)_V = 13.5$  (blue thick solid line in Figure 36(a)) calculated from the time-stretching method in the Appendix (Figure 50). We obtained another distance-reddening relation by UV 1455Å fitting (magenta solid line in Figure 36(a)), which is calculated in the Appendix (Figure 50(a)).

Four trends,  $E(B-V) = 0.55$  (vertical black solid line),  $(m-M)_V = 13.5$  (blue solid line), UV 1455Å fitting (magenta solid line), and distance-reddening relation of Marshall et al. (2006), consistently cross at  $E(B-V) \sim 0.55$  and  $d \sim 2.3$  kpc in Figure 36(a). The NASA/IPAC galactic dust absorption map gives  $E(B-V) = 0.55 \pm 0.03$  in the direction toward QU Vul, which is also consistent with our estimate.

### 6.12. OS And 1986

OS And was discovered on UT 1986 December 5.44 at about 8.0 mag (Beckmann & Collins 1987). The  $V$  and UV 1455Å light curves are plotted in Figure 11 with those of V1668 Cyg. The  $V$  light curve and the  $(B-V)_0$  and  $(U-B)_0$  color evolution are plotted in the Appendix (Figure 49). The optical maximum of  $m_{V,\max} = 6.2$  was reached on UT December 7.5 $\pm$ 1.0 (Kikuchi et al. 1988). Then it gradually decayed with  $t_3 \sim 20$  days, followed by a sudden drop by  $\sim 1.5$  mag about 30 days after discovery because of dust formation (Kikuchi et al. 1988). Here we adopted

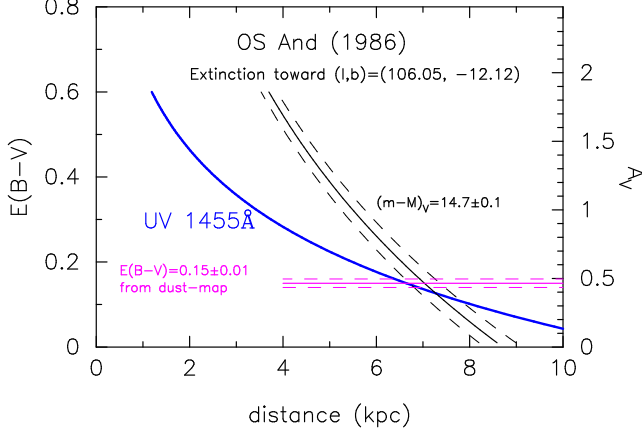


FIG. 38.— Same as Figure 12, but for OS And. Two distance-reddening relations are plotted: one is calculated from the UV 1455Å flux fit (blue solid line), and the other is the optical V fit with our free-free emission model light curve of the  $1.0 M_{\odot}$  WD in Figure 11. We also plot the extinction estimate from the dust-map calculated on NASA/IPAC web site (magenta solid line flanked by dashed lines). These three trends cross at  $d \approx 7.0$  kpc and  $E(B-V) \approx 0.15$ .

the *UBV* data from Kikuchi et al. (1988); IAU Circular Nos. 4306, 4342, and 4452; and Ohmori & Kaga (1987). Because Ohmori & Kaga (1987) gave only the differences between OS And and the comparison star 7 And, we used the *UBV* magnitudes of 7 And given by Harmanec et al. (1994) and obtained the *UBV* magnitudes of OS And. Kikuchi et al.'s *UBV* data were converted from the magnitudes of several narrower bands, and they could differ greatly from the true *UBV* magnitudes when emission lines contribute strongly to the *UBV* bands. We compared Kikuchi et al.'s (red filled circles) and Ohmori & Kaga's (red open triangles) data with the other *B-V* and *U-B* colors taken from IAU Circulars Nos. 4282, 4293, 4306, 4342, and 4452 (red open diamonds), and we shifted Kikuchi et al.'s data by  $\Delta(B-V) = -0.1$  and  $\Delta(U-B) = -0.15$ , and Ohmori & Kaga's data by  $\Delta(B-V) = 0.2$  and  $\Delta(U-B) = -0.15$  in this study.

We plot the color-color diagram of OS And in Figure 31(d). The small number of data points prevents us from confidently estimating the color excess using our general tracks. Therefore, we determined the color excess by other methods.

The reddening toward OS And was estimated as  $E(B-V) = 0.26 \pm 0.04$  (Kikuchi et al. 1988) from  $(B-V)_{0,t2} = -0.02 \pm 0.04$  together with  $(B-V)_{t2} = 0.24 \pm 0.02$ , and  $E(B-V) = 0.25 \pm 0.05$  (Schwarz et al. 1997) from an average of four values based on four empirical relations, i.e.,  $E(B-V) = 0.27$  from  $(B-V)_{0,t2} = -0.02 \pm 0.04$  (van den Bergh & Younger 1987),  $E(B-V) = 0.21$  from  $(B-V)_{0,max} = 0.2$  (Allen 1973) together with  $(B-V)_{max} = +0.41$ ,  $E(B-V) = 0.34$  from  $(B-V)_{0,ss} = -0.11$  at the stabilization stage (Miroshnichenko 1988), and  $E(B-V) = 0.24$  from the extinction map toward OS And.

On the other hand, the recent NASA/IPAC galactic dust absorption map gives  $E(B-V) = 0.15 \pm 0.01$  in the direction toward OS And, whose galactic coordinates are  $(l, b) = (106^{\circ}05'14'', -12^{\circ}11'73'')$ . This value is not consistent with the above estimates but is somewhat smaller.

It has been noted that OS And is similar to V1668 Cyg except for the depth of the dust blackout. Thus, we plot light curves of these two novae in Figure 11 with the free-free emission model light curves taken from Hachisu & Kato (2010). This figure also shows the UV 1455Å light curves corresponding to each optical light curve model. The  $1.0 M_{\odot}$  WD (red

solid line) model shows the best fit with both the optical and *IUE* UV 1455Å fluxes of OS And. Here, we assumed a chemical composition of the WD envelope of  $X = 0.35$ ,  $Y = 0.33$ ,  $Z = 0.02$ ,  $X_{C+O} = 0.30$ . From the optical light curve fitting, we obtained a distance modulus of  $(m-M)_V = m_w - M_w = 16.1 - (+1.4) = 14.7$ , where  $m_w = 16.1$  was read directly from the end point of the free-free emission model light curve (large open circle at the bottom of the line) in Figure 11, and  $M_w$  is taken from Table 2 of Hachisu & Kato (2010) as  $M_w = +1.4$  for the  $M_{WD} = 1.0 M_{\odot}$  model. We also obtained a distance-reddening relation from the UV1455Å light curve fitting of Equation(10) for OS And. We plot these two distance-reddening relations in Figure 38. We see that three trends, the distance modulus  $(m-M)_V = 14.7$  together with Equation (2), the UV 1455Å fitting in Figure 11 together with Equation (10), and the dust-map  $E(B-V) = 0.15$ , cross consistently at  $d \approx 7.0$  kpc and  $E(B-V) \approx 0.15$ . Therefore, we adopted  $E(B-V) = 0.15$  for OS And. Using this value, we plot the color-color diagram in Figure 31(d). The resultant distribution of the data seems to be reasonable, although the number of data points is small.

### 6.13. QV Vul 1987

QV Vul was discovered on UT 1987 November 15 at about 7.0 mag (Beckmann & Collins 1987). The *V* light curve,  $(B-V)_0$  and  $(U-B)_0$  color evolution are plotted in the Appendix (Figure 51), where the *UBV* data are taken from Ohshima (1988). The optical maximum had already been reached at discovery (Ohshima 1988). It gradually decayed and suddenly dropped about 60 days after discovery because of dust formation. We also plot the color-color evolution of QV Vul in Figure 32(a). There are several data points just after maximum, so we set Ohshima's data points (red filled circles) on the nova-giant sequence as shown in the figure and obtained a reddening of  $E(B-V) = 0.60 \pm 0.05$ .

The reddening toward QV Vul was also determined to be  $E(B-V) = 0.40 \pm 0.05$  (Scott et al. 1994) from the  $H\gamma/H\beta$  line ratio and to be  $E(B-V) = A_V/3.1 = 1.0/3.1 = 0.32$  (Gehrz et al. 1992) from various loose constraints on the luminosities and spectra of QV Vul. To further examine the reddening, we plot the distance-reddening relation toward QV Vul in Figure 36(b), whose galactic coordinates are  $(l, b) = (53^{\circ}85'55'', +6^{\circ}97'41'')$ . Here we plot four nearby directions from the data of Marshall et al. (2006):  $(l, b) = (53^{\circ}75', +6^{\circ}75')$  (red open squares),  $(54^{\circ}00', +6^{\circ}75')$  (green filled squares),  $(53^{\circ}75', +7^{\circ}00')$  (blue asterisks), and  $(54^{\circ}00', +7^{\circ}00')$  (magenta open circles). The closest one is that denoted by blue asterisks or magenta open circles. We also plot the distance-reddening relation of  $(m-M)_V = 14.0$  (blue thick solid line) calculated by the time-stretching method in the Appendix (Equation(A14)). These trends cross at  $E(B-V) \approx 0.60$  and  $d \approx 2.7$  kpc, which are consistent with our estimate above. The NASA/IPAC galactic dust absorption map gives  $E(B-V) = 0.64 \pm 0.02$  in the direction toward QV Vul, which is also consistent with our estimate.

### 6.14. V443 Sct 1989

V443 Sct was discovered on UT 1989 September 20 at about 10.5 mag (Wild 1989). The optical maximum ( $\sim 7.5$  mag) was already reached a week before discovery (see, e.g., Figure 1 of Rosino et al. 1999). We plot the *V* light curve, and  $(B-V)_0$  and  $(U-B)_0$  color evolution of V443 Sct in the Appendix (red symbols in Figure 52), which shows a semi-

periodic oscillation with a periodicity of  $\sim 17$  days. The light curve is similar to that of PW Vul (denoted by blue symbols in the same figure). We plot the color-color evolution of V443 Sct in Figure 32(b), where the  $UBV$  data are taken from IAU Circular Nos. 4862, 4868, and 4873. Although there are only several data points after optical maximum, we determine the reddening to be  $E(B-V) = 0.40 \pm 0.05$ .

The reddening toward V443 Sct was estimated by Anupama et al. (1992) to be  $E(B-V) = 0.40$  from the Balmer/Paschen line ratios, which is consistent with our estimate. To further examine the reddening, we plot the distance-reddening relation toward V443 Sct, whose galactic coordinates are  $(l, b) = (27^\circ 2183, -2^\circ 4211)$ , in Figure 36(c). Here we plot four nearby directions from the data of Marshall et al. (2006):  $(l, b) = (27^\circ 00, -2^\circ 25)$  (red open squares),  $(27^\circ 25, -2^\circ 25)$  (green filled squares),  $(27^\circ 00, -2^\circ 50)$  (blue asterisks), and  $(27^\circ 25, -2^\circ 50)$  (magenta open circles). The closest one is that denoted by magenta open circles. We also plot the distance-reddening relation of  $(m-M)_V = 15.5$  calculated in the Appendix (Equation (A15)). Our two trends intersect at  $E(B-V) \approx 0.40$  and the distance  $d \approx 7.1$  kpc. Considering the small number of data points in Figure 32(b), our estimated extinction is barely consistent with the distance-reddening relation given by Marshall et al. (2006).

#### 6.15. V1419 Aql 1993

V1419 Aql was discovered by Yamamoto on UT 1993 May 14 at about 7.6 mag (Hirayama et al. 1993). The  $V$  light curve and  $(B-V)_0$  and  $(U-B)_0$  color evolution are plotted in the Appendix (Figure 45), where the  $UBV$  data are taken from Munari et al. (1994a) and IAU Circular Nos. 5794, 5802, 5807, and 5829. The  $V$  magnitude reached a maximum of  $m_V = 7.5$  on May 23. Then it gradually decayed and sharply dropped about 35–40 days after discovery owing to dust shell formation. We also plot the color-color evolution of V1419 Aql in Figure 32(c). The color data in the IAU Circulars are scattered, so we used mainly Munari et al.'s data in our fitting procedure. The first color data were obtained near maximum, on May 26, so we set this point on the nova-giant sequence, as shown in Figure 32(c), and estimated the reddening to be  $E(B-V) = 0.50 \pm 0.05$ . The color evolution of V1419 Aql started near point D and remained there for a while, as seen in Figures 45(b) and (c). After that, the nova suddenly darkened owing to dust shell formation. We do not follow the color evolution after the dust blackout in the color-color diagram.

Lynch et al. (1995) obtained the following values for the reddening toward V1419 Aql:  $E(B-V) = 1.02 \pm 0.19$  from an average of  $E(B-V) = 0.74 \pm 0.46$  in June and  $E(B-V) = 1.10 \pm 0.32$  in September, both from the Paschen series line ratios,  $E(B-V) = 1.22 \pm 0.13$  in June and  $E(B-V) = 1.05 \pm 0.12$  in September, both from the O I lines  $\lambda 8446$ ,  $\lambda 11287$ , and  $\lambda 13164$ . On the other hand, Munari et al. (1994b) estimated the reddening to be  $E(B-V) = 0.55 \pm 0.15$  from the star's color, i.e., the average of  $E(B-V) = 0.6$  from the intrinsic color at  $t_2$  time (van den Bergh & Younger 1987) and  $E(B-V) = 0.5$  from the intrinsic color at maximum (Allen 1973). Thus, these reddening estimates show a large difference between these two groups.

To further examine the reddening, we plot the distance-reddening relation of Marshall et al. (2006) in Figure 36(d), where the galactic coordinates of V1419 Aql are  $(l, b) = (36^\circ 8110, -4^\circ 1000)$ . We plot four nearby directions from

the data from Marshall et al. (2006):  $(l, b) = (36^\circ 75, -4^\circ 00)$  (red open squares),  $(37^\circ 00, -4^\circ 00)$  (green filled squares),  $(36^\circ 75, -4^\circ 25)$  (blue asterisks), and  $(37^\circ 00, -4^\circ 25)$  (magenta open circles). The closest one is that denoted by red open squares. We also plot the distance-reddening relation of  $(m-M)_V = 14.6$  calculated by the time-stretching method in the Appendix (Equation (A8)). The two trends of  $(m-M)_V = 14.6$  and  $E(B-V) = 0.50$  cross at  $d \approx 4.1$  kpc and  $E(B-V) \approx 0.50$ , which are consistent with the distance-reddening relation of Marshall et al. (2006). The NASA/IPAC galactic dust absorption map gives  $E(B-V) = 0.55 \pm 0.01$  in the direction toward V1419 Aql, which is also consistent with our estimate.

#### 6.16. V705 Cas 1993

V705 Cas was discovered by Kanatsu on UT 1993 December 7 at about 6.5 mag (Nakano et al. 1993). The  $V$  light curve and  $(B-V)_0$  and  $(U-B)_0$  color evolution are plotted in the Appendix (Figure 51), where the  $UBV$  data are taken from Munari et al. (1994b), Hric et al. (1998), and IAU Circular Nos. 5920 and 5929. It rose to  $m_V = 5.5$  10 days after discovery, i.e., on UT December 17. A deep minimum appeared about 60 days after discovery because of dust shell formation. Therefore, we only plot the data for  $t < 60$  days for the color-color evolution of V705 Cas in Figure 32(d). The color-color data of Munari et al. are scattered, so we determine the reddening to be  $E(B-V) = 0.45 \pm 0.05$ , mainly from the data of Hric et al. and the IAU Circulars. Combining the distance modulus of  $(m-M)_V = 13.6$  calculated in the Appendix (Equation (A14)) and  $E(B-V) = 0.45$ , we obtained a distance of  $d = 2.8$  kpc. The color-color evolution of V705 Cas started near point 3 (or point C). Then, the nova ascended along the nova-giant sequence to near point 4'' (near point F) and stayed there for a while. After that, the nova suddenly darkened owing to dust shell formation.

The reddening toward V705 Cas was estimated by Hric et al. (1998) to be  $E(B-V) = 0.38$  from an intercomparison of the color indices of stars surrounding the nova selected from the SAO catalog. They also obtained  $E(B-V) = (B-V)_{ss} - (B-V)_{0,ss} = 0.32 - (-0.11) = 0.43$  from the intrinsic color at the stabilization stage (Miroshnichenko 1988). Hauschildt et al. (1995) obtained  $E(B-V) = 0.5$  assuming that the total (optical + UV) luminosity in the early phase is constant (see also Shore et al. 1994). The simple arithmetic mean of these values is  $E(B-V) = 0.44 \pm 0.05$ , which is consistent with our estimate of  $E(B-V) = 0.45 \pm 0.05$ . If we use the relations given by van den Bergh & Younger (1987), we obtain  $E(B-V) = (B-V)_{\max} - (B-V)_{0,\max} = 0.56 - (+0.23) = 0.33$  and  $E(B-V) = (B-V)_{t_2} - (B-V)_{0,t_2} = 0.34 - (-0.02) = 0.36$ , the color data of which are taken from Hric et al. (1998). These values are slightly smaller than our value of  $E(B-V) = 0.45 \pm 0.05$ . The galactic coordinates of V705 Cas are  $(l, b) = (113^\circ 6595, -4^\circ 0959)$ . Unfortunately, there are no data on the dust extinction map calculated by Marshall et al. (2006) because their data are given for  $-100^\circ 0 \leq l \leq 100^\circ 0$  and  $-10^\circ 0 \leq b \leq +10^\circ 0$ . The NASA/IPAC galactic dust absorption map gives  $E(B-V) = 0.48 \pm 0.02$  in the direction toward V705 Cas, which is consistent with our value.

#### 6.17. V382 Vel 1999

V382 Vel is a very fast nova identified as a neon nova (Woodward et al. 1999). The  $V$  light curve and  $(B-V)_0$  and  $(U-B)_0$  color evolution are plotted in the Appendix (Figures 42). The nova reached  $m_V = 2.7$  at maximum on UT 1999 May



23. The *UBV* color-color evolution is plotted in Figure 33(a), where the data are taken from IAU Circular Nos. 7176, 7179, 7196, 7209, 7216, 7226, and 7232 (observed mainly by A. C. Gilmore and P. M. Kilmartin). We obtained  $E(B-V) = 0.15 \pm 0.05$  by fitting. Mukai & Ishida (2001) obtained a hydrogen column density toward V382 Vel of  $N_H = (1.01 \pm 0.05) \times 10^{21}$  from early hard X-ray spectrum fittings. This value can be converted to  $E(B-V) = N_H / 5.8 \times 10^{21} \approx 0.2$  (Bohlin et al. 1978) or  $E(B-V) = N_H / 8.3 \times 10^{21} \approx 0.12$  (Liszt 2014), which are consistent with our estimated value. Shore et al. (2003) obtained  $E(B-V) = 0.20$  and della Valle et al. (2002) estimated  $E(B-V) = 0.05-0.099$  from various line ratios and the Na I D interstellar absorption features. These values are all consistent with our estimated value of  $E(B-V) = 0.15 \pm 0.05$ .

The galactic coordinates of V382 Vel are  $(l, b) = (284^\circ 16' 74'', +5^\circ 77' 15'')$ . We plot the distance-reddening relation calculated by Marshall et al. (2006) in Figure 37(a). Here we plot four nearby directions:  $(l, b) = (284^\circ 00', +5^\circ 75')$  (red open squares),  $(284^\circ 25', +5^\circ 75')$  (green filled squares),  $(284^\circ 00', +6^\circ 00')$  (blue asterisks), and  $(284^\circ 25', +6^\circ 00')$  (magenta open circles). The closest one is that denoted by green filled squares. We also plot the distance-reddening relation  $(m-M)_V = 11.4$  calculated in the Appendix (Equation (A5)). It seems that our estimate of  $E(B-V) = 0.15$  is slightly smaller than Marshall et al.'s distance-reddening relation.

#### 6.18. V2274 Cyg 2001#1

V2274 Cyg was discovered by Nakamura on UT 2001 July 13.65 at about 11.9 mag (Sato et al. 2001). We plot the *V* light curve and  $(B-V)_0$  and  $(U-B)_0$  color evolution in the Appendix (Figure 48), where the *UBV* data are taken from Voloshina & Metlova (2002b). It rose to  $m_V = 11.8$  on UT August 20.09 (Waagen et al. 2001). Then it declined with large oscillatory variations until dust blackout began about 50 days after discovery. We also plot the color-color evolution of V2274 Cyg in Figure 33(b); we obtained  $E(B-V) = 1.35 \pm 0.1$  by fitting. There is large scatter in the color-color data, so we have a relatively large error of determination.

Rudy et al. (2003) estimated the reddening to be  $E(B-V) = 1.30 \pm 0.2$  from three O I line fluxes based on the reddening law given by Draine (1989), which is consistent with our estimate of  $E(B-V) = 1.35 \pm 0.1$ . Rudy et al. (2003) also obtained a distance of  $d = 10.8^{+4.2}_{-3.1}$  kpc to the nova from della Valle & Livio's (1995) MMRD relation together with  $t_2 = 33 \pm 4$ . Then the apparent distance modulus in *V* becomes  $(m-M)_V = 19.16 \pm 0.7$ , including  $3\sigma$  scatter in the MMRD relation.

The galactic coordinates of V2274 Cyg are  $(l, b) = (73^\circ 04' 15'', +1^\circ 99' 10'')$ , and we plot the distance-reddening relation calculated by Marshall et al. (2006) in Figure 37(b). Here we plot four nearby directions:  $(l, b) = (73^\circ 00', 2^\circ 00')$  (red open squares),  $(73^\circ 25', 2^\circ 00')$  (green filled squares),  $(73^\circ 00', 1^\circ 75')$  (blue asterisks), and  $(73^\circ 25', 1^\circ 75')$  (magenta open circles). The closest one is that denoted by red open squares. Our two trends,  $(m-M)_V = 18.7$  (thick blue solid line) calculated in the Appendix (Equation (A11)) and  $E(B-V) = 1.35$  (vertical black solid line), cross at  $d = 8.0$  kpc. This point is consistent with Marshall et al.'s distance-reddening relation.

#### 6.19. V475 Sct 2003

V475 Sct was discovered by Nishimura on UT 2003 August 28.58 at about 8.5 mag (Nakano et al. 2003). We plot

the *V* light curve and  $(B-V)_0$  and  $(U-B)_0$  color evolution of V475 Sct in the Appendix (Figure 43) together with those of DQ Her, NQ Vul, and T Pyx. It rose to  $m_V = 8.4$  on UT September 2 (e.g., Stringfellow & Walter 2006). Then it gradually declined with  $t_2 = 48$  days and  $t_3 = 53$  days (e.g., Chochol et al. 2005). The nova started a dust blackout about 60 days after discovery. We plot the color-color evolution of V475 Sct in Figure 33(c), where the *UBV* data are taken from Chochol et al. (2005). The color evolution followed the nova-giant sequence in the early phase, as shown in Figure 33(c), so we determine the reddening to be  $E(B-V) = 0.55 \pm 0.10$ .

Chochol et al. (2005) obtained a value of  $E(B-V) = 0.69 \pm 0.05$  for the reddening toward V475 Sct averaging various estimates:  $E(B-V) = (B-V)_{\max} - (B-V)_{0,\max} = 0.91 - 0.2 = 0.71$ ,  $E(B-V) = (B-V)_{t_2} - (B-V)_{0,t_2} = 0.45 - (-0.02) = 0.47$ ,  $E(B-V) = (B-V)_{ss} - (B-V)_{0,ss} = 0.61 - (-0.11) = 0.72$ ,  $E(B-V) = (B-V)_{F2} - (B-V)_{0,F2} = 1.08 - (0.23) = 0.85$ , where the spectral type of V475 Sct observed on UT August 31.97 is F2 supergiant and  $(B-V)_{0,F2}$  is the intrinsic color of F2 supergiants (Cox 2000), and  $E(B-V) = 0.70$  from the interstellar K I line. Chochol et al. (2005) derived values of  $(m-M)_V = 15.57 \pm 0.15$  and  $d = 4.8 \pm 0.9$  kpc for the distance modulus in the *V* band and the distance, respectively. The distance was also estimated by Stringfellow & Walter (2006) to be  $(m-M)_0 = 13.7$  ( $d \sim 5.5$  kpc) from the MMRD relations with  $t_2 = 46$ , and  $t_3 = 53$  days together with  $E(B-V) = (B-V)_{F2} - (B-V)_{0,F2} = 0.78 - 0.23 = 0.55$ . The latter value of  $E(B-V) = 0.55$  is consistent with our estimated value.

To examine the distance-reddening relation toward V475 Sct, we compared our results with that of Marshall et al. (2006). The galactic coordinates of V475 Sct are  $(l, b) = (24^\circ 20' 15'', -3^\circ 94' 66'')$ . We plot the distance-reddening relation calculated by Marshall et al. (2006) in Figure 37(c). Here we plot four nearby directions:  $(l, b) = (24^\circ 00', -4^\circ 00')$  (red open squares),  $(24^\circ 25', -4^\circ 00')$  (green filled squares),  $(24^\circ 00', -3^\circ 75')$  (blue asterisks), and  $(24^\circ 25', -3^\circ 75')$  (magenta open circles). The closest one is that denoted by green filled squares. We also plot the distance-reddening relation of  $(m-M)_V = 15.6$  calculated in the Appendix (Equation (A6)). The two trends of  $(m-M)_V = 15.6$  (thick blue solid line) and  $E(B-V) = 0.55$  (black solid line) cross at  $d = 6.0$  kpc, which is consistent with Marshall et al.'s trend. The NASA/IPAC galactic dust absorption map gives  $E(B-V) = 0.59 \pm 0.05$  in the direction toward V475 Sct, which is also consistent with our estimate.

#### 6.20. V5114 Sgr 2004

V5114 Sgr was discovered independently by Nishimura on UT 2004 March 15.82 at about 9.4 mag and by Liller on 2004 March 17.34 at about 8.2 mag (Nishimura et al. 2004). We plot the *V* light curve and  $(B-V)_0$  and  $(U-B)_0$  color evolution in the Appendix (Figure 44). It rose to  $m_V = 8.0$  on UT March 17.17 (Ederoclite et al. 2006). Then it gradually declined with  $t_2 = 11$  days and  $t_3 = 21$  days. We plot the color-color evolution of V5114 Sgr in Figure 33(d), where the *UBV* data are taken from Ederoclite et al. (2006). The color evolution followed the nova-giant sequence in the very early phase from point D to point 4'' and then followed the path from point 4'' to 5'', so we obtained a reddening of  $E(B-V) = 0.45 \pm 0.05$ . This color-evolution path is very similar to that of V1974 Cyg. Here we omitted some data that differ greatly from the others to reduce the scatter in the color data.

The reddening toward V5114 Sgr was determined by

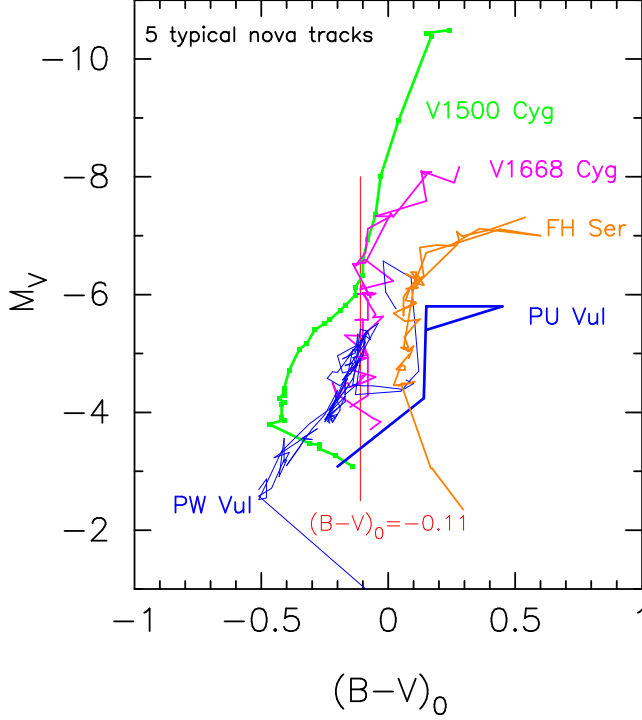


FIG. 39.— Five typical nova tracks in the color-magnitude diagram: from left to right, V1500 Cyg (green solid), V1668 Cyg (magenta solid), PW Vul (blue thin solid), FH Ser (ocher solid), and PU Vul (blue thick solid line). Vertical red solid line indicates stabilization track of  $(B-V)_0 = -0.11$  (Miroshnichenko 1988).

Ederoclite et al. (2006) to be  $E(B-V) = 0.45$  from the equivalent width of the interstellar line K I  $\lambda 7699$ ,  $E(B-V) = (B-V)_{\max} - (B-V)_{0,\max} = 0.66 - (0.23 \pm 0.06) = 0.43 \pm 0.06$ ,  $E(B-V) = (B-V)_{t_2} - (B-V)_{0,t_2} = 0.38 - (-0.02 \pm 0.04) = 0.40 \pm 0.04$ ,  $E(B-V) = 0.58$  from the galactic dust map (Schlegel et al. 1998),  $E(B-V) = 0.57$  from the line ratio of He II  $\lambda 4686$  and  $\lambda 10124$ ,  $E(B-V) = 0.65$  from the line ratio of He I  $\lambda 4861$  and  $\lambda 10049$ , and so on. We checked the NASA/IPAC galactic dust absorption map and obtained  $E(B-V) = 0.49 \pm 0.02$  in the direction toward V5114 Sgr, whose galactic coordinates are  $(l, b) = (3^\circ 9429, -6^\circ 3121)$ . The simple arithmetic mean of the first six values above, given by Ederoclite et al. (2006), is  $E(B-V) = 0.51 \pm 0.09$ , which is consistent with our value of  $E(B-V) = 0.45 \pm 0.05$ .

To further check the reddening-distance relation toward V5114 Sgr, we compared our results with that of Marshall et al. (2006). In Figure 37(d), we plot four nearby directions:  $(l, b) = (3^\circ 75, -6^\circ 50)$  (red open squares),  $(4^\circ 00, -6^\circ 50)$  (green filled squares),  $(3^\circ 75, -6^\circ 25)$  (blue asterisks), and  $(4^\circ 00, -6^\circ 25)$  (magenta open circles). The closest one is that denoted by magenta open circles. These three trends, Marshall et al.'s magenta open circles,  $(m-M)_V = 16.5$  (thick blue solid line) calculated in the Appendix (Equation (A7)), and  $E(B-V) = 0.45$  (vertical black solid line), are all consistent with  $d \sim 10.5$  kpc and  $E(B-V) \sim 0.45$ .

## 7. DISCUSSION

### 7.1. Comparison with Miroshnichenko's Relation

Miroshnichenko (1988) identified a trend in which the  $B-V$  and  $U-B$  colors remain constant for a while soon after optical maximum, which usually has the reddest color, and further that this stage showed a general trend of  $(B-V)_{0,ss} = -0.11 \pm 0.02$ . He called this stage “the stabilization stage”

and determined the  $V$  band absorptions ( $A_V$ ) of 23 novae assuming that they all have the same intrinsic  $(B-V)_0$  color at this stabilization stage, i.e.,  $E(B-V) = (B-V)_{ss} - (B-V)_{0,ss} = (B-V)_{ss} + 0.11$  and  $A_V = R_V E(B-V) = 3.13 E(B-V)$ , where  $(B-V)_{ss}$  is the observed  $B-V$  color at the stabilization stage. This method looks fascinating but sometimes results in a large difference from our value (see Table 2).

Figure 39 summarizes the color-magnitude diagram for our 28 novae. There are five typical nova tracks, each of which represents a similar speed class as well as other characteristic properties. We found that the two types of V1668 Cyg and FH Ser clearly show a stabilization stage, in which the  $B-V$  color is almost constant during a decay of a few magnitudes in  $V$ . In the V1668 Cyg type of novae (fast novae with optically-thin dust formation) the stabilization stage clearly appears as a straight vertical track of  $(B-V)_0 \approx -0.05$  (point 4’), which is close to  $(B-V)_0 = -0.11$  (the red vertical line). On the other hand, the FH Ser type (moderately fast/slow novae with optically thick dust formation) lies between  $(B-V)_0 = 0.0$  and  $0.1$ . In the V1500 Cyg and PW Vul types of novae, the  $(B-V)_0$  colors are close to  $(B-V)_0 \sim -0.03$  at  $t_2$  because they remain for a while near point F (see Section 7.2). Because their colors gradually become blue around  $t_2$ , their color could be consistent with  $(B-V)_{0,ss} = -0.11$ . In the PU Vul type of novae, including V723 Cas and HR Del, the color path is much redder because they stay near point 0, whose color is  $(B-V)_0 = +0.13$  (see Figure 17 for PU Vul and Figure 26 for V723 Cas/HR Del). Thus, three types, the V1668 Cyg, V1500 Cyg, and PW Vul types, could have a stabilization stage with  $(B-V)_{0,ss} \approx -0.11$ . For the other two types, the FH Ser and PU Vul types, Miroshnichenko's method may result in a larger extinction than the true value, as seen in Table 2.

### 7.2. Comparison with van den Bergh and Younger's Relations

van den Bergh & Younger (1987) derived the general trends of color evolution in nova light curves, i.e.,  $(B-V)_{0,\max} = 0.23 \pm 0.06$  at maximum and  $(B-V)_{0,t_2} = -0.02 \pm 0.04$  at  $t_2$ . Using these relations, one can obtain  $E(B-V)$  for individual novae. These two methods, however, often give very different values from those obtained by other methods. Table 2 summarizes these values of  $E(B-V)$ , including our results from the previous sections. Here we examine van den Bergh and Younger's empirical relations for our 28 novae.

In this paper, we showed that novae generally follow the nova-giant sequence when the photospheric emission dominates the spectrum in the optical region. The optical maximum corresponds to the reddest point of the journey along the nova-giant sequence. This reddest point varies among novae. Thus, the color at maximum,  $(B-V)_{0,\max}$ , is not the same for all the novae. To understand the difference among various types of novae, we plot five typical nova tracks in the color-magnitude diagram (Figure 39). A nova outburst evolves from the peak magnitude (top of a line) and then moves down. V1500 Cyg and V1668 Cyg showed colors consistent with  $(B-V)_{0,\max} = 0.23 \pm 0.06$  at maximum (van den Bergh & Younger 1987). In this way, many fast and very fast novae are consistent with van den Bergh & Younger's  $(B-V)_{0,\max} = 0.23 \pm 0.06$  except for some novae like V1974 Cyg. V1974 Cyg is not consistent with this because of its too-short journey along the nova-giant sequence from point D, where  $(B-V)_{0,D} = +0.04$  (see Figure 8(d)). For the other types of novae, e.g., FH Ser and PU Vul are also

not consistent with this, because their long journeys along the nova-giant sequence reach  $(B-V)_0 \sim 0.6$  far beyond  $(B-V)_0 = 0.23$ . Thus, van den Bergh and Younger's law of  $(B-V)_{0,\max} = 0.23 \pm 0.06$  is usually not applicable to slow/very slow novae and sometimes fast novae like V1974 Cyg.

The second law of  $(B-V)_{0,t2} = -0.02 \pm 0.04$  at  $t_2$ , on the other hand, shows rough agreement with our estimated values. This is because  $(B-V)_{0,t2} = -0.02 \pm 0.04$  is very close to the  $(B-V)_0$  color at point F ( $-0.03$ ), point 4'' ( $-0.05$ ), and point 4' ( $-0.08$ ), where fast novae usually remain for a while when free-free emission dominates the spectrum after optical maximum (see Figure 39). However, some of the very slow novae, e.g., PU Vul, V5558 Sgr, V723 Cas, and HR Del, remain near point 0 (not point F) for a while as mentioned in Sections 4 and 5, and its color is  $(B-V)_0 = +0.13$ , which is not consistent with  $(B-V)_{0,t2} = -0.02 \pm 0.04$ . Thus, the PU Vul and FH Ser type tracks show much redder colors at  $t_2$ .

## 8. CONCLUSIONS

We extensively examined the color-color evolutions of nova outbursts and found several important properties of nova color evolution. Our main results are summarized as follows.

1. We compiled or obtained the distance and extinction for eight well-observed novae including all the speed classes. Based on the revised distances and extinctions, we plotted the dereddened  $(B-V)_0$  versus  $(U-B)_0$  color-color diagrams of these novae and found a general course for the color evolution of nova outbursts. We further found that a number of novae follow this general course in the color-color diagram.
2. The general tracks of nova outbursts consist mainly of three branches, i.e., the nova-giant sequence phase and free-free emission (point F) phase, followed by development of strong emission lines (horizontal blueward excursion): (1) In the early phase of a nova outburst, i.e., in the pre-maximum phase, a nova evolves from near the blackbody sequence and follows a new sequence redward. After optical maximum, the nova quickly evolves back blueward along this new sequence. This new sequence is located parallel to, but  $\Delta(U-B) \approx -0.2$  mag bluer than, the supergiant sequence. We call the new sequence "the nova-giant sequence" after the supergiant sequence. The spectra of novae on the nova-giant sequence resemble those of A-F type supergiants. (2) Subsequently, the spectra of novae become that of free-free emission in the optical and near IR regions. Therefore, novae stay at the point of free-free emission ( $B-V = -0.03$ ,  $U-B = -0.97$ ) for a while. Thus, we call this point "point F" in the color-color diagram after free-free emission. (3) After this stage, novae

evolve leftward (blueward in  $B-V$  but almost constant in  $U-B$ ) mainly because of the development of strong emission lines. In this work, we stopped following the color evolution when the  $V$  magnitude drops by 3–4 mag from the maximum because strong emission lines make an increasingly large contribution to the  $(U-B)_0$  and  $(B-V)_0$  colors, and their effects cloud the overall evolution of colors.

3. We can determine the color excess  $E(B-V)$  of a target nova by fitting its color evolution track with our general course in the color-color diagram. This is a new and convenient method for obtaining accurate color excesses for classical novae. In this paper, we redetermined the color excesses of 19 novae by fitting with our general track. They are shown in Figures 29–33, and the obtained values are tabulated in Table 2.

4. Using a time-stretching method for nova light curves (Hachisu & Kato 2010), we can estimate the apparent distance modulus  $(m-M)_V$  of a target nova. We have confirmed that this time-stretching method is applicable for several novae with known distances. Then, we determined the distance moduli of other novae, which are shown in Figures 40–52, and the obtained values of  $(m-M)_V$  are tabulated in Table 2. Comparing some other available distance-reddening relations with our apparent distance modulus  $(m-M)_V$  for a target nova, we examined and confirmed our estimated color excess for each nova in Figures 34–37 and showed that our estimated values of  $E(B-V)$  are in good agreement with these relations, thus supporting the validity of our new method.

We are grateful to S. Shugarov and D. Chochol for permitting us to use digital data for PU Vul's  $UBV$  magnitudes, and also to R. González-Riestra for providing us with her new reddening estimates of V723 Cas 1995, and A. Casatella for providing us with their machine readable UV 1455 Å data for various novae. We also thank the American Association of Variable Star Observers (AAVSO) and the Variable Star Observers League of Japan (VSOLJ) for archival nova data. We are also grateful to the anonymous referee for useful comments to improve the manuscript. This research used the NASA/IPAC Infrared Science Archive, which is operated by the Jet Propulsion Laboratory, California Institute of Technology, under contract with the National Aeronautics and Space Administration. This research was supported in part by Grants-in-Aid for Scientific Research (22540254, 24540227) from the Japan Society for the Promotion of Science.

## APPENDIX

### TIME-STRETCHING METHOD FOR NOVA LIGHT CURVES

Hachisu & Kato (2006) found that nova light curves follow a universal decline law when free-free emission dominates the optical and IR flux. Using the universal decline law, Hachisu & Kato (2010) found that, if two nova light curves overlap each other after one of the two is squeezed/stretched by a factor of  $f_s$  ( $t' = t/f_s$ ) in the time direction, the brightnesses of the two novae obey the relation of  $m'_V = m_V - 2.5 \log f_s$ . Using this result and calibrated nova light curves, we can estimate the absolute magnitude of a target nova. In the following, we determine the distance moduli of 28 novae. The results are tabulated in Table 2.

First, we calibrate the distance modulus of V1500 Cyg with those of GK Per and V603 Aql, because the distances to GK Per and V603 Aql were recently obtained by Harrison et al. (2013) using trigonometric parallax, i.e.,  $d = 477^{+28}_{-25}$  pc for GK Per and  $d = 249^{+9}_{-8}$  pc for V603 Aql. The value of GK Per is consistent within a  $1\sigma$  error with the previous estimate of  $d = 455$  pc by Slavin et al. (1995) using the nebular expansion parallax method. The distance modulus of GK Per is  $(m-M)_V = 5 \log 477^{+28}_{-25}/10 + 3.1 \times 0.3 = 9.3 \pm 0.1$  for  $E(B-V) = 0.3$  (Wu et al. 1989). The distance modulus of V603 Aql is  $(m-M)_V = 5 \log 249^{+9}_{-8}/10 + 3.1 \times$

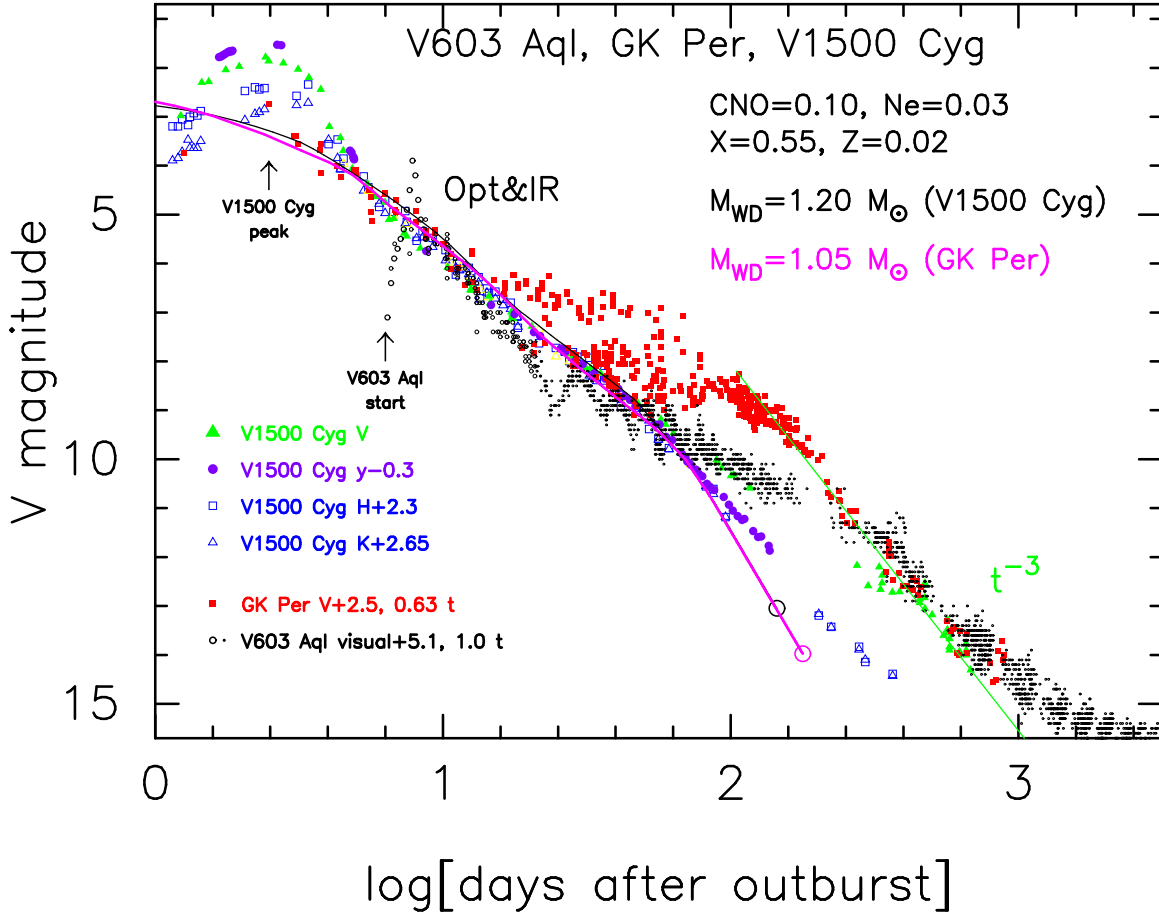


FIG. 40.— Light curves of V1500 Cyg, GK Per, and V603 Aql. Light curves of free-free emission are almost independent of wavelength, so the  $V$ ,  $y$ ,  $H$ , and  $K$  light curves of V1500 Cyg almost overlap from several days to  $\sim 65$  days after the outburst. The  $V$  light curve of GK Per is shifted downward by  $\Delta V = 2.5$  mag and leftward by  $\Delta \log t = -0.2$ , whereas the visual light curve of V603 Aql is shifted downward by  $\Delta V = 5.1$  mag but not shifted in the time direction. The smooth light curve of V1500 Cyg is fitted with the bottom line of the GK Per light curve during the transition oscillations of GK Per, whereas it is fitted with the top line of the V603 Aql light curve during the transition oscillations of V603 Aql. We added two model light curves of free-free emission for WDs with masses of  $1.2 M_{\odot}$  (black solid line) and  $1.05 M_{\odot}$  (magenta solid line). The light curve of the  $1.05 M_{\odot}$  WD is shifted against that of the  $1.2 M_{\odot}$  WD by  $\Delta \log t = \log f_s = -0.2$  and by  $\Delta V = -2.5 \log f_s = 0.50$  mag to make them overlap, as shown in the figure.

$0.07 = 7.2 \pm 0.07$  for  $E(B-V) = 0.07$  (Gallagher & Holm 1974).

Figure 40 shows the light curves of V1500 Cyg in the  $V$  and near-infrared (NIR) bands. The NIR data are taken from Ennis et al. (1977), Gallagher & Ney (1976), and Kawara et al. (1976) and the  $y$  and  $V$  data are from Lockwood & Millis (1976) and Tempesti (1979). When we shift each light curve of V1500 Cyg in the vertical direction, all the light curves merge into one line in the mid-time region. This property was explained by Hachisu & Kato (2006) as a characteristic property of free-free emission. Figure 40 also shows the light curves of GK Per and V603 Aql. The optical  $V$  data for GK Per are those in Figure 2 of Hachisu & Kato (2007). The data for V603 Aql are taken from Campbell & Shapley (1923) and the AAVSO. These light curves are shifted in the vertical direction so that they overlap with the free-free emission model light curves (black and magenta solid lines explained later). In addition, the light curve of GK Per is shifted by  $\Delta \log t = -0.2$  in the horizontal direction so that it overlaps with the final decline of the  $t^{-3}$  law for V1500 Cyg shown in Figure 40. We do not shift the light curve of V603 Aql in the time direction because its  $t^{-3}$  slope accidentally overlaps with that of V1500 Cyg. This means that the timescale of V603 Aql is almost the same as that of V1500 Cyg. Thus, we can determine the time-scaling factors as 0.63 for GK Per and 1.0 for V603 Aql, and the vertical shifts as  $\Delta V = 2.5$  mag for GK Per and  $\Delta V = 5.1$  mag for V603 Aql. The start time of V603 Aql is located in the middle because of its smaller envelope mass.

GK Per shows transition oscillations in the middle part of the light curve, and the bottom line of these oscillations almost coincides with our free-free emission model light curve. V603 Aql also shows transition oscillations, and its top line almost overlaps our model light curve. Both of these light curves agree with that of V1500 Cyg in the early phase and in the later phase of the  $t^{-3}$  law. The time-stretching method proposed by Hachisu & Kato (2010) is based on the relation  $m'_V = m_V - 2.5 \log f_s$  between two light curves that overlap each other. In Figure 40, we obtain the following relation among the apparent distance moduli of the three novae:

$$\begin{aligned}
 (m-M)_{V, \text{V1500 Cyg}} &= 12.3 \\
 &= (m-M)_{V, \text{GK Per}} + \Delta V - 2.5 \log 0.63 / 1.0 \\
 &\approx 9.3 \pm 0.1 + 2.5 + 0.50 = 12.3 \pm 0.1 \\
 &= (m-M)_{V, \text{V603 Aql}} + \Delta V + 2.5 \log 1.0 / 1.0
 \end{aligned}$$

$$= 7.2 \pm 0.07 + 5.1 - 0.0 = 12.3 \pm 0.07, \quad (\text{A1})$$

where we use distance moduli of  $(m-M)_V = 9.3 \pm 0.1$  for GK Per and  $(m-M)_V = 7.2 \pm 0.07$  for V603 Aql from Harrison et al.'s results obtained using the trigonometric parallax method. The latter two values in the third and fifth lines of Equation (A1) agree very well with our distance modulus in the first line of Equation (A1) presented in Section 3.4. Moreover, the mutual agreement in the two novae with their known trigonometric distances indicates that the time-stretching method is reliable.

Now we determine the WD masses of V1500 Cyg, GK Per, and V603 Aql using model light curve analysis of free-free emission. The model light curves are taken from Hachisu & Kato (2010). The best-fit model is  $M_{\text{WD}} = 1.20 M_{\odot}$  (black solid line) for V1500 Cyg. We select the  $1.20 M_{\odot}$  WD from the position at which a bend or break appears on the  $y$ ,  $H$ , and  $K$  light curves at  $\sim 65$  days ( $\log t_{\text{break}} \sim 1.8$ ) after the outburst (see Hachisu & Kato 2006, for more details). Here we search for the best-fit model by eye by changing the WD mass in  $0.05 M_{\odot}$  steps. This figure also shows the model light curve for a  $1.05 M_{\odot}$  WD shifted in the time direction by a scaling factor of 0.63 to overlap that of  $1.2 M_{\odot}$  WD. The resultant curve fits that of GK Per shifted by the same scaling factor of 0.63. Therefore, we adopted  $M_{\text{WD}} = 1.05 M_{\odot}$  for GK Per. For V603 Aql, the timescale is almost the same as that of V1500 Cyg. The WD mass of V603 Aql is almost the same, i.e.,  $M_{\text{WD}} = 1.20 M_{\odot}$ . This is very consistent with the dynamical mass of  $M_{\text{WD}} = 1.2 \pm 0.2 M_{\odot}$  obtained by Arenas et al. (2000).

Hachisu & Kato (2010) calibrated the absolute magnitudes of their free-free model light curves. Using their absolute magnitudes, we obtained the distance modulus of GK Per as

$$[(m-M)_{V,\text{GK Per}}]_{\text{FF}} = m_w - M_w = 10.9 - 1.6 = 9.3 \quad (\text{A2})$$

from  $m_w = 10.9$  and  $M_w = 1.6$  ( $M_{\text{WD}} = 1.05 M_{\odot}$ ) in Table 3 of Hachisu & Kato (2010). We obtained the distance modulus of V1500 Cyg as

$$[(m-M)_{V,\text{V1500 Cyg}}]_{\text{FF}} = m_w - M_w = 13.0 - 0.7 = 12.3 \quad (\text{A3})$$

from  $m_w = 13.0$  and  $M_w = 0.7$  ( $M_{\text{WD}} = 1.20 M_{\odot}$ ) in Table 3 of Hachisu & Kato (2010). Here,  $m_w/M_w$  is the apparent/absolute magnitude at the end point of optically-thick winds (denoted by a large open circle at the end of each black or magenta free-free model light curve). The value of  $m_w$  is read directly from Figure 40 and  $M_w$  was calibrated and given in Table 3 of Hachisu & Kato (2010). These results from Equations (A2) and (A3) are consistent with the results of Equation (A1). Thus, we confirm the validity of our time-stretching method; at the same time, we show that the absolute magnitudes of our model light curves, which are based on the free-free emission light curves, are consistently calibrated with the absolute magnitudes of GK Per and V603 Aql, which are based on trigonometric parallax.

Figure 41 shows the  $V$  light curves and  $(B-V)_0$  and  $(U-B)_0$  color evolution of PW Vul, V1500 Cyg, V1668 Cyg, and V1974 Cyg as well as those of V533 Her. We squeezed the light curves of PW Vul, V1668 Cyg, V1974 Cyg, and V533 Her in the time direction by factors of 0.21, 0.44, 0.50, and 0.54 and shifted them by  $\Delta V = -1.6$ ,  $\Delta V = -2.6$ ,  $\Delta V = -0.4$ , and  $\Delta V = +0.8$  mag, respectively, against that of V1500 Cyg. Then, we obtained the apparent distance modulus in the  $V$  band as

$$\begin{aligned} (m-M)_{V,\text{V1500 Cyg}} &= 12.3 \\ &= (m-M)_{V,\text{PW Vul}} + \Delta V - 2.5 \log 0.21/1.0 \\ &\approx 13.0 - 2.4 + 1.7 = 12.3 \\ &= (m-M)_{V,\text{V1668 Cyg}} + \Delta V - 2.5 \log 0.44/1.0 \\ &\approx 14.25 - 2.9 + 0.90 = 12.25 \\ &= (m-M)_{V,\text{V1974 Cyg}} + \Delta V - 2.5 \log 0.50/1.0 \\ &\approx 12.2 - 0.6 + 0.75 = 12.35 \\ &= (m-M)_{V,\text{V533 Her}} + \Delta V - 2.5 \log 0.54/1.0 \\ &\approx 10.8 + 0.8 + 0.67 = 12.27, \end{aligned} \quad (\text{A4})$$

where the apparent distance moduli of PW Vul, V1500 Cyg, V1668 Cyg, and V1974 Cyg were already obtained as  $(m-M)_{V,\text{PW Vul}} = 13.0$  in Section 3.1,  $(m-M)_{V,\text{V1500 Cyg}} = 12.3$  in Section 3.4,  $(m-M)_{V,\text{V1668 Cyg}} = 14.25$  in Section 3.5, and  $(m-M)_{V,\text{V1974 Cyg}} = 12.2$  in Section 3.6. These are all consistent with each other. Therefore, we can use this method to obtain the distance modulus of a target nova; the distance modulus of V533 Her is found to be  $(m-M)_{V,\text{V533 Her}} = 10.8$ .

In Figure 41, we also plotted UV 1455Å fluxes for PW Vul (magenta open circles with plus sign), V1668 Cyg (black filled squares), and V1974 Cyg (green filled triangles). UV 1455Å fluxes of V1974 Cyg and PW Vul are scaled down by 0.005 and 0.88 to fit its shape with those of V1668 Cyg. In this figure we adopted  $M_{\text{WD}} = 0.83 M_{\odot}$  for PW Vul as a best-fit model for our assumed chemical composition of  $X = 0.55$ ,  $Y = 0.23$ ,  $Z = 0.02$ , and  $X_{\text{CNO}} = 0.20$  (magenta solid lines). The distance-reddening relation (magenta solid line in Figure 35(d)) of UV 1455Å flux fitting is calculated from Equation (10) for PW Vul. We adopted  $F_{\lambda}^{\text{obs}} = 4.5 \times 10^{-12} \text{ erg s}^{-1} \text{ cm}^{-2} \text{ Å}^{-1}$ , which is the observed flux at  $\lambda = 1455\text{Å}$  corresponding to the upper bound of Figure 41(a), and  $F_{\lambda}^{\text{mod}} = 1.1 \times 10^{-11} \text{ erg s}^{-1} \text{ cm}^{-2} \text{ Å}^{-1}$ , which is the model flux of the  $0.83 M_{\odot}$  WD corresponding to the upper bound of Figure 41(a).

In this way, we obtained the distance moduli for various novae studied in Section 6, using the time-stretching method. From Figure 42, we obtain the apparent distance moduli in the  $V$  band as

$$\begin{aligned} (m-M)_{V,\text{RS Oph}} &= 12.8 \\ &= (m-M)_{V,\text{V1500 Cyg}} + \Delta V - 2.5 \log 1.0/5.6 \\ &= 12.3 + (+0.0 - 1.4) + 1.88 = 12.78 \\ &= (m-M)_{V,\text{V1668 Cyg}} + \Delta V - 2.5 \log 0.44/5.6 \end{aligned}$$



$$\begin{aligned}
&\approx 14.25 + (-2.9 - 1.4) + 2.76 = 12.71 \\
&= (m-M)_{V,V446 \text{ Her}} + \Delta V - 2.5 \log 1.41/5.6 \\
&\approx 11.7 + (+1.0 - 1.4) + 1.50 = 12.80 \\
&= (m-M)_{V,V382 \text{ Vel}} + \Delta V - 2.5 \log 0.89/5.6 \\
&\approx 11.4 + (+0.8 - 1.4) + 2.0 = 12.80.
\end{aligned} \tag{A5}$$

In Figure 42, we also plotted the UV 1455Å fluxes of the 1985 RS Oph outburst (red filled triangles) together with those of V1668 Cyg (black filled squares) and V1974 Cyg (blue filled circles). The UV 1455Å flux of RS Oph is scaled down by 0.0625 (= 1/16) to fit its shape with those of V1974 Cyg/V1668 Cyg. In this figure we adopted  $M_{\text{WD}} = 1.37 M_{\odot}$  for RS Oph as a best-fit model for our assumed chemical composition of  $X = 0.55$ ,  $Y = 0.23$ ,  $Z = 0.02$ , and  $X_{\text{CNO}} = 0.20$  (magenta solid lines). The distance-reddening relation (magenta solid line in Figure 34(a)) of UV 1455Å flux fitting is calculated from Equation (10) for RS Oph. We adopted  $F_{\lambda}^{\text{obs}} = 5.0 \times 10^{-11} \text{ erg s}^{-1} \text{ cm}^{-2} \text{ Å}^{-1}$ , which is the observed flux at  $\lambda = 1455\text{Å}$  corresponding to the upper bound of Figure 42(a), and  $F_{\lambda}^{\text{mod}} = 1.7 \times 10^{-11} \text{ erg s}^{-1} \text{ cm}^{-2} \text{ Å}^{-1}$ , which is the model flux of the  $1.37 M_{\odot}$  WD corresponding to the upper bound of Figure 42(a).

In Figure 43, the  $V$  light curve of T Pyx almost overlaps that of DQ Her from the maximum to the final  $t^{-3}$  decline law (thin solid black line) except for the dust blackout period of DQ Her. The final  $t^{-3}$  decline law can be explained as free-free emission from a homologously expanding nebula (see, e.g., Hachisu & Kato 2006) after the optically-thick winds ended. In this figure, we took a start of day about 20 days after the outburst of T Pyx in order to make the final declines of each nova overlap. Because the overall timescales of these four novae (DQ Her, NQ Vul, V475 Sct, and T Pyx) are almost the same, we consider that their brightnesses are almost the same, i.e.,

$$\begin{aligned}
(m-M)_{V,T \text{ Pyx}} &= 13.8 \\
&= (m-M)_{V,DQ \text{ Her}} + \Delta V \\
&= 8.2 + (+5.4 + 0.2) = 13.8 \\
&= (m-M)_{V,NQ \text{ Vul}} + \Delta V \\
&= 13.6 + (+0.0 + 0.2) = 13.8 \\
&= (m-M)_{V,V475 \text{ Sct}} + \Delta V \\
&= 15.6 + (-2.0 + 0.2) = 13.8.
\end{aligned} \tag{A6}$$

From Figure 44, we derive

$$\begin{aligned}
(m-M)_{V,LV \text{ Vul}} &= 11.9 \\
&= (m-M)_{V,V1500 \text{ Cyg}} + \Delta V - 2.5 \log 1.0/0.45 \\
&\approx 12.3 + (+0.0 + 0.5) - 0.87 = 11.93 \\
&= (m-M)_{V,IV \text{ Cep}} + \Delta V - 2.5 \log 0.40/0.45 \\
&\approx 14.7 + (-3.4 + 0.5) + 0.13 = 11.93 \\
&= (m-M)_{V,V1494 \text{ Aql}} + \Delta V - 2.5 \log 1.0/0.45 \\
&\approx 13.1 + (-0.8 + 0.5) - 0.87 = 11.93 \\
&= (m-M)_{V,V5114 \text{ Sgr}} + \Delta V - 2.5 \log 0.56/0.45 \\
&\approx 16.5 + (-4.8 + 0.5) - 0.24 = 11.96.
\end{aligned} \tag{A7}$$

From Figure 45,

$$\begin{aligned}
(m-M)_{V,V1419 \text{ Aql}} &= 14.6 \\
&= (m-M)_{V,V1668 \text{ Cyg}} + \Delta V - 2.5 \log 1.26/0.79 \\
&\approx 14.25 + (+1.5 - 0.6) - 0.51 = 14.64 \\
&= (m-M)_{V,V1065 \text{ Cen}} + \Delta V - 2.5 \log 1.0/0.79 \\
&= 15.5 + (+0.0 - 0.6) - 0.26 = 14.64 \\
&= (m-M)_{V,V496 \text{ Sct}} + \Delta V - 2.5 \log 0.50/0.79 \\
&\approx 13.6 + (+1.1 - 0.6) + 0.50 = 14.59.
\end{aligned} \tag{A8}$$

From Figure 46,

$$\begin{aligned}
(m-M)_{V,IV \text{ Cep}} &= 14.7 \\
&= (m-M)_{V,V1500 \text{ Cyg}} + \Delta V - 2.5 \log 1.0/0.40 \\
&\approx 12.3 + (+0.0 + 3.4) - 0.99 = 14.71 \\
&= (m-M)_{V,V1668 \text{ Cyg}} + \Delta V - 2.5 \log 0.54/0.40 \\
&\approx 14.25 + (-2.6 + 3.4) - 0.33 = 14.72 \\
&= (m-M)_{V,V2468 \text{ Cyg}} + \Delta V - 2.5 \log 0.45/0.40 \\
&\approx 15.6 + (-4.1 + 3.4) - 0.13 = 14.77 \\
&= (m-M)_{V,V2491 \text{ Cyg}} + \Delta V - 2.5 \log 1.41/0.40 \\
&\approx 16.5 + (-3.8 + 3.4) - 1.34 = 14.73,
\end{aligned} \tag{A9}$$

From Figure 47,

$$\begin{aligned}
(m-M)_{V,IV \text{ Cep}} &= 14.7 \\
&= (m-M)_{V,V1668 \text{ Cyg}} + \Delta V - 2.5 \log 0.54/0.40
\end{aligned}$$

$$\begin{aligned}
&\approx 14.25 + (-2.6 + 3.4) - 0.33 = 14.72 \\
&= (m-M)_{V,V2467 \text{ Cyg}} + \Delta V - 2.5 \log 0.50/0.40 \\
&\approx 16.2 + (-4.6 + 3.4) - 0.24 = 14.76 \\
&= (m-M)_{V,V2468 \text{ Cyg}} + \Delta V - 2.5 \log 0.45/0.40 \\
&\approx 15.6 + (-4.1 + 3.4) - 0.13 = 14.77.
\end{aligned} \tag{A10}$$

From Figure 48,

$$\begin{aligned}
(m-M)_{V,V496 \text{ Sct}} &= 13.6 \\
&= (m-M)_{V,FH \text{ Ser}} + \Delta V \\
&= 11.7 + (+1.9 - 0.0) = 13.6 \\
&= (m-M)_{V,NQ \text{ Vul}} + \Delta V \\
&= 13.6 + (+0.0 - 0.0) = 13.6 \\
&= (m-M)_{V,V2274 \text{ Cyg}} + \Delta V \\
&= 18.7 + (-5.1 - 0.0) = 13.6.
\end{aligned} \tag{A11}$$

From Figure 49,

$$\begin{aligned}
(m-M)_{V,V1370 \text{ Aql}} &= 15.2 \\
&= (m-M)_{V,V1668 \text{ Cyg}} + \Delta V - 2.5 \log 0.50/1.0 \\
&\approx 14.25 + 0.2 + 0.75 = 15.2 \\
&= (m-M)_{V,OS \text{ And}} + \Delta V - 2.5 \log 0.63/1.0 \\
&\approx 14.7 + 0.0 + 0.50 = 15.2.
\end{aligned} \tag{A12}$$

From Figure 50,

$$\begin{aligned}
(m-M)_{V,GQ \text{ Mus}} &= 15.7 \\
&= (m-M)_{V,V1974 \text{ Cyg}} + \Delta V - 2.5 \log 1.0/0.26 \\
&= 12.2 + (-0.0 + 5.0) - 1.46 = 15.74 \\
&= (m-M)_{V,PW \text{ Vul}} + \Delta V - 2.5 \log 0.42/0.26 \\
&= 13.0 + (-1.8 + 5.0) - 0.52 = 15.68 \\
&= (m-M)_{V,QU \text{ Vul}} + \Delta V - 2.5 \log 0.42/0.26 \\
&= 13.5 + (-2.3 + 5.0) - 0.52 = 15.68.
\end{aligned} \tag{A13}$$

In Figure 50, we plotted UV 1455Å fluxes for PW Vul (blue open circles with plus sign), GQ Mus (magenta filled circles), V1974 Cyg (red filled squares), and QU Vul (green open circles). In this figure we adopted  $M_{\text{WD}} = 0.65 M_{\odot}$  for GQ Mus as a best-fit model for our assumed chemical composition of  $X = 0.35$ ,  $Y = 0.33$ ,  $Z = 0.02$ , and  $X_{\text{CNO}} = 0.30$  (blue solid lines). The distance-reddening relation (magenta solid line in Figure 35(c)) of UV 1455Å flux fitting is calculated from Equation (10) for GQ Mus. We adopted  $F_{\lambda}^{\text{obs}} = 5.0 \times 10^{-13} \text{ erg s}^{-1} \text{ cm}^{-2} \text{ Å}^{-1}$ , which is the observed flux at  $\lambda = 1455\text{Å}$  corresponding to the upper bound of Figure 50(a), and  $F_{\lambda}^{\text{mod}} = 8.5 \times 10^{-12} \text{ erg s}^{-1} \text{ cm}^{-2} \text{ Å}^{-1}$ , which is the model flux of the  $0.65 M_{\odot}$  WD corresponding to the upper bound of Figure 50(a). We also adopted  $M_{\text{WD}} = 0.95 M_{\odot}$  for QU Vul as a best-fit model for our assumed chemical composition of  $X = 0.65$ ,  $Y = 0.27$ ,  $Z = 0.02$ ,  $X_{\text{CNO}} = 0.03$ , and  $X_{\text{Ne}} = 0.03$ . The distance-reddening relation (magenta solid line in Figure 36(a)) of UV 1455Å flux fitting is calculated from Equation (10) for QU Vul. We adopted  $F_{\lambda}^{\text{obs}} = 3.0 \times 10^{-12} \text{ erg s}^{-1} \text{ cm}^{-2} \text{ Å}^{-1}$ , which is the observed flux at  $\lambda = 1455\text{Å}$  corresponding to the upper bound of Figure 50(a), and  $F_{\lambda}^{\text{mod}} = 1.1 \times 10^{-11} \text{ erg s}^{-1} \text{ cm}^{-2} \text{ Å}^{-1}$ , which is the model flux of the  $0.95 M_{\odot}$  WD corresponding to the upper bound of Figure 50(a).

From Figure 51,

$$\begin{aligned}
(m-M)_{V,QV \text{ Vul}} &= 14.0 \\
&= (m-M)_{V,FH \text{ Ser}} + \Delta V \\
&= 11.7 + (-0.0 + 2.3) = 14.0 \\
&= (m-M)_{V,V705 \text{ Cas}} + \Delta V \\
&= 13.4 + (-1.7 + 2.3) = 14.0 \\
&= (m-M)_{V,V2615 \text{ Oph}} + \Delta V \\
&= 16.5 + (-4.8 + 2.3) = 14.0.
\end{aligned} \tag{A14}$$

From Figure 52,

$$\begin{aligned}
(m-M)_{V,V443 \text{ Sct}} &= 15.5 \\
&= (m-M)_{V,PW \text{ Vul}} + \Delta V - 2.5 \log 1.0 \\
&= 13.0 + 2.5 + 0.0 = 15.5 \\
&= (m-M)_{V,V458 \text{ Vul}} + \Delta V - 2.5 \log 2.0 \\
&\approx 15.5 + 0.7 - 0.75 = 15.45.
\end{aligned} \tag{A15}$$

The obtained values of  $(m-M)_V$  are summarized in Table 2.

#### REFERENCES

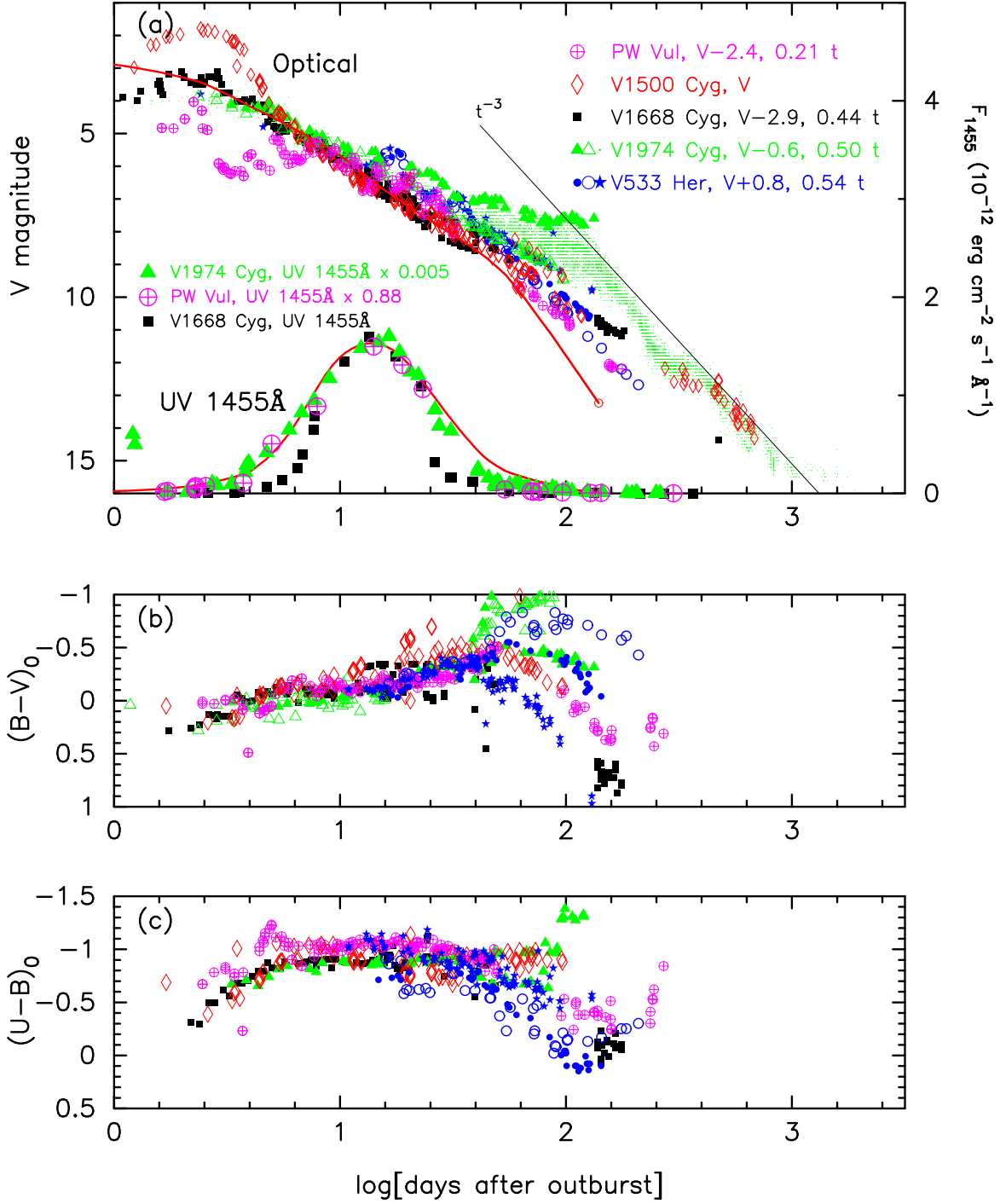


FIG. 41.— (a) V band and UV 1455Å narrow band light curves, (b)  $(B-V)_0$ , and (c)  $(U-B)_0$  color curves for PW Vul (magenta open circles with plus sign), V1500 Cyg (red open diamonds), V1668 Cyg (black filled squares), and V1974 Cyg (green open and filled triangles). Those of V533 Her are also shown for comparison. Blue filled circles are taken from van Genderen (1963), blue open circles are from Chincarini (1964), and blue star symbols are from Shen et al. (1964). To make them overlap in the early decline phase, we stretched the light curves of PW Vul, V1668 Cyg, V1974 Cyg, and V533 Her by 0.21, 0.44, 0.50, and 0.54, and shifted their magnitudes by -2.4, -2.9, -0.6, and +0.8 mag, respectively, as indicated in the figure. UV 1455Å fluxes of each nova are also rescaled as indicated in the figure.

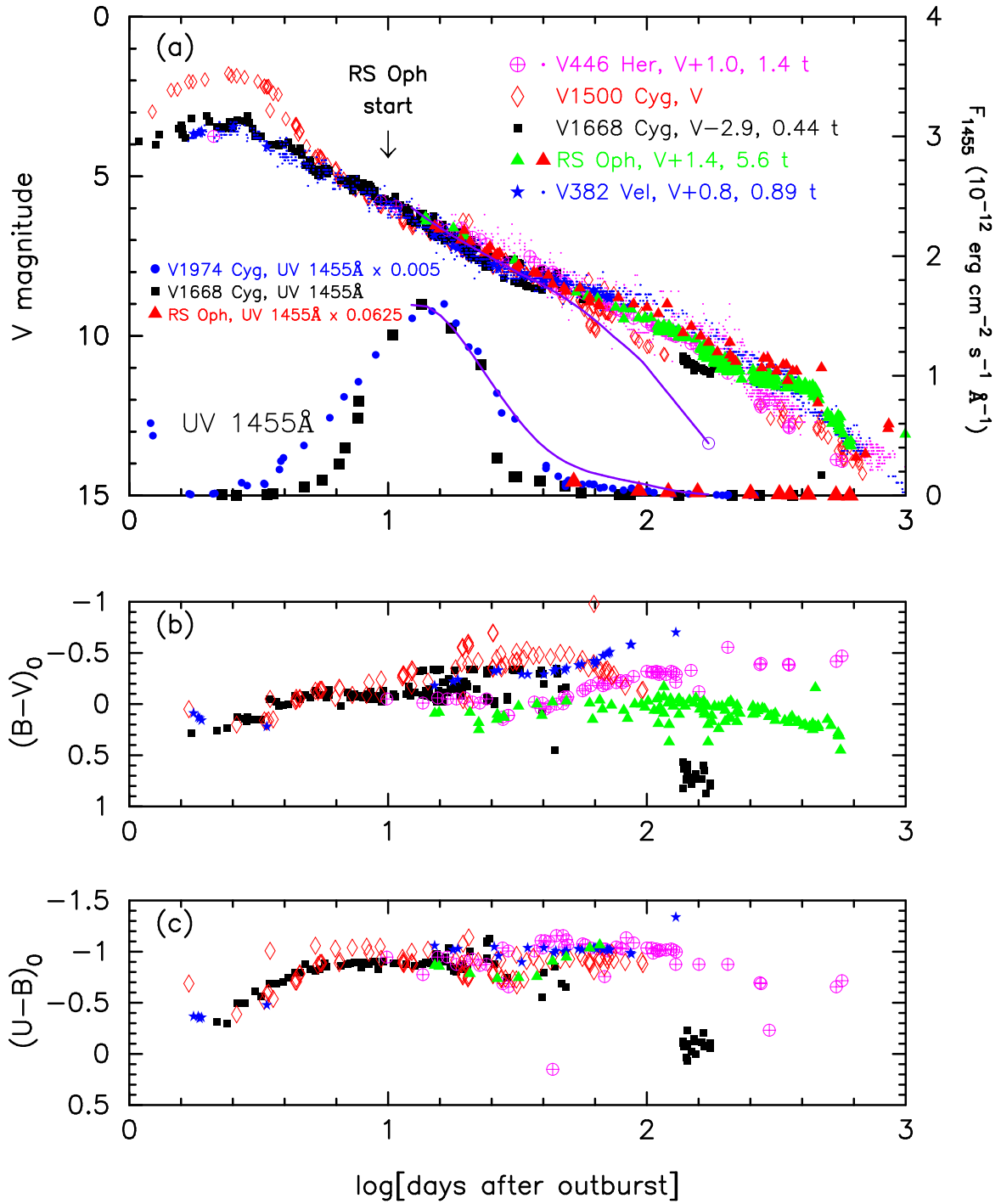


FIG. 42.— Same as Figure 41, but for V446 Her, V1500 Cyg, V1668 Cyg, RS Oph, and V382 Vel. Time-stretching factors and vertical shifts of these novae are shown in the figure. We arranged the origin of the time of RS Oph according to that of V1668 Cyg. The UV 1455Å fluxes of V1668 Cyg, V1974 Cyg, and RS Oph are added. Model light curve is also added for RS Oph ( $1.37 M_{\odot}$  WD, purple solid lines). See text for more details.

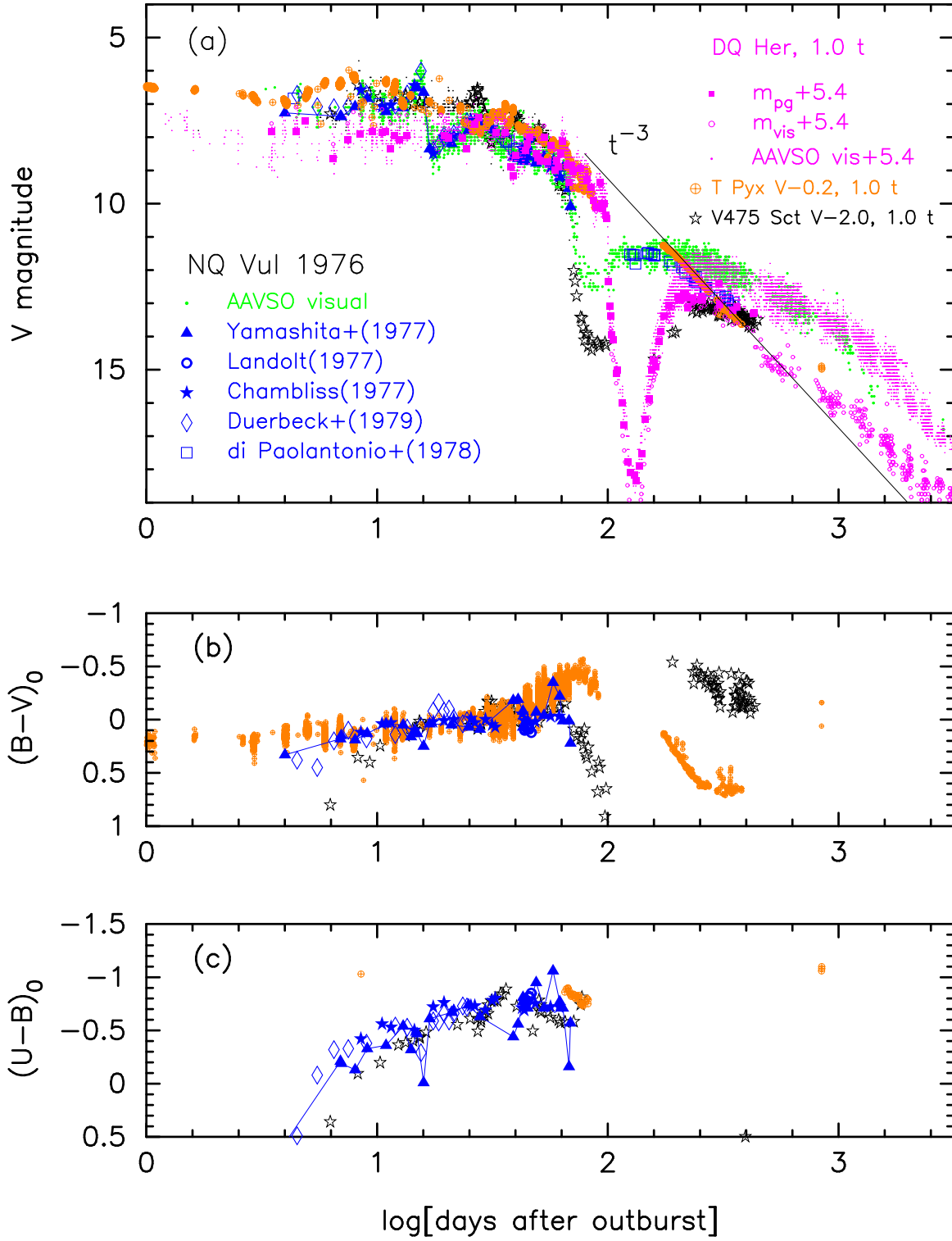


FIG. 43.— Same as Figure 41, but for DQ Her, NQ Vul, V475 Sct, and T Pyx. For T Pyx, we take the start of the day about 20 days after the outburst.



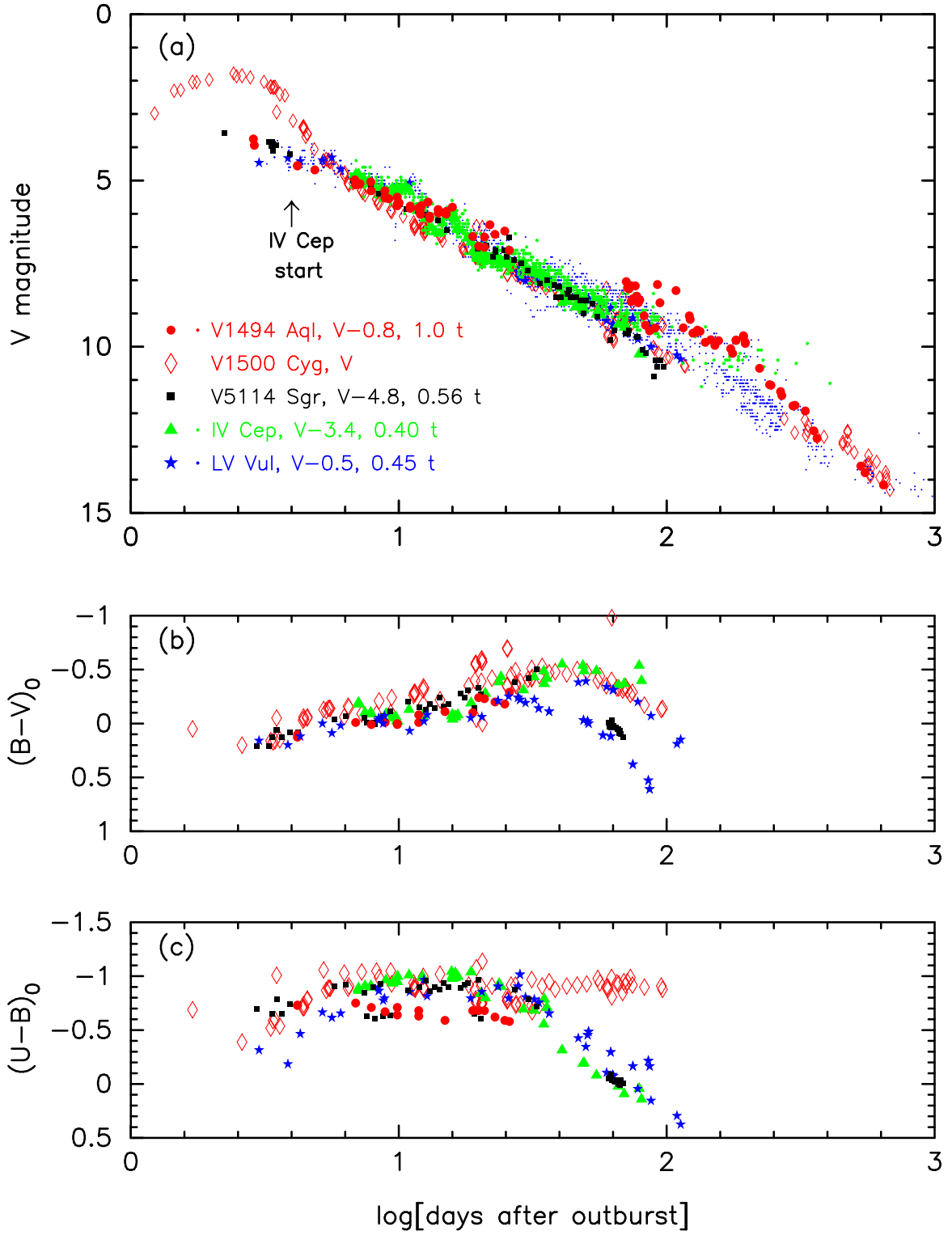


FIG. 44.— Same as Figure 41, but for LV Vul (blue filled star symbols and dots), IV Cep (green filled triangles and dots), V1494 Aql (red filled circles), V5114 Sgr (black filled squares), and V1500 Cyg (red open diamonds). The visual data (small dots) of each nova are taken from the AAVSO archive. To make them overlap in the early decline phase, we stretched the light curves of LV Vul, IV Cep, V1494 Aql, and V5114 Sgr by 0.45, 0.40, 1.0, and 0.56, and shifted their magnitudes up by 0.5, 3.4, 0.8, and 4.8 mag, respectively, against V1500 Cyg, as indicated in the figure.

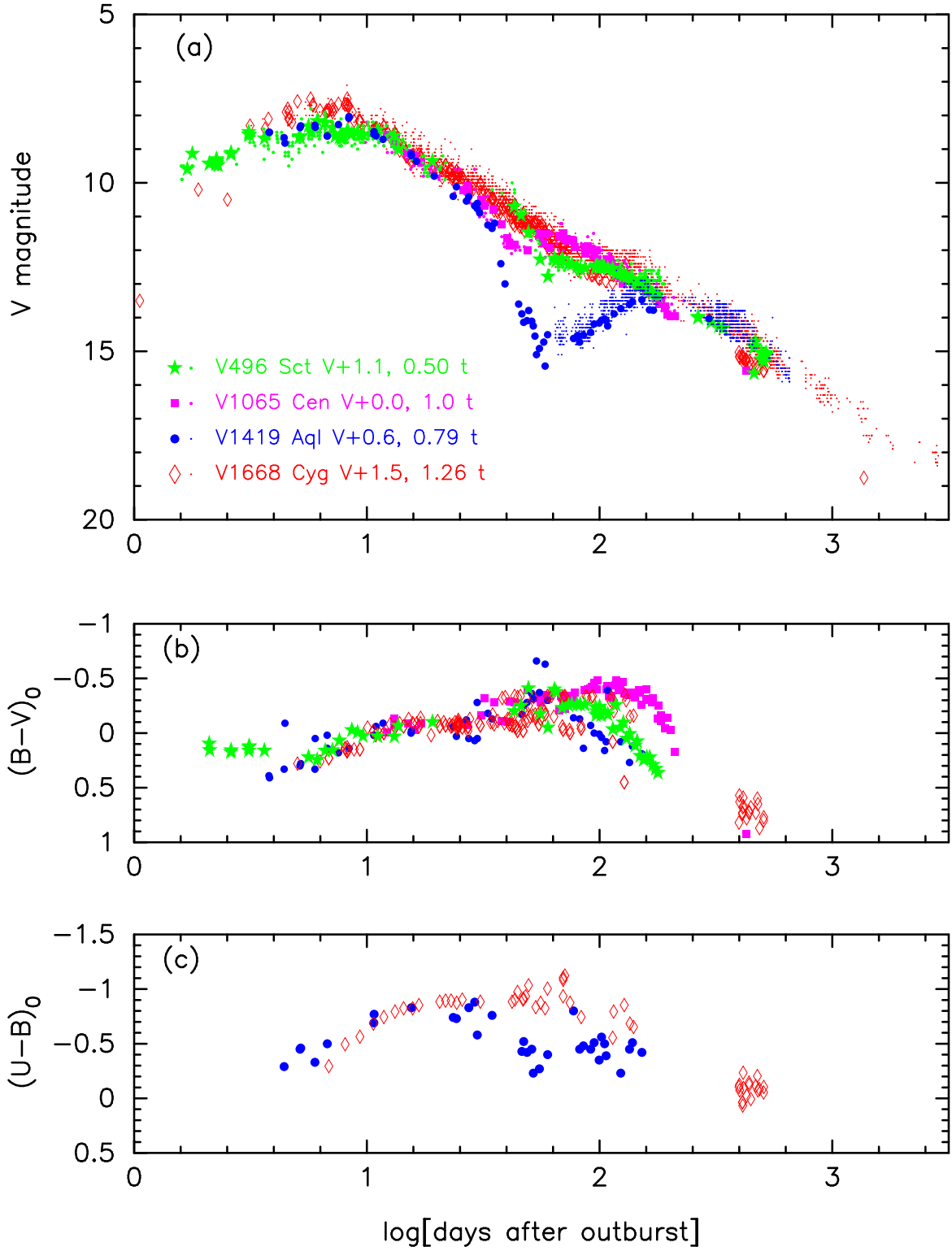


FIG. 45.— Same as Figure 41, but for V496 Sct (green star symbols and dots), V1065 Cen (magenta filled squares and dots), V1419 Aql (blue filled circles and dots), and V1668 Cyg (red open diamonds and dots). The time of V1668 Cyg, V1419 Aql, V1065 Cen, and V496 Sct are stretched by a factor of 1.26, 0.79, 1.0, and 0.50, respectively. We shifted the visual and  $V$  light curves of V1668 Cyg, V1419 Aql, V1065 Cen, and V496 Sct, down by 1.5, 0.6, 0.0, and 1.1 mag, respectively. These four  $V$  light curves almost overlap in the early decline phase.

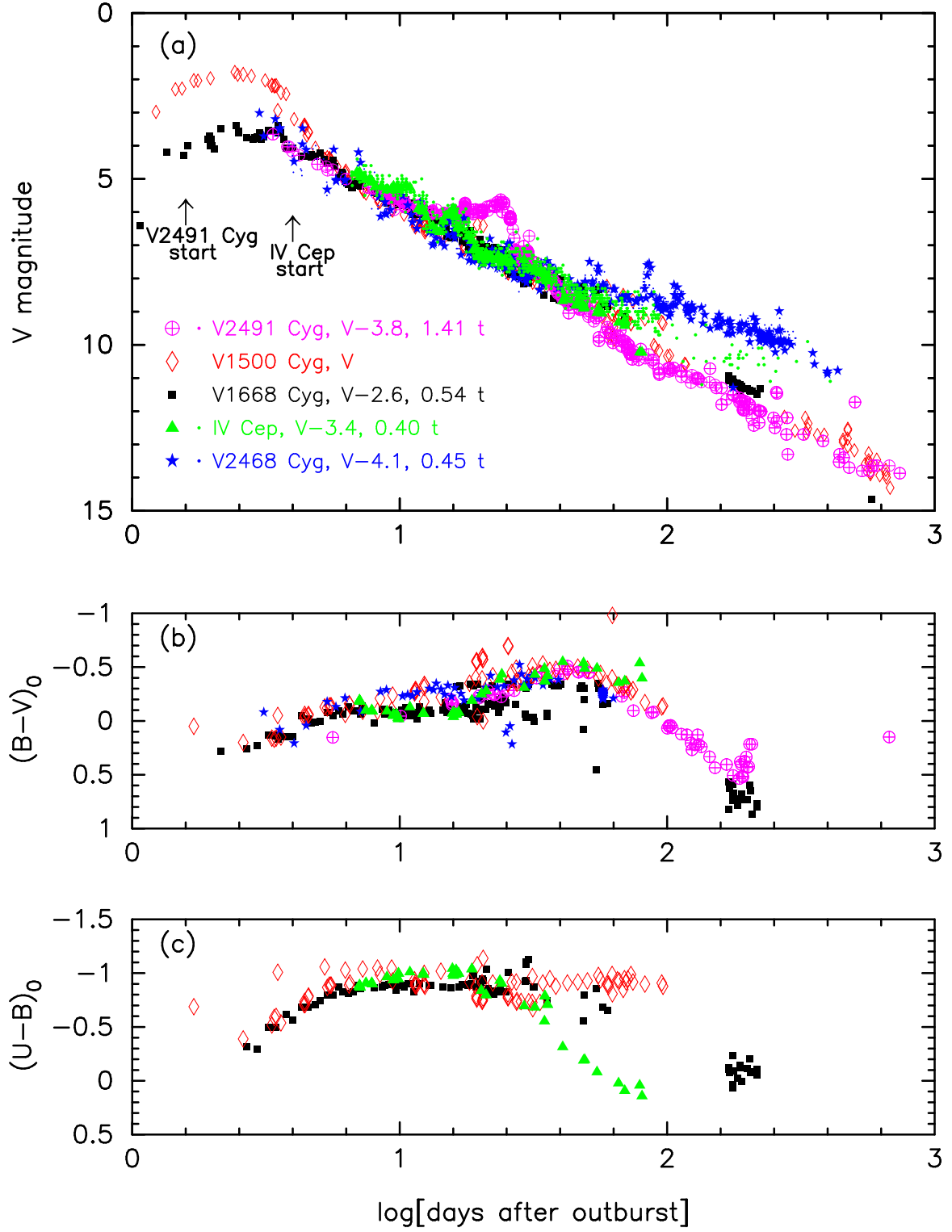


FIG. 46.— Same as Figure 41, but for V2491 Cyg, V1500 Cyg, V1668 Cyg, IV Cep, and V2468 Cyg. The start of the outburst is indicated by an arrow for IV Cep and V2491 Cyg.

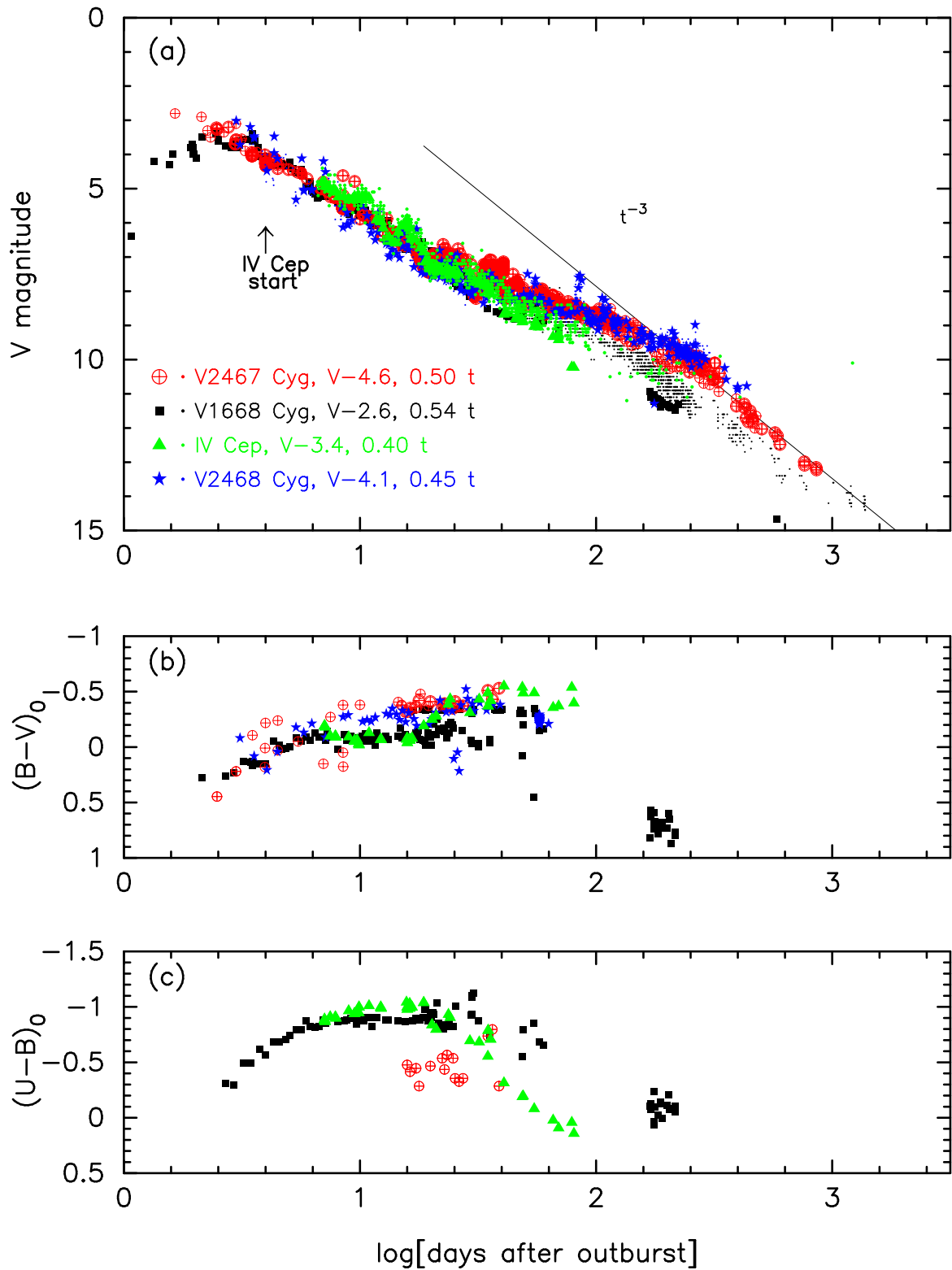


FIG. 47.— Same as Figure 41, but for V2467 Cyg, V1668 Cyg, IV Cep, and V2468 Cyg.

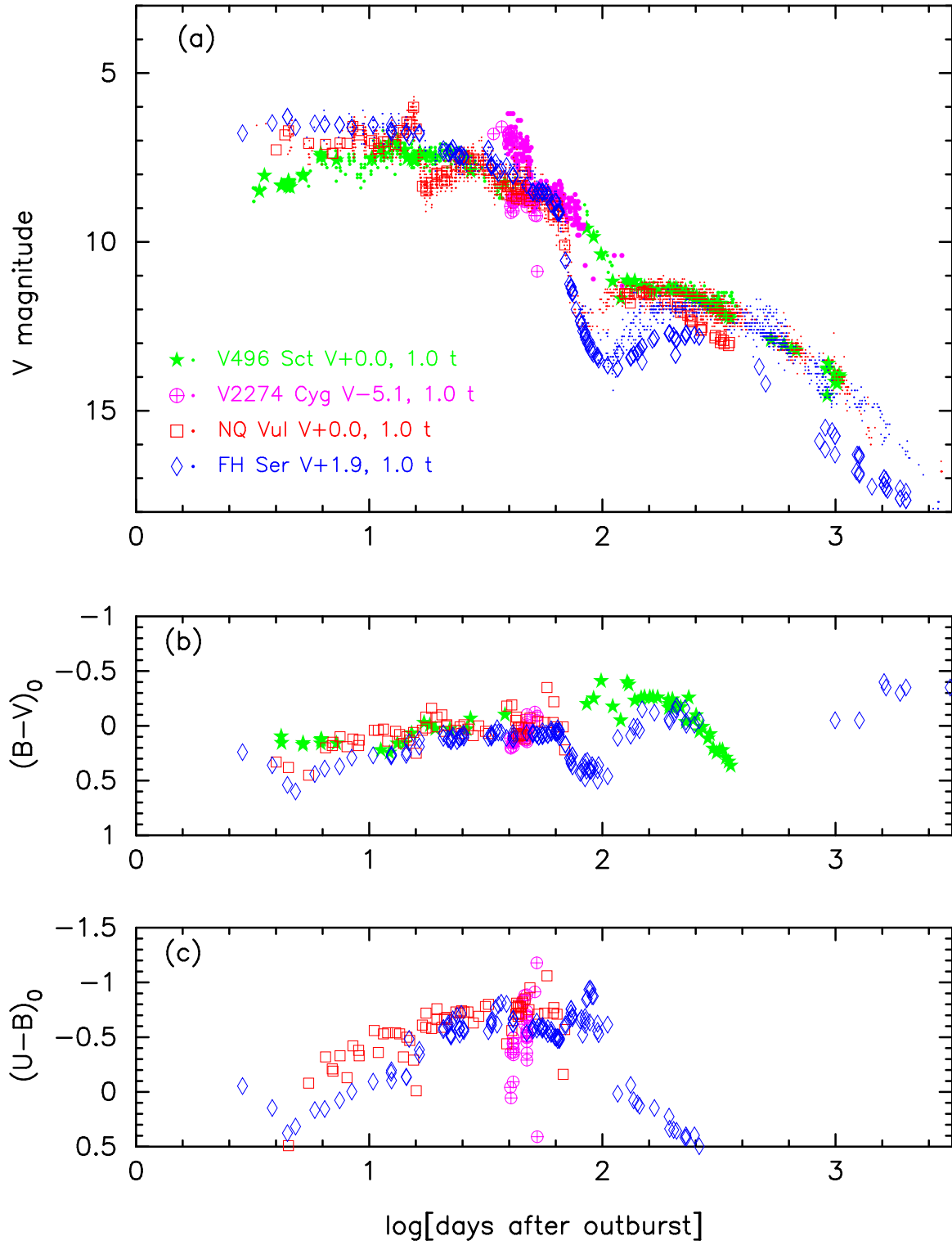


FIG. 48.— Same as Figures 43, but for V496 Sct (green symbols), V2274 Cyg (magenta symbols), NQ Vul (red symbols, including the data from all the authors in Figure 43), and FH Ser (blue symbols, including the data from all the authors in Figure 43). The data for V2274 Cyg are taken from Voloshina et al. (2002a), Voloshina & Metlova (2002b), and IAU Circular Nos. 7666 and 7668 (open circles with a plus sign inside), and the AAVSO archive (small dots).



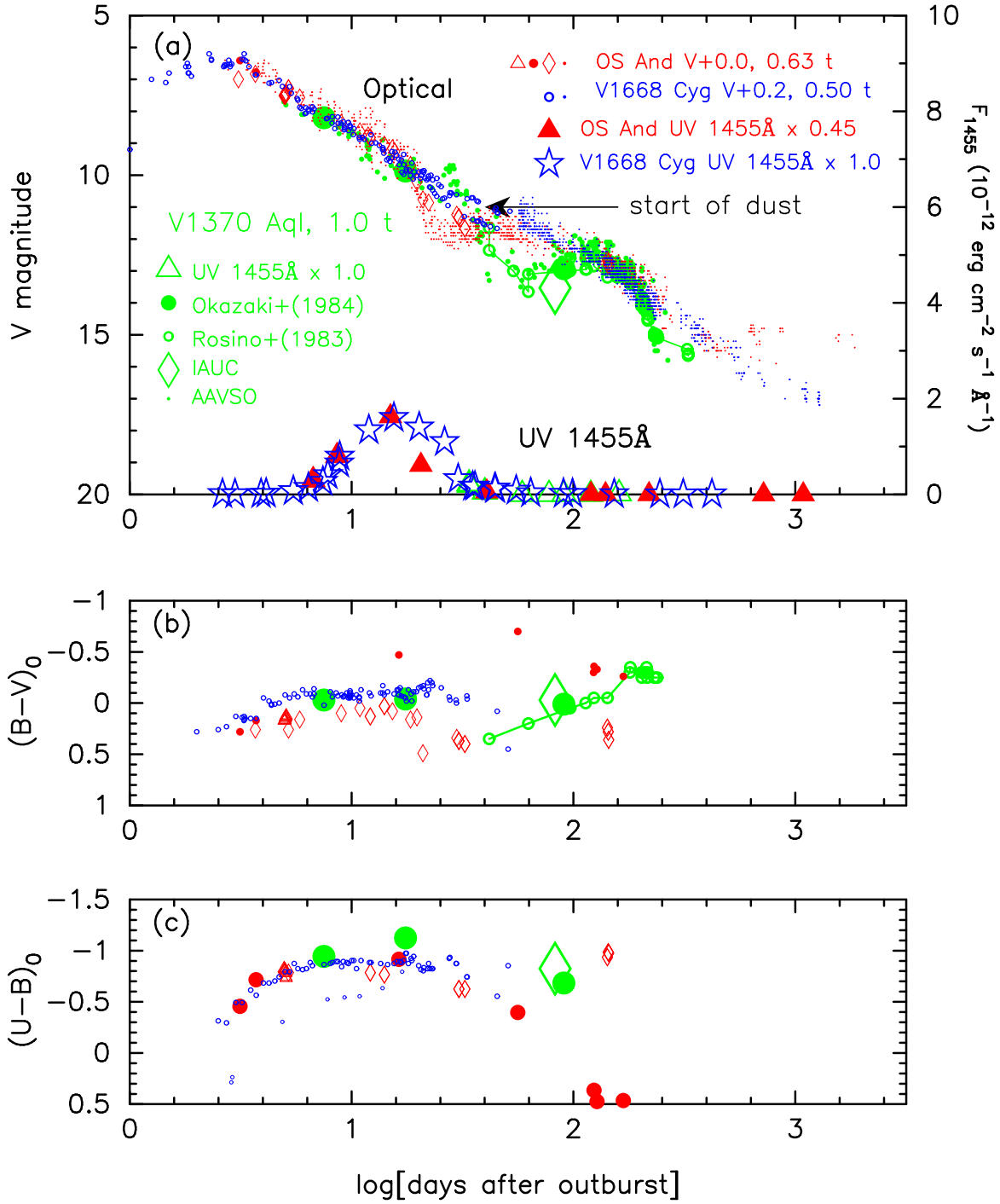


FIG. 49.— Same as Figure 41, but for V1370 Aql, V1668 Cyg, and OS And. The  $V$  light curves of V1668 Cyg and OS And are squeezed by factors of 0.50 and 0.63 and shifted down by 0.2 and 0.0 mag, respectively, against that of V1370 Aql. The UV 1455Å data for OS And and V1668 Cyg are also plotted. The flux scale is linear between 0.0 and  $1.0 \times 10^{-11} \text{ erg s}^{-1} \text{ cm}^{-1} \text{ Å}^{-1}$  for V1668 Cyg (from the bottom to the top of the frame) but scaled down by 2.2 times for OS And to match them with those of V1668 Cyg.

Alcock, G. E. D. 1976, IAU Circ., 2997, 1  
 Allen, C. W. 1973, *Astrophysical Quantities* (3rd ed.; London: Athlone)  
 Ando, H., & Yamashita, Y. 1976, PASJ, 28, 171  
 Andrae, J., Drechsel, H., Snijders, M. A. J., & Cassatella, A. 1991, A&A, 244, 111  
 Andrillat, Y., Antipova, L. I., & Babaev, M. B. 1986, SvA, 30, 79  
 Anupama, G. C., Duerbeck, H. W., Prabhu, T. P., & Jain, S. K. 1992, A&A, 263, 87  
 Arenas, J., Catalán, M. S., Augusteijn, T., & Retter, A. 2000, MNRAS, 311, 135  
 Arkhipova, V. P., & Zaitseva, G. V. 1976, SvAL, 2, 35

Austin, S. J., Wagner, R. M., Starrfield, S., et al. 1996, AJ, 111, 869  
 Balman, S., Krautter, J., & Ögelman, H. 1998, ApJ, 499, 395  
 Barnes, T. G., & Evans, N. R. 1970, PASP, 82, 889  
 Becker, H. J., & Duerbeck, H. W. 1980, PASP, 92, 792  
 Beckmann, K., & Collins, P. 1987, IAU Circ., 4488, 1  
 Belyakina, T. S., Bondar, N. I., Chochol, D., et al., 1989, A&A, 223, 119  
 Bergner, Iu. K., Miroshnichenko, A. S., Iudin, R. V., Iutanov, N. Iu., & Dzakusheva, K. G. 1988, Ap&SS, 149, 63  
 Bohlin, R. C., Savage, B. D., & Drake, J. F. 1978, ApJ, 224, 132  
 Borra, E. F., & Andersen, P. H. 1970, PASP, 82, 1070  
 Bronkalla, W., & Notni, P. 1961, AN, 286, 179

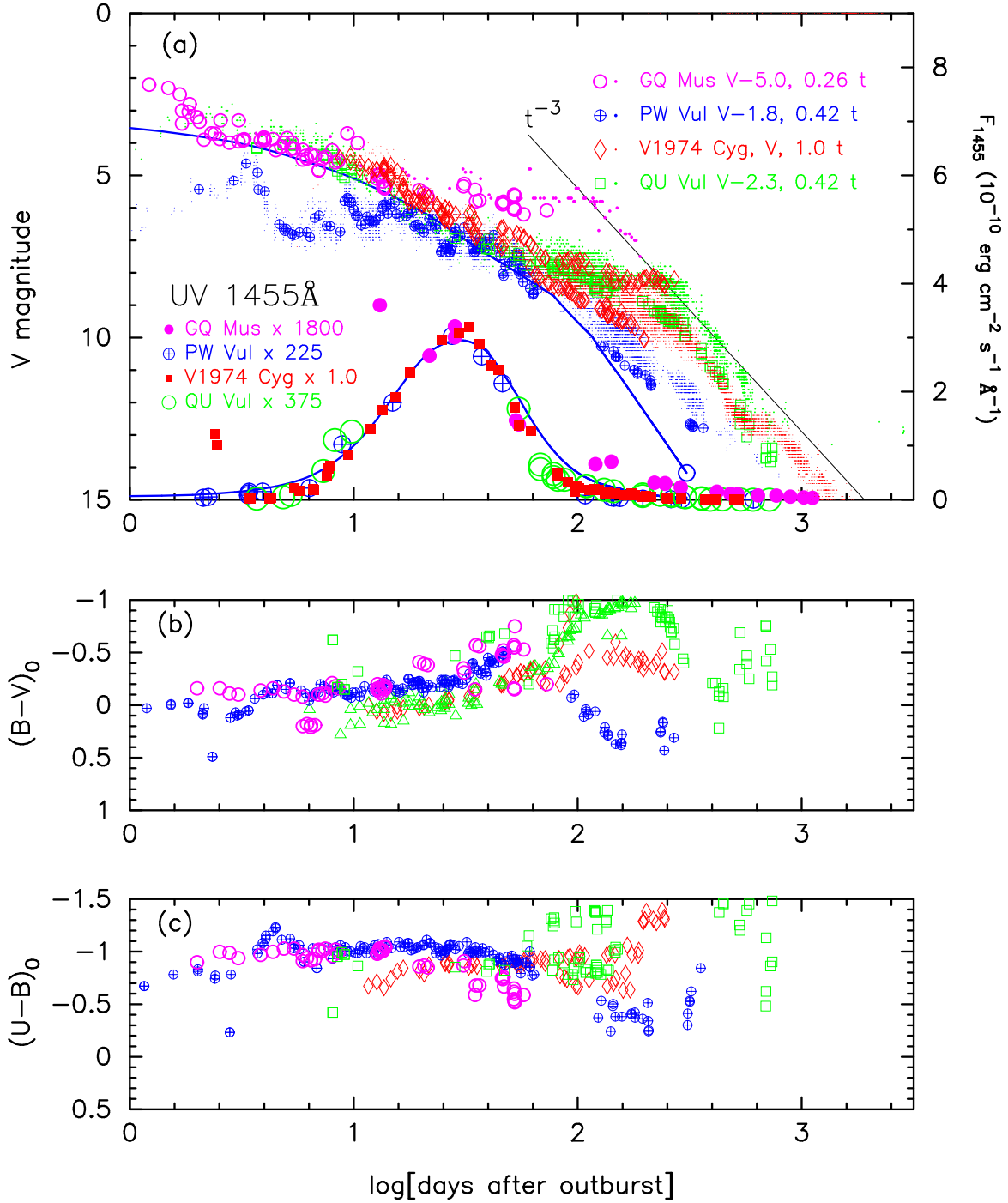


FIG. 50.— Same as Figure 41, but for GQ Mus (magenta open circles for optical/magenta filled circles for UV 1455Å), PW Vul (blue circles with a plus sign for both optical and UV 1455Å), V1974 Cyg (red open diamonds/red filled squares), and QU Vul (green open squares/open circles). Model light curves are also added for PW Vul ( $0.83 M_{\odot}$  WD, blue solid lines). See text for more details.

Budding, E. 1983, IAU Circ., 3853, 2  
 Burkhead, M. S., Penhallow, W. S., & Honeycutt, R. K. 1971, PASP, 83, 338  
 Campbell, L., & Shapley, H. 1923, Annals of the Astronomical Observatory of Harvard College, 81, 113  
 Candy, M. P., Alcock, G. E. D., & Zissell, R. E. 1967, IAU Circ., 2022, 1  
 Carney, B. W. 1977, BAAS, 9, 556  
 Cassatella, A., Altamore, A., & González-Riestra, R. 2002, A&A, 384, 1023  
 Chambliss, C. R. 1977, IBVS, 1233, 1  
 Chincarini, G. 1964, PASP, 76, 289  
 Chochol, D., Grygar, J., Pribulla, T., et al. 1997, A&A, 318, 908  
 Chochol, D., Hric, L., Urban, Z., Komzik, R., Grygar, J., & Papousek, J. 1993, A&A, 277, 103

Chochol, D., & Pribulla, T. 1997, CoSka, 27, 53  
 Chochol, D., & Pribulla, T. 1998, CoSka, 28, 121  
 Chochol, D., Katysheva, N. A., Pribulla, T., et al. 2005, CoSka, 35, 107  
 Cohen, J. G. 1985, ApJ, 292, 90  
 Cohen, J. G., & Rosenthal, A. J. 1983, ApJ, 268, 689  
 Collins, P. 1992, IAU Circ., 5454, 1  
 Collins, P., Hurst, G. M., Wils, P., et al. 1984, IAU Circ., 4023, 1  
 Connelley, M., & Sandage, A. 1970, PASP, 70, 600  
 Contadakis, M. E. 1980, IBVS, 1818, 1  
 Cox, A. (ed.) 2000, Allen's Astrophysical Quantities (New York: Springer)  
 Cragg, T. A. 1960, PASP, 72, 475  
 Dawson, B. H. 1926, AJ, 36, 148

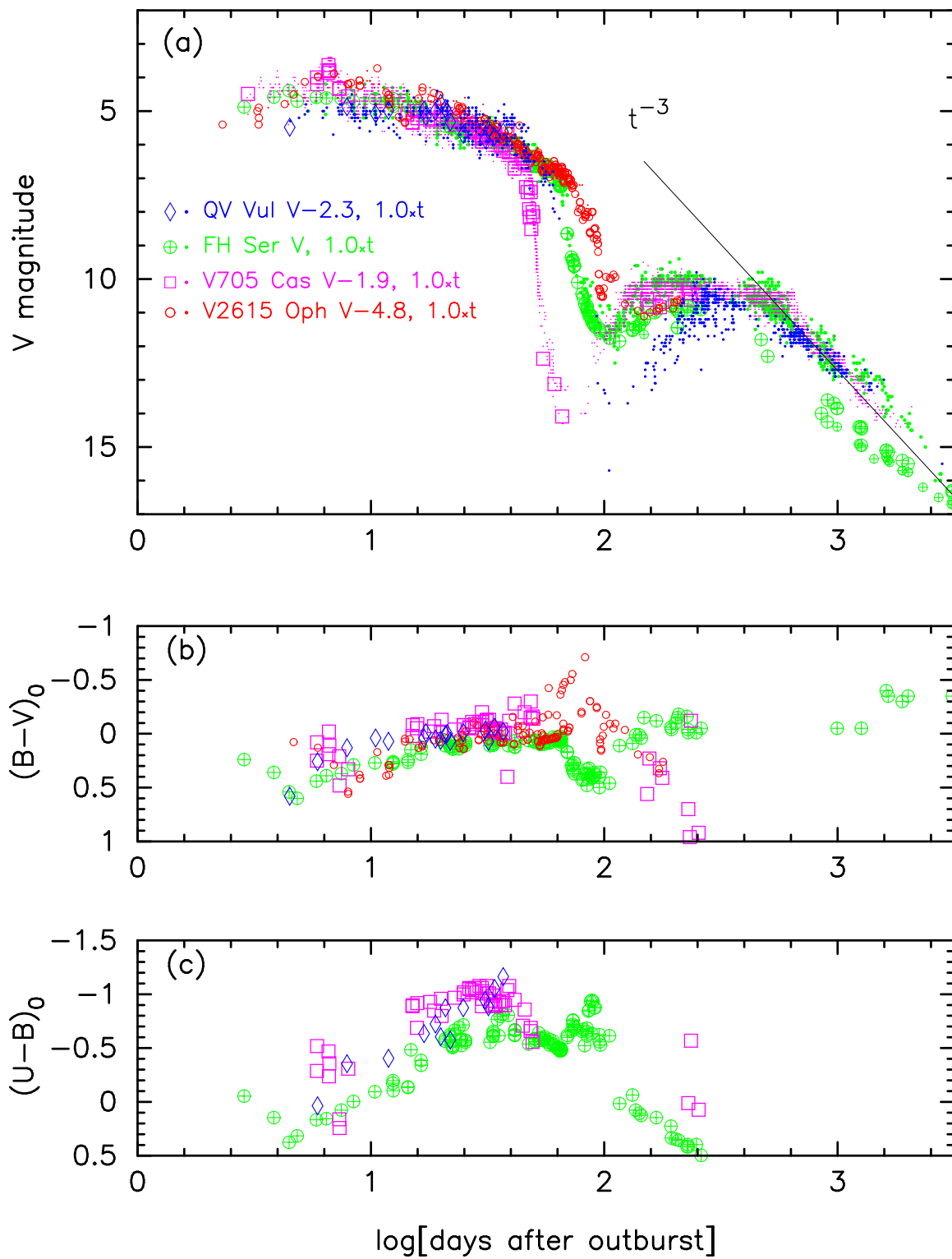


FIG. 51.— Same as Figures 43, but for QV Vul (blue symbols), FH Ser (green symbols), V705 Cas (magenta symbols), and V2615 Oph (red symbols).

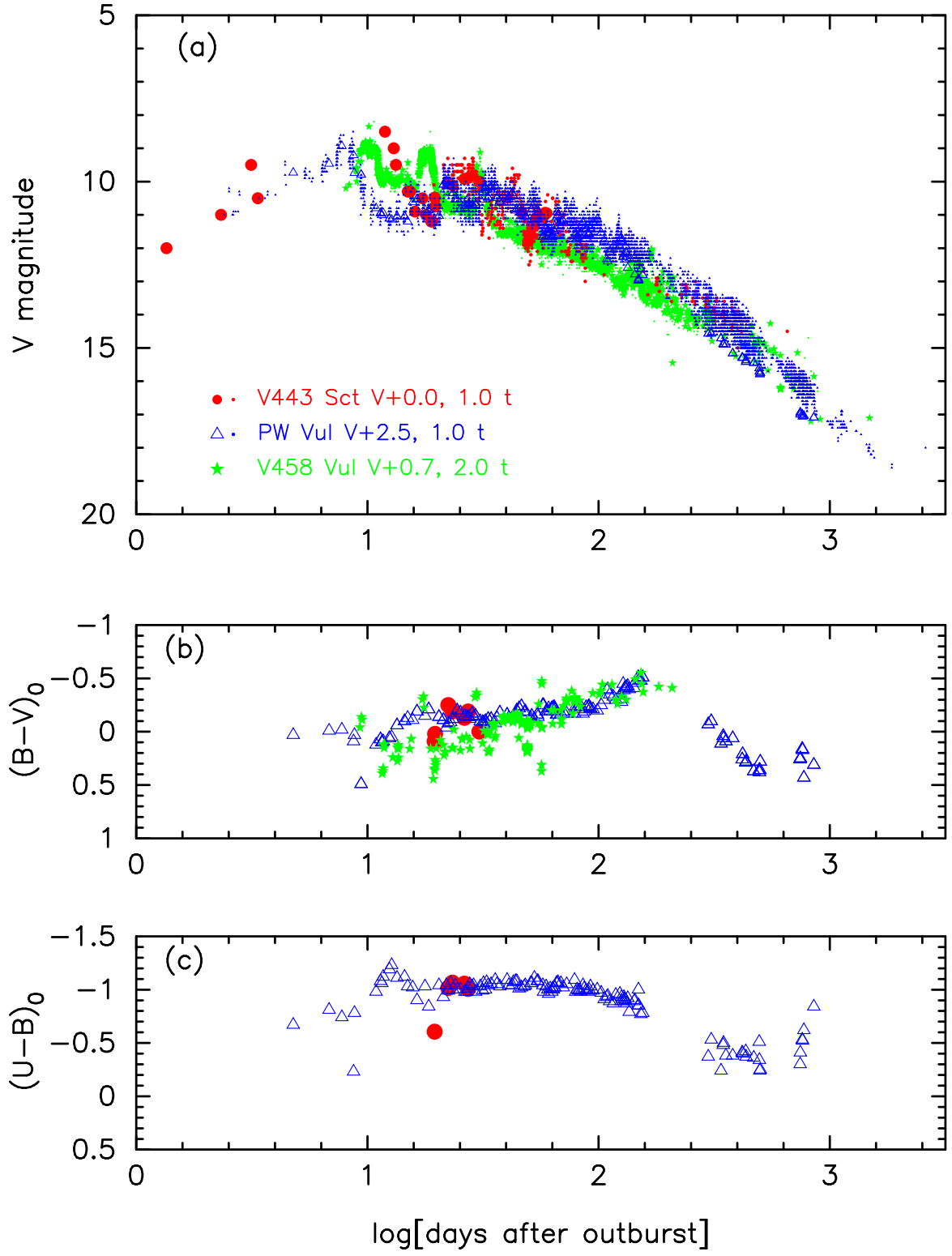


FIG. 52.— Same as Figure 41, but for V443 Sct and V458 Vul together with PW Vul.

- de Freitas Pacheco, J. A., & Codina, S. J. 1985, *MNRAS*, 214, 481
- della Valle, M., Gilmozzi, R., Bianchini, A., & Esenoglu, H. 1997, *A&A*, 325, 1151
- della Valle, M., & Livio, M. 1995, *ApJ*, 452, 704
- della Valle, M., Pasquini, L., Daou, D., & Williams, R. E. 2002, *A&A*, 390, 155
- deRoux, J. K. 1978, *IBVS*, 1519, 1
- Dickey, J. M., & Lockman, F. J. 1990, *ARA&A*, 28, 215
- di Paolantonio, A., & Patriarca, R. 1978, *IBVS*, 1516, 1.
- Dorschner, J., Friedemann, C., & Pfau, W. 1969, *AN*, 291, 217
- Downes, R. A., & Duerbeck, H. W. 2000, *AJ*, 120, 2007
- Draine, B. T. 1989, in *Proc. 22nd ESLAB Symp., Infrared Spectroscopy in Astronomy*, ed. B. H. Kaldeich (ESA SP-290; Paris: ESA), 93
- Drechsel, H., Rahe, J., Duerbeck, H. W., Kohoutek, L., & Seitter, W. C. 1977, *A&AS*, 30, 323
- Duerbeck, H. W. 1981, *PASP*, 93, 165
- Duerbeck, H. W., Geffert, M., Nelles, B., Dummmler, R., & Nolte, M. 1984, *IBVS*, 2641, 1
- Duerbeck, H. W., Rindermann, R., & Seitter, W. C. 1980, *A&A*, 81, 157
- Duerbeck, H. W., & Seitter, W. C. 1979, *A&A*, 75, 297
- Duerbeck, H. W., & Wolf, B. 1977, *A&AS*, 29, 297
- Eggen, O. J., Mathewson, D. S., & Serkowski, K. 1967, *Natur*, 213, 1216
- Ederoclitte, A., Mason, E., della Valle, M., et al. 2006, *A&A*, 459, 875
- Ennis, D., Becklin, E. E., Beckwith, S., Elias, J., Gatley, I., Matthews, K., Neugebauer, G., & Willner, S. P. 1977, *ApJ*, 214, 478
- Evans, A., Callus, C. M., Whitlock, P. A., & Laney, D. 1990, *MNRAS*, 246, 527
- Evans, A., Gehrz, R. D., Geballe, T. R., et al. 2003, *AJ*, 126, 1981
- Ferland, G. J. 1977, *ApJ*, 215, 873
- Ferland, G. J., Lambert, D. L., & Woodman, J. H. 1986, *ApJS*, 60, 375
- Fernie, J. D. 1969, *PASP*, 81, 374
- Friedjung, M. 1992, *A&A*, 262, 487
- Friedjung, M., & Iijima, T. 2002, in *AIP Conf. Proc.* 637, *Classical Nova Explosions*, ed. M. Hernanz, & J. José (Melville, NY: AIP), 308
- Friedman, S. D., York, D. G., McCall, B. J., et al. 2011, *ApJ*, 727, 33
- Gallagher, J. S., & Holm, A. V. 1974, *ApJL*, 189, L123
- Gallagher, J. S., & Ney, E. P. 1976, *ApJL*, 204, L35
- Gaposchkin, S. 1956, *AJ*, 61, 36
- Garnavich, P. M. 1996, *The Journal of the American Association of Variable Star Observers*, 24, 81
- Gehrz, R. D., Grasdalen, G. I., & Hackwell, J. A. 1985, *ApJL*, 298, L47
- Gehrz, R. D., Grasdalen, G. I., & Hackwell, J. A. 1986, *ApJL*, 298, L47 (erratum 306, L49)
- Gehrz, R. D., Harrison, T. E., Ney, E. P., et al. 1988, *ApJ*, 329, 894
- Gehrz, R. D., Jones, T. J., Woodward, C. E., et al. 1992, *ApJ*, 400, 671
- Gilmozzi, R., & Selvelli, P. 2007, *A&A*, 461, 593
- Gilmozzi, R., Selvelli, P. L., & Cassatella, A. 1994, *MmSAI*, 65, 199
- González-Riestra, R., Shore, S. N., Starrfield, S., & Krautter, J. 1996, *IAU Circ.*, 6295, 1
- Hachisu, I., & Kato, M. 2004, *ApJL*, 612, L57
- Hachisu, I., & Kato, M. 2006, *ApJS*, 167, 59
- Hachisu, I., & Kato, M. 2007, *ApJ*, 662, 552
- Hachisu, I., & Kato, M. 2009, *ApJL*, 694, L103
- Hachisu, I., & Kato, M. 2010, *ApJ*, 709, 680
- Hachisu, I., Kato, M., & Cassatella, A. 2008, *ApJ*, 687, 1236
- Hakkila, J., Myers, J. M., Stidham, B. J., & Hartmann, D. H. 1997, *AJ*, 114, 2043
- Harrison, T. E., Bornak, J., McArthur, B. E., & Benedict, G. F. 2013, *ApJ*, 767, 7
- Harman, D. J., & O'Brien, T. J. 2003, *MNRAS*, 344, 1219
- Harmanec, P., Horn, J., & Juza, K. 1994, *A&AS*, 104, 121
- Hassall, B. J. M., Snijders, M. A. J., Harris, A. W., et al. 1990, in *Physics of Classical Novae*, ed. A. Cassatella & R. Viotti (Berlin: Springer), 202
- Hauschildt, P. H., Starrfield, S., Shore, S. N., Allard, F., & Baron, E. 1995, *ApJ*, 447, 829
- Hirayama, T., Yamamoto, M., Camilleri, P., et al. 1993, *IAU Circ.*, 5791, 1
- Hric, L., Petrík, K., Urban, Z., & Hanžl, D. 1998, *A&AS*, 133, 211
- Iijima, T. 1989, *A&A*, 215, 57
- Iijima, T. 2006, *A&A*, 451, 563
- Iijima, T., Rosino, L., & della Valle, M. 1998, *A&A*, 338, 1006
- Kalberla, P. M. W., Burton, W. B., Hartmann, D., Arnal, E. M., Bajaja, E., Morras, R., & Pöppel, W. G. L. 2005, *A&A*, 440, 775
- Kamath, U. S., & Ashok, N. M. 1999, *A&AS*, 136, 107
- Kanamitsu, O., 1991, *PASJ*, 43, 225
- Kato, M. 1983, *PASJ*, 35, 507
- Kato, M., & Hachisu, I., 1994, *ApJ*, 437, 802
- Kato, M., & Hachisu, I., 2007, *ApJ*, 657, 1004
- Kato, M., & Hachisu, I., 2009, *ApJ*, 699, 1293
- Kato, M., & Hachisu, I., 2011, *ApJ*, 743, 157
- Kato, M., Hachisu, I., & Cassatella, A. 2009, *ApJ*, 704, 1676
- Kato, M., Hachisu, I., Cassatella, A., & González-Riestra, R. 2011, *ApJ*, 727, 72
- Kato, M., Mikołajewska, J., & Hachisu, I. 2012, *ApJ*, 750, 5
- Kawara, K., Maihara, T., Noguchi, K., et al. 1976, *PASJ*, 28, 163
- Kikuchi, S., Mikami, Y., & Kondo, M. 1988, *PASJ*, 40, 491
- Klare, G., Wolf, B., & Krautter, J. 1980, *A&A*, 89, 282
- Kodaira, K. 1970, *PASJ*, 22, 447
- Kohoutek, L. 1981, *MNRAS*, 196, 87P
- Kohoutek, L., & Klawitter, P. 1973, *A&AS*, 11, 347
- Kolotilov, E. A. 1980, *SvAL*, 6, 268
- Kolotilov, E. A., Munari, U., & Yudin, B. F. 1995, *MNRAS*, 275, 185
- Kolotilov, E. A., & Shenavrin, V. I. 1988, *SvAL*, 14, 29
- Kosai, H. 1984, *IAU Circ.*, 3963, 2
- Kosai, H., Honda, M., Nishimura, S., et al. 1982, *IAU Circ.*, 3661, 1
- Kosai, H., Ohshima, O., Ohkura, N., et al. 1992, *IAU Circ.*, 5455, 1
- Krautter, J., Beuermann, K., Leitherer, C., et al. 1984, *A&A*, 137, 307
- Krautter, J., Ögelman, H., Starrfield, S., Wichmann, R., & Pfeiffermann, E. 1996, *ApJ*, 456, 788
- Kuwano, Y., Ishida, K., Ichimura, K., et al. 1971, *IAU Circ.*, 2340, 1
- Lance, C. M., McCall, M. L., & Uomoto, A. K. 1988, *ApJS*, 66, 151
- Landolt, A. U. 1970, *PASP*, 82, 86
- Landolt, A. U. 1977, *PASP*, 89, 574
- Liszt, H. S. 2014, *ApJ*, 780, 10
- Lockwood, G. W., & Millis, R. L. 1976, *PASP*, 88, 235
- Lyke, J. E., & Campbell, R. D. 2009, *AJ*, 138, 1090
- Lynch, D. K., Rossano, G. S., Rudy, R. J., & Puetter, R. C. 1995, *AJ*, 110, 2274
- MacConnell, D. J., & Thomas, J. C. 1972, *IBVS*, 706, 1
- Malakpur, I. 1975, *Ap&SS*, 38, 403
- Mallama, A. D., & Skillman, D. R. 1979, *PASP*, 91, 99
- Mannery, E. J. 1970, *PASP*, 82, 626
- Marshall, D. J., Robin, A. C., Reylé, C., Schultheis, M., & Picaud, S. 2006, *A&A*, 453, 635
- Martin, P. G., & Maza, J. 1977, *Natur*, 265, 314
- Mayall, M. W. 1963, *JRASC*, 57, 279
- Milbourn, S. W., Alcock, G. E. D., Harlan, E. A., et al. 1976, *IAU Circ.*, 2997, 1
- Miroshnichenko, A. S. 1988, *SvA*, 32, 298
- Mollerus, B. 1969, *A&A*, 3, 376
- Morrison, W., Beckman, K., Baroni, S., & Cavagna, N. 1978, *IAU Circ.*, 3264, 3
- Mukai, K., & Ishida, M. 2001, *ApJ*, 551, 1024
- Munari, U., Goranskij, V. P., Popova, A. A., et al. 1996, *A&A*, 315, 166
- Munari, U., Orio, M., Valentini, M., et al. 2007, *CBET*, 1010, 1
- Munari, U., Tomov, T. V., Hric, L., & Hazucha, P. 1994a, *IBVS*, 3977, 1
- Munari, U., Yudin, B. F., Kolotilov, E. A., et al. 1994b, *A&A*, 284, L9
- Mürset, U., & Nussbaumer, H. 1994, *A&A*, 282, 586
- Nakano, S., Kanatsu, K., Kawanishi, K., et al. 1993, *IAU Circ.*, 5902, 1
- Nakano, S., Sakurai, Y., Itagaki, K., & Koff, R. 2007, *IAU Circ.*, 8832, 1
- Nakano, S., Sato, H., Nishimura, H., et al. 2003, *IAU Circ.*, 8190, 1
- Neckel, Th. 1967, *Veroeff. Landessternwarte Heidelberg-Koenigstuhl*, 19, 1
- Ness, J.-U., Schwarz, G., Starrfield, S., et al. 2008, *AJ*, 135, 1328
- Nishimaki, Y., Yamamuro, T., Motohara, K., Miyata, T., & Tanaka, M. 2008, *PASJ*, 60, 191
- Nishimura, H., Nakano, S., Liller, W., et al. 2004, *IAU Circ.*, 8306, 1
- Nussbaumer, H., & Vogel, M. 1996, *A&A*, 307, 470
- O'Connell, D. J. K. 1968, *IBVS*, 313, 1
- Ohmori, S., & Kaga, T. 1987, *IBVS*, 2988, 1
- Ohshima, O. 1988, *IBVS*, 3135, 1
- Okazaki, A., & Yamasaki, A. 1986, *Ap&SS*, 119, 89
- Onderlička, B., & Vetešník, M. 1968, *BAICz*, 19, 99
- Osawa, K. 1970, *IBVS*, 429, 1
- Payne-Gaposchkin, C. 1957, *The Galactic Novae* (Amsterdam: North-Holland)
- Péquignot, D., Petitjean, P., Boisson, C., & Krautter, J. 1993, *A&A*, 271, 219
- Pfau, W. 1976, *IBVS*, 1106, 1
- Poggiani, R. 2010, *NewA*, 15, 657
- Rafanelli, P., & Rosino, L. 1978, *A&AS*, 31, 337
- Rieke, G. H., & Lebofsky, M. J. 1985, *ApJ*, 288, 618
- Robb, R. M., & Scarfe, C. D. 1995, *MNRAS*, 273, 347
- Robinson, L. J., & Ashbrook, J. 1968, *IBVS*, 252, 1
- Rosino, L. 1975, in *Variable Stars and Stellar Evolution*, (Dordrecht: Reidel), 347



- Rosino, L., Benetti, S., Iijima, T., Rafanelli, P., & della Valle, M. 1991, *AJ*, 101, 1807
- Rosino, L., Iijima, T., Benetti, S., et al. 1992, *A&A*, 257, 603
- Rosino, L., Iijima, T., & Ortolani, S. 1983, *MNRAS*, 205, 1069
- Ross, L. W. 1960, *PASP*, 72, 413
- Rudy, R. J., Dimpfl, W. L., Lynch, D. K., et al. 2003, *ApJ*, 596, 1229
- Rudy, R. J., Lynch, D. K., Russell, R. W., & Woodward, C. E. 2007, *IAU Circ.*, 8884, 2
- Rudy, R. J., Venturini, C. C., Lynch, D. K., Mazuk, S., & Puetter, R. C. 2002, *ApJ*, 573, 794
- Saizar, P., Starrfield, S., Ferland, G. J., et al. 1991, *ApJ*, 367, 310
- Saizar, P., Starrfield, S., Ferland, G. J., et al. 1992, *ApJ*, 398, 651
- Sato, H., Nakamura, Y., Fukushima, H., Yamaoka, H., & Kadota, K. 2001, *IAU Circ.*, 7666, 1
- Sato, S., Maihara, T., & Okuda, H. 1973, *PASJ*, 25, 571
- Schlaflly, E. F., & Finkbeiner, D. P. 2011, *ApJ*, 737, 103
- Schlegel, D., Finkbeiner, D. P., & Davis, M. 1998, *ApJ*, 500, 525
- Schmidt, Th. 1957, *ZA*, 41, 182
- Schwarz, G. J. 2002, *ApJ*, 577, 940
- Schwarz, G. J., Starrfield, S., Shore, S. N., & Hauschildt, P. H. 1997, *MNRAS*, 290, 75
- Scott, A. D., Evans, A., & Rawlings, J. M. C. 1994, *MNRAS*, 269, L21
- Seaton, M. J. 1979, *MNRAS*, 187, 73P
- Selvelli, P. 2004, *BaltA*, 13, 93
- Shen, L.-Z., et al. 1964, *AcASn*, 12, 83
- Shore, S. N., Augusteijn, T., Ederoclite, A., & Uthas, H. 2011, *A&A*, 533, L8
- Shore, S. N., Schwarz, G., Bond, H. E., et al. 2003, *AJ*, 125, 1507
- Shore, S. N., Starrfield, S., Gonzalez-Riestrat, R., Hauschildt, P. H., & Sonneborn, G. 1994, *Natur*, 369, 539
- Shugarov, S., Chochol, D., & Kolotilov, E. 2012, *BaltA*, 21, 150
- Sion, E. M., Shore, S. N., Ready, C. J., & Scheible, M. P. 1993, *AJ*, 106, 2118
- Skopal, A. 2007, *NewA*, 12, 597
- Slavin, A. J., O'Brien, T. J., & Dunlop, J. S. 1994, *MNRAS*, 266, L55
- Slavin, A. J., O'Brien, T. J., & Dunlop, J. S. 1995, *MNRAS*, 276, 353
- Slovak, M. H. & Vogt, S. S. 1979, *Natur*, 277, 114
- Snijders, M. A. J. 1987, *Ap&SS*, 130, 243
- Snijders, M. A. J., Seaton, M. J., & Blades, J. C. 1982, in *Advances in Ultraviolet Astronomy: Four Years of IUE Research*, ed. Y. Kondo, J. M. Mead, & R. D. Chapman (NASA CP-2238; Greenbelt, MD: NASA), 625
- Sokoloski, J. L., Crotts, A. P. S., Lawrence, S., & Uthas, H. 2013, *ApJL*, 770, L33
- Solf, J. 1983, *ApJ*, 273, 647
- Stickland, D. J., Penn, C. J., Seaton, M. J., Snijders, M. A. J., & Storey, P. J. 1981, *MNRAS*, 197, 107
- Stringfellow, G. S., & Walter, F. M. 2006, *Ap&SS*, 304, 401
- Strope, R., Schaefer, B. E., & Henden, A. A. 2010, *AJ*, 140, 34
- Tanaka, J., Nogami, D., Fujii, M., et al. 2011, *PASJ*, 63, 911
- Tempesti, P. 1972, *A&A*, 20, 63
- Tempesti, P. 1979, *AN*, 300, 51
- Terzan, A. 1968, *JO*, 51, 329
- Thomas, J. C., Cowley, A. P., MacConnell, D. J., & Toney, J. 1973, *PASP*, 85, 309
- Tomkin, J., Lambert, D. L., & Woodman, J. 1976, *A&A*, 48, 319
- Tomov, T., Zamanov, R., Iliev, L., Mikolajewski, M., & Georgiev, L. 1991, *MNRAS*, 252, 31P
- van den Bergh, S., & Younger, P. F. 1987, *A&AS*, 70, 125
- van Genderen, A. M. 1963, *BAN*, 17, 293
- Verbunt, F. 1987, *A&AS*, 71, 339
- Vogel, M., & Nussbaumer, H. 1992, *A&A*, 259, 525
- Voloshina, I., Rovithis-Livaniou, H., & Metlova, N. 2002a, in *AIP Conf. Proc. 637, Classical Nova Explosions: International Conference on Classical Nova Explosions*, ed. M. Hernanz & J. José (Melville, NY: AIP), 315
- Voloshina, I. B., & Metlova, N. V. 2002b, in *ASP Conf. Ser. 261, The Physics of Cataclysmic Variables and Related Objects*, ed. B. T. Gänsicke, K. Beuermann, & K. Reinsch (San Francisco, CA: ASP), 669
- Waagen, E. O., Price, A., O'Connor, S., & Royer, R. 2001, *IAU Circ.*, 7668, 4
- Wade, R. A., Ciardullo, R., Jacoby, G. H., & Sharp, N. A. 1991, *AJ*, 102, 1738
- Warner, B. 1995, *Cataclysmic Variable Stars*, (Cambridge: Cambridge Univ. Press)
- Whitelock, P. A., Carter, B. S., Feast, M. W., et al. 1984, *MNRAS*, 211, 421
- Wild, P. 1989, *IAU Circ.*, 4861, 1
- Williams, P. M., & Longmore, A. J. 1984, *MNRAS*, 207, 139
- Woodward, C. E., Wooden, D. H., Pina, R. K., & Fisher, R. S. 1999, *IAU Circ.*, 7220, 3
- Wright, A. E., & Barlow, M. J. 1975, *MNRAS*, 70, 41
- Wu, C.-C., Holm, A. V., Panek, R. J., et al. 1989, *ApJ*, 339, 443
- Yamaoka, H., Haseda, K., & Nakamura, Y. 2007, *IAU Circ.*, 8832, 2
- Yamashita, Y., Ichimura, K., Nakagiri, M., et al. 1977, *PASJ*, 29, 527
- Young, P. J., Corwin, H. G., Bryan, J., & de Vaucouleurs, G. 1976, *ApJ*, 209, 882
- Younger, J. W. 1980, *AJ*, 85, 1232